DESIGN AND ANALYSIS OF MINE RESISTANT AMBUSH PROTECTED VEHICLE ROLLOVER SIMULATOR

SERHAT KÖKSAL

DECEMBER 2020

DESIGN AND ANALYSIS OF MINE RESISTANT AMBUSH PROTECTED
VEHICLE ROLLOVER SIMULATOR

A THESIS SUBMITTED TO

THE GRADUATE SCHOOL OF NATURAL AND APPLIED

SCIENCES OF
ÇANKAYA UNIVERSITY

BY
SERHAT KÖKSAL

IN PARTIAL FULFILLMENT OF THE REQUIREMENTS FOR
THE DEGREE OF
MASTER OF SCIENCE
IN
MECHANICAL ENGINEERING
DEPARTMENT

DECEMBER 2020

ABSTRACT

DESIGN AND ANALYSIS OF MINE RESISTANT AMBUSH PROTECTED VEHICLE ROLLOVER SIMULATOR

KÖKSAL, Serhat

M.Sc., Department of Mechanical Engineering

Supervisor: Asst.Prof.Dr. Özgün Selvi (Cankaya University)

December 2020, 74 pages

In this study, design, static structural analysis and, dynamic simulation of Mine Resistant Ambush Protected Vehicle Rollover Simulator which is designed for egress training, was carried out. Especially for military requirements, types and necessity of emergency egress training are explained and, according to MRAP vehicles in use, a generic cabin and rollover mechanism designed and their structural resistance has been examined. The Figures of the components of the simulator were shared. Unlike the conventional type of rollover simulators, a lateral movement mechanism is added to the simulator for better rollover sentiment and eventually better training. According to this design, a member of the vehicle crew was modeled and a planar movement simulation was created in the MATLAB Simulink Multibody Environment. The most sensitive part was determined as his/her neck for rollover situation and based on the outcomes that are taken from the neck part, the maximum velocity and acceleration to avoid any injury while training, was determined. This assembly system was simulated with the MATLAB Simulink program, and the results were shared.

Keywords: Rollover Simulator, Emergency Egress Trainer, Planar Movement Simulation.

ÖZ

MAYINA DAYANIKLI ZIRHLI ARAÇ DEVRİLME SİMULATÖRÜ TASARIM VE ANALİZLERİ

KÖKSAL, Serhat

Yüksek Lisans, Makine Mühendisliği Anabilim Dalı

Tez Yöneticisi: Dr. Öğr. Üyesi. Özgün Selvi (Çankaya Üniversitesi)

Aralık 2020, 74 Sayfa

Bu çalışmada, kaçış eğitimi için tasarlanan Mayına Dayanıklı Zırhlı Araç Devrilme Simülatörünün tasarımı, yapısal dayanım analizleri ve dinamik hareket simulasyonu yapılmıştır. Özellikle askeri alanda ihtiyaç duyulan acil durum kaçış eğitimlerinin türleri ve gerekliliği açıklanmış, kullanımda olan MRAP araçları baz alınarak, genel bir kabin ile devrilme mekanizması tasarlanmış ve yapısal dayanımları incelenmiştir. Simülatör modelinin bileşenlerinin görselleri paylaşılmıştır. Geleneksel devrilme simülatörlerinden farklı olarak, daha iyi bir takla atma hissi ve nihayetinde daha iyi eğitim için simülatöre yanal bir hareket mekanizması eklenmiştir. Bu tasarıma göre, araç ekibi üyelerinden biri modellenmiş ve MATLAB Simulink Multibody ortamda düzlemsel bir hareket simülasyonu oluşturulmuştur. Devrilme durumunda personelin en hassas bölgesi boynu olarak değerlendirilmiş ve boyundan alınan sonuçlara göre, eğitim esnasında herhangi bir sakatlanmaya sebep olmadan eğitimin tamamlanabileceği en yüksek hız, ivme değerleri belirlenmiştir. Bu montaj sistemi MATLAB Simulink programı ile simüle edilmiş ve sonuçlar paylaşılmıştır.

Anahtar Kelimeler: Devrilme Simulatörü, Acil Durum Kaçış Eğitmeni, Düzlemsel Hareket Simulasyonu

ACKNOWLEDGEMENTS

TABLE OF CONTENTS

LIST OF FIGURES

LIST OF TABLES

LIST OF ABBREVIATIONS

FEM   Finite Elements Method

HUET   Helicopter Underwater Egress

MRAP   Mine-Resistant Ambushed Vehicle

MRET   MRAP Egress Trainer

NHTSA   National Highway Traffic Safety Administration

NIC   Neck Injury Criteria

OPITO   Offshore Petroleum Industry Training Organization

PITB   Petroleum Industry Training Board

CHAPTER 1

INTRODUCTION

1.1 Motivation

This thesis provides information about the design of a military egress training simulator that simulates the rollover of military vehicles. The purpose of these simulators is to create a proper simulation environment for egress training. So they do not simulate the exact similar rollover incident. The commonly used ones simulate rollover incidents with one degree of freedom. These simulators only represent the rotational movement and are used both for military and civil applications. This work purposes to improve the accuracy, fidelity, and performance of this kind of simulators by adding a lateral movement. Additionally, there is no scientific research in literature that determines the limiting velocity and acceleration of this kind of simulators. So, one other motivation is determining the design limitations of the simulator with dynamic simulation according to effects on its crew.

1.2 Literature Review

1.2.1 Simulators

Simulators are devices that are developed to create a realistic imitation environment of different situations. There are many different types of simulators but roughly, they can be divided into two categories, namely: training simulators and research simulators. Training simulators can be defined as the devices that are used for training purposes and certificated by accredited institutions according to simulation and usage similarity to actual platforms. On the other hand, research simulators can be defined as devices that are designed for investigating effects of certain situations like human-machine interaction, effects of motion platforms' dynamic behavior on humans or researching on extreme dangerous situations, etc. [1] Research simulators can sample as hydraulic blast simulators which generate g-shock over a building to experiment the strength of the concrete structure [2].

In this thesis, training simulators are focused on. Pieces of training are usually

performed to prepare the trainee for real-life experience. Up to tool, vehicle, or the environment that are used, the real-life experience can be extremely dangerous. Simulators create these cases in a safer environment with adjustable and repeatable scenarios. The reasons for using simulators can be listed as:

- Cost-effective training solutions,

- Simulating dangerous cases without any risk,

- Training under different scenarios and conditions,

- Preparing the trainee for possible accidents and emergency conditions.

So, in this era with developed technology, simulators became a solid part of civil and military training.

Simulations have had a complex history in many areas like aviation, military training, driving education, and health care. The first necessity of training simulators was felt in the aviation industry because of military applications at the beginning of the 1900s. The flight training studies were achieved on real planes but this training style caused lots of plane crashes with casualties. Then, the first flight simulator was built and called Antoinette.[3]

Figure 1 First Vehicle Simulator for Military Flight Trainings *[3]*

After that, a simulator called Link Trainer was built by Edwin Link in the late 1920s and became the first commercial aviation simulator. [4] Because of safe and cost-effective training skills, aviation simulators became a major member of pilot training and pioneered to simulation business being developed in different types. With time and developed technology, the importance of the simulators is more understood by

armies, and the scale of the simulator types got widen. For example, in the 1980s US Army started to improve the primary live training of ground forces by using laser devices that simulate gunfire. During the 1990's they started to use driving simulators that are configurable to replicate the variety of vehicles. [5]

There are many types of simulators in different Armed Forces but in this thesis egress training versions are focused on.

1.2.2   Egress Training Simulators

According to the nature of training, trainees are usually got trained to respond to emergency conditions. Emergency response training is a challenging and stressful training that forces the individuals to understand the emergency, detect the threats, and safely mitigate the risks with learned reactions. [6] The common purpose of this training is surviving under difficult conditions and egressing from them. So, as part of development in the simulators area, the simulators which simulate the mentioned conditions are started to be designed and commonly named "Egress trainer". These simulators can be classified under three conditions in which they are used:

- Wet condition / Helicopter Underwater Egress Trainer Simulators (HUET) [7]

- Air conditions / Egress with Parachute Simulator. [8]

- Dry condition / Rollover Simulators (MRET). [9]

Helicopter Underwater Egress Training Simulators (HUET)

Since the invention of flying machines people use them for faster traveling. To shorten the travel duration, pilots usually select the shortest distance which can pass ground with also water. Flying over water on a plane or helicopter comes with its challenges like ditching into the water because of technical problems or bad weather conditions etc. [10] The first reported helicopter ditching happened on the 1st of November, 1944 in the Pacific Ocean, but, up to 1971, no one paid attention to casualties in helicopter ditching. With the discovery of the oil reserves in the North Sea the helicopter ditching accidents started to increase, and in 1971 Glancy wrote the first report about this situation. [11] According to her study, 55% of aircrew died in case of helicopter ditching. The survival rate was low because, after the contact to the water surface, helicopters usually capsized and rapidly filled with water approximately %70 of the cases. [12]

Figure 2 A Ditched and Capsized Helicopter in the North Sea [13]

Unless the crew can egress before the helicopter was filled with water, the underwater egress situation starts. Underwater egress is a very time-limited, challenging, and stressful situation, and unfortunately sometimes ends up with casualties. According to Taber and McCabe's review of a reported helicopter ditching all around the world between 1971 and 2005, there were 511 cases with %66 survival rate of 2478 people. [14] To prepare the crew for this harsh situation, the underwater egress training began with the design and manufacture of HUET simulators and got very beneficial results.
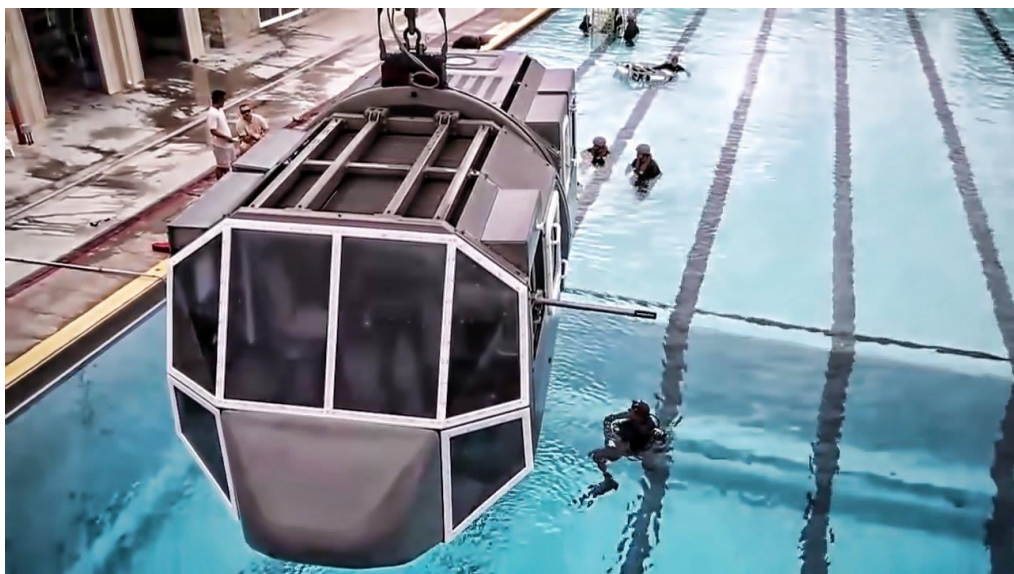
Figure 3 An example of HUET Simulator [15]

According to Cunningham's report [12] survival rate in the ditching situation was %66 without HUET and %91.5 with HUET. This big gap between survival rates shows the importance of the Helicopter Underwater Egress Simulator. So, in 1977, the Petroleum Industry Training Board (PITB) was established, and PITB be split in 1982; the formed Offshore Petroleum Industry Training Organization (OPITO) standardized the training procedure for Offshore Industry including HUET. Since then 375.000 military and civil personnel from more than 50 countries were trained for Underwater Egress. [16] In Kocaeli/Turkey one training center which is designed for the Turkish Navy according to OPITO Standards is under construction by Meteksan Defence Company.
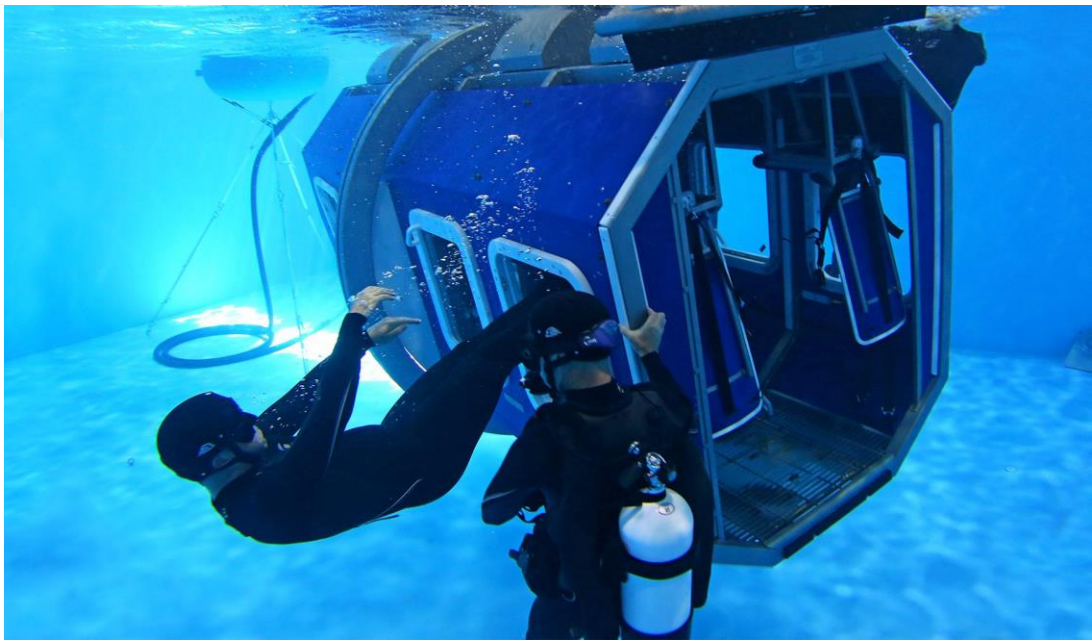
Figure 4 Egressing from HUET Simulator [17]

Parachute with Egress Training Simulators

R.Hogue and et al. [8] gives the details of the parachute simulator which is used for one or other type of egress training in the air includes after egressing from a plane in an emergency and managing the parachute that failed to open as required. This is a very rare type of egress simulator and is not commonly used.

MRAP Rollover Egress Training (MRET) Simulators

Rollover accident is an issue since the invention of ground vehicles. The roof deformation and passenger injuries in such accidents have been the subject of investigation for the last 40 years. [18] Scientists have been designing experimental

setups and simulators to investigate this topic. As mentioned at the beginning of this chapter, these setups can be divided into two categories which are built for training and research. The research ones mostly simulate the same rollover incident with dummies inside actual vehicles and collect real-time information for improving vehicle and road technologies. [19] [20] [21] On the other hand, rollover training simulators mostly focus on two topics. The first type of these simulators is a driving simulator which trains the drivers to prevent rollover situations. They simulate the rollover incident in a virtual environment according to the reactions of the driver without fully physical rollover movement. [22] [23]

Figure 5 An example of a Computer Based Real-Time Driving Simulator [22]

Figure 6 An example of tractor cab roll simulator, with simulator tilted to 30°. [23]

Meanwhile, some training simulators are designed for egress training. These simulators mostly educate occupants on how to respond to a rollover accident and egress from a capsized vehicle. These simulators can be used for civil reasons with commercial automobile models. For example, in 2016 more than 25813 people experienced the rollover simulator which encourages the use of seatbelt in Ireland. [24] Also, they can be used for military reasons with simulated military vehicle cabins. [25] In this thesis, a military type Rollover Simulator that simulates, the rollover accident of mine-resistant ambush-protected land vehicles is focused.

Mine resistant Ambush Protected (MRAP) Vehicles are heavy vehicles that usually serve for transferring soldiers to dangerous operation areas with mine and bullet protection. For this protection, vehicles are equipped with thick metal plates with a V-shaped hull and bulletproofed windows, but these heavy accessories increase heavy curb weight ranging from 7 to 22 tons with high ground clearance from the center of gravity point to the ground. Under this condition, the vehicle design gives required protection, but in most cases increases the vehicular accidents primarily vehicle rollovers. According to the analysis of 420 MRAP accidents that occurred from November 2007 through August 2009, % 42 of these accidents are related to the rollover situation. Because of these accidents, 215 injuries are reported. [26]

Figure 7 An example of MRAP Rollover accident [27]

Nearly %75 percent of rollover accidents happens outside of the urban areas with low-quality road conditions. In this case, the crew could not get immediate help and some causalities occur especially when they could not exit the vehicle in time, in case of fire or drawing into a river or water channel. [28] Especially behind the dangerous line, MRAP vehicles attend lots of operations with personnel transferring duties. While these transfers the counter forces usually ambush handmade explorers to the sides of the roads to damage the operational forces. These explosions harm the vehicles and can cause rollover situations. These kinds of rollover situations are physically and emotionally more devastating than regular traffic accident rollovers. Examples of it are given in Figures 8 and 9. These situations increase the importance of egress training because of the necessity of self-surviving.

Figure 8 Example of MRAP side explosion – 1 [29]

Figure 9 Example of MRAP side explosion – 2 [29]

So, to avoid rollover accidents and decrease the number of causalities, militaries usually process some training programs which include common driver training, operator driving training, and egress training. These training programs educate the crew of the vehicle because nearly 60 percentages of these accidents occur in lack of training. [28]

Egress simulator is one of the major parts of the training. As mentioned in previous sentences, MRAP Egress Trainer (MRET) is a specially designed simulator that occurs from an MRAP vehicle simulated cabin with 360º rotation ability. And a unique version's design details, static analysis, and dynamic simulation is given in the following chapters of this thesis.

Figure 10 Example of 1 DoF Military Rollover Simulator [30]

1.3 Thesis Overview

The Rollover simulator which is a major part of egress training was chosen for modification and development. In Section 1.2 Literature review and information about egress training types and simulators are given.

In Chapter 2 the general design of the rollover simulator is introduced. The subparts, dimensions, and sitting plans are defined in section 2.1. In the next section, the selection methodology and calculations of lateral and rotational movement motors are performed.

In Chapter 3, the static structural analysis of simulator parts is performed, separately. Section 3.1 focuses on Simulator Cabin. The structural design details, the types, positions, and thicknesses of the materials are defined. In the following parts of the same section, static structural analysis' inputs and results are given. The same procedure processed in section 3.1 is processed in section 3.2 for the movable platform.

In Chapter 4, dynamic simulation of the simulator is performed in Matlab Simulink Multibody environment. The simulation methodology and the properties of the human model used in the simulation are defined in Section 4.1. After that, the simulation components, Simulink diagrams, and planar kinematics calculations for calculation inputs are given in Section 4.2. Results of the simulation are given in Section 4.3.

And finally, in Chapter 5, the conclusion of the study is defined.

CHAPTER 2
DESIGN

2.1 Rollover Simulator Configuration

The rollover simulator is designed according to the necessity of better training, so it includes many different parts assembled with different manufacturing methods; but basically, it can be categorized under three main parts which are:

- Simulator Cabin: is a part which is designed as the main place of the training. It is rotational, and it is a design copy of the MRAP vehicle's cabin. Its main structure is planned to be produced by welding the sheet metal plates and steel profiles.

- Movable platform: is a part that is designed to carry the simulator cabin and provides lateral movement. It is planned to be produced with welding of the standard steel profiles.

- Fixed platform: is a part that provides the necessary height to trainees for proper entrance and exit. It is planned to be produced with welding of the standard steel profiles and sheet metals.
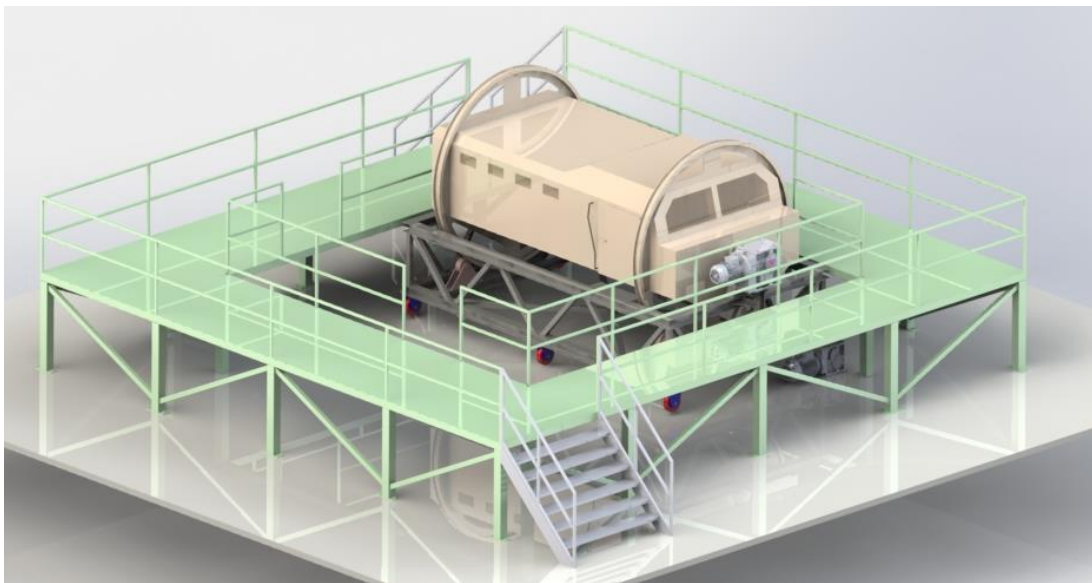
Figure 11 General View of Simulator
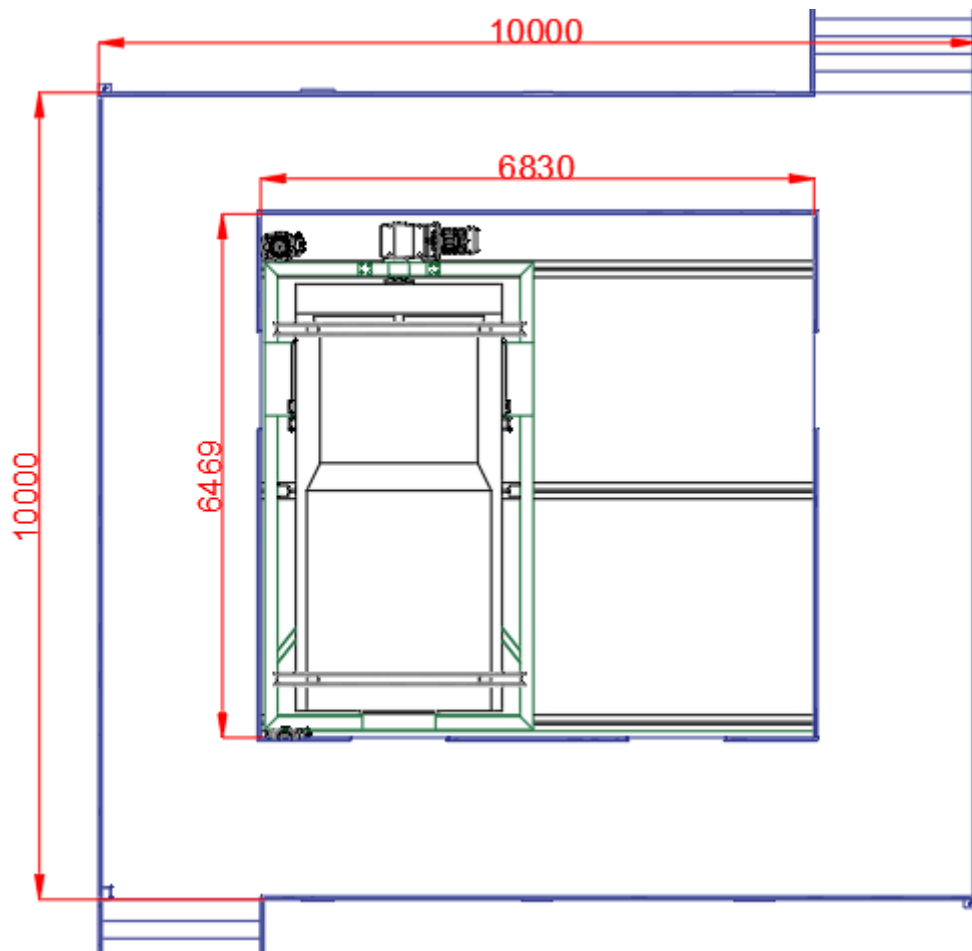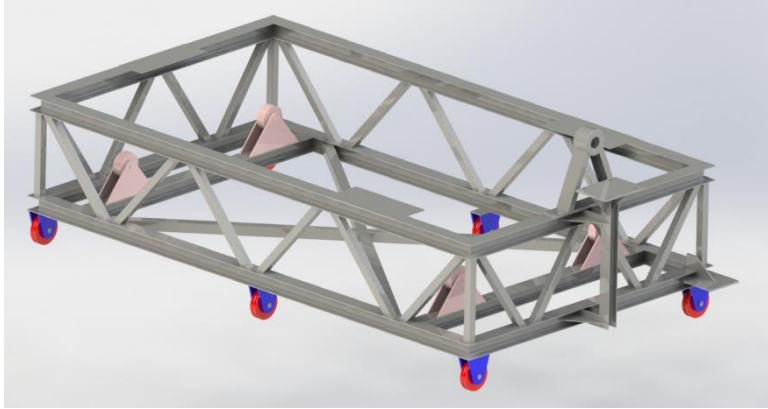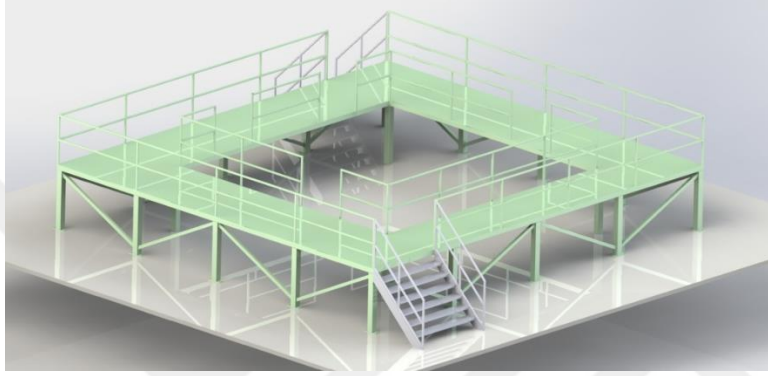
Figure 12 General Layout of Simulator

Table 1 Components of Simulator

	Simulator Cabin

	Movable Platform
	Fixed Platform

The design of the simulator cabin has internal and external structural members. The mission of the internal members is mostly strengthening and stabilizing the model. On the other hand, the shell parts have the same mission, additionally with providing the same feeling that the trainees feel themselves like they are in a real MRAP vehicle which is called fidelity. [31] Some thicknesses of material used especially in the simulator cabin are needed structurally because providing the same fidelity as MRAP was a major aim. The thicknesses of the sheet metals are given in the following figures.
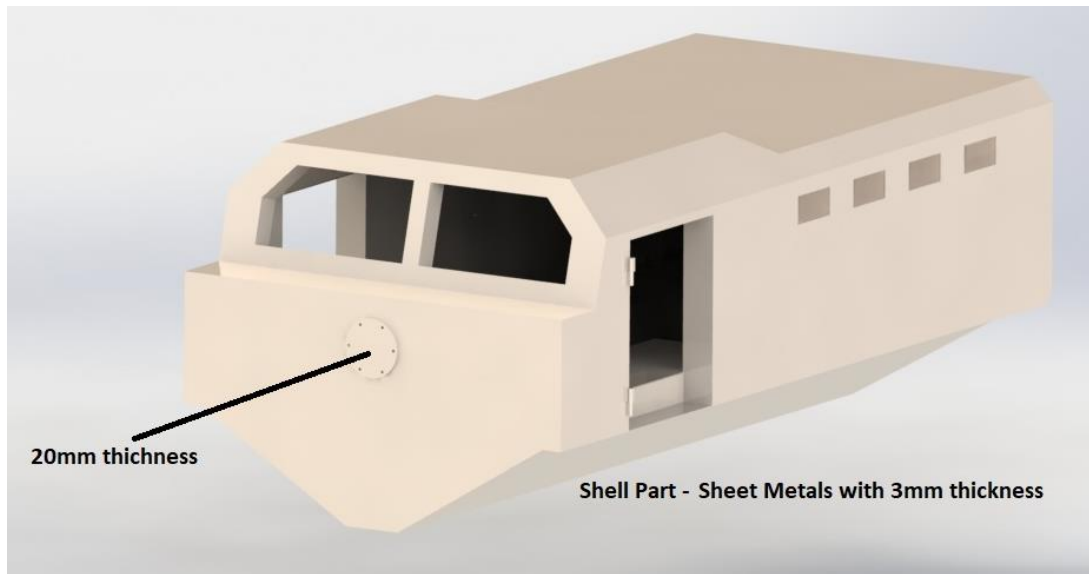
Figure 13 Thickness of Shell Metals
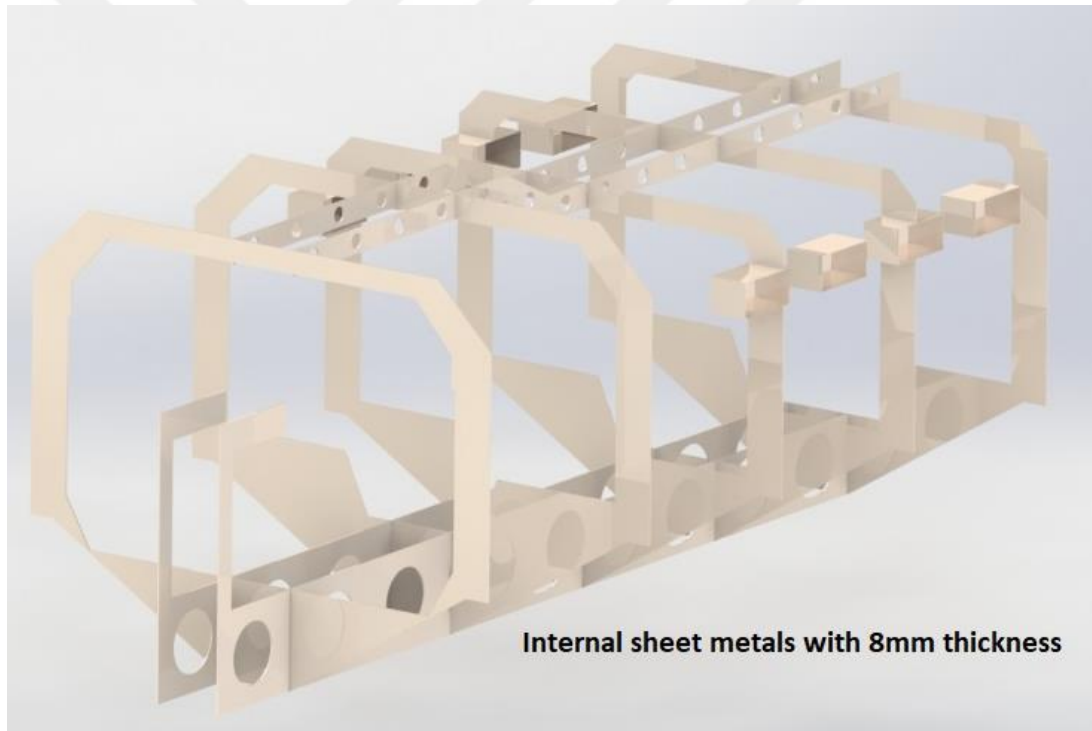
Figure 14 Thickness of the Internal Metals
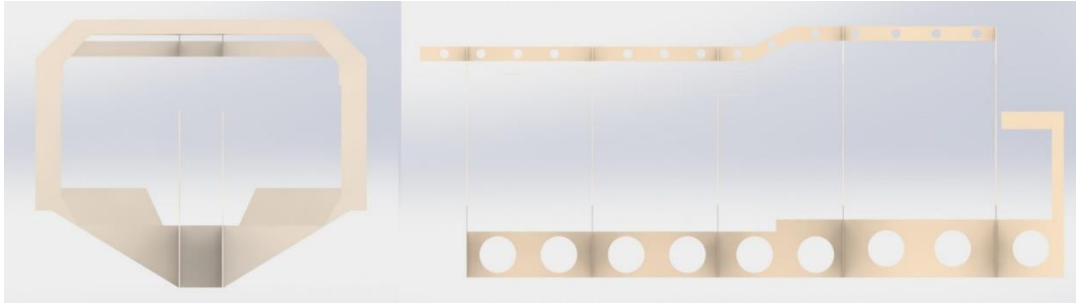
Figure 15 Front and Rear Views of the Internal Metals
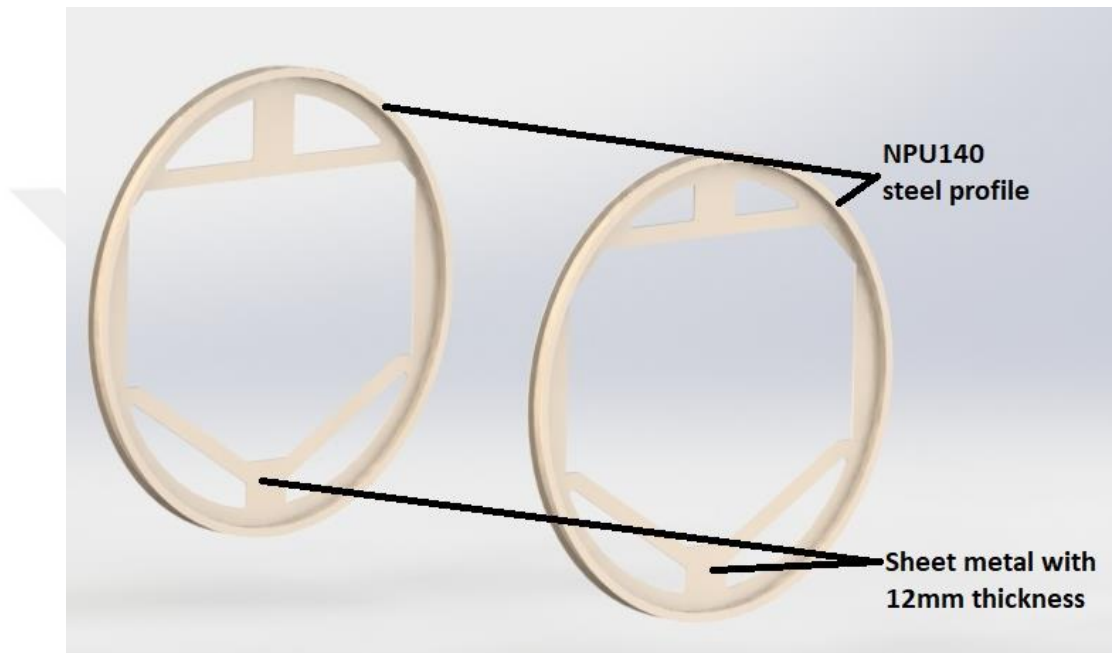
Figure 16 Thickness of Rotation Frame
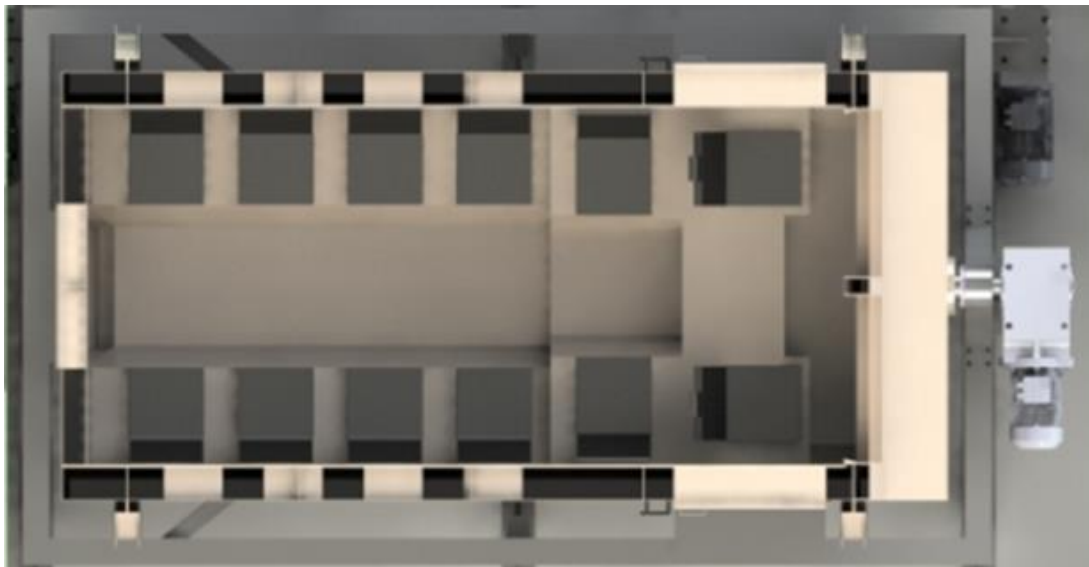
Figure 17 Sitting Configuration of Simulator

The dimensions of the simulator cabin are given in the following figure. Especially the diameter of the support circle will be used in electrical motor calculations.
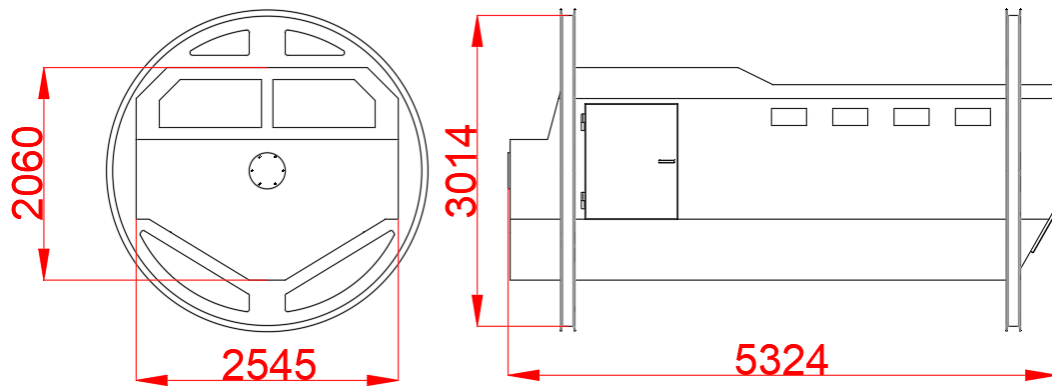
Figure 18 Dimensions of Simulator Cabin

The design of the movable platform includes two types of profiles that have the same material type with different sizes. The profile details are given in Figure 19. The steel type is St37-2, and its material properties are given in Figure 30.
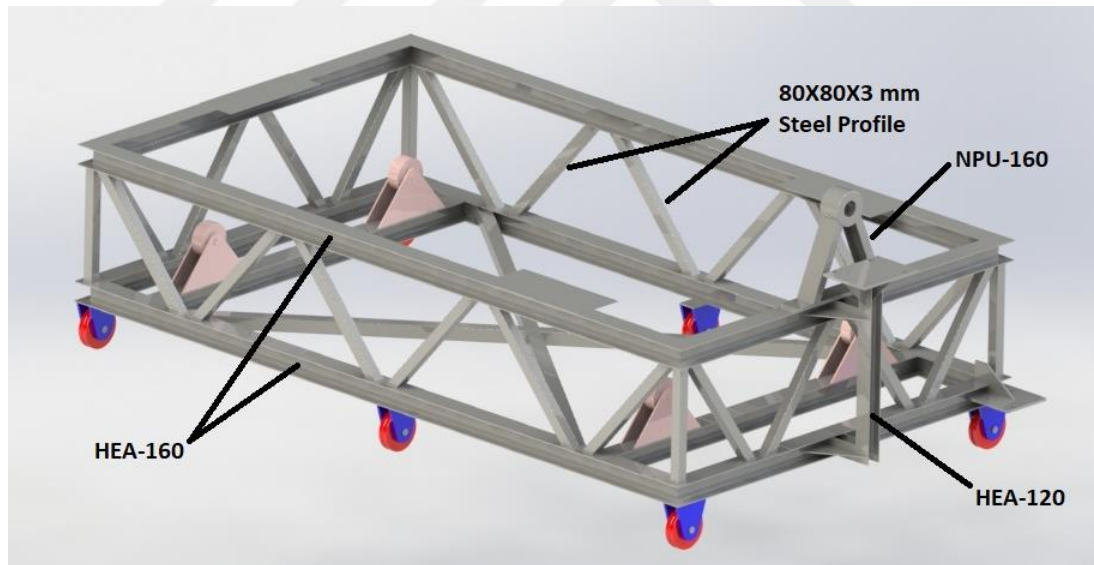
Figure 19 Movable Platform Profile Type

The rotational and lateral movements are provided by electrical motors. There are two-wheel coupled electrical motors that are used for lateral movement, and one shaft coupled electrical motor is used for rotational movement. The duration of the training under the normal procedure is selected as 10 seconds. So, the simulator completes the 180º rolling movement with 3.315m lateral movement within 10 seconds. For both

types of movements, the maximum velocity is reached at the half time of the training duration with constant acceleration and deceleration. The velocity profile of the simulator is given in Figures 20 and 21.
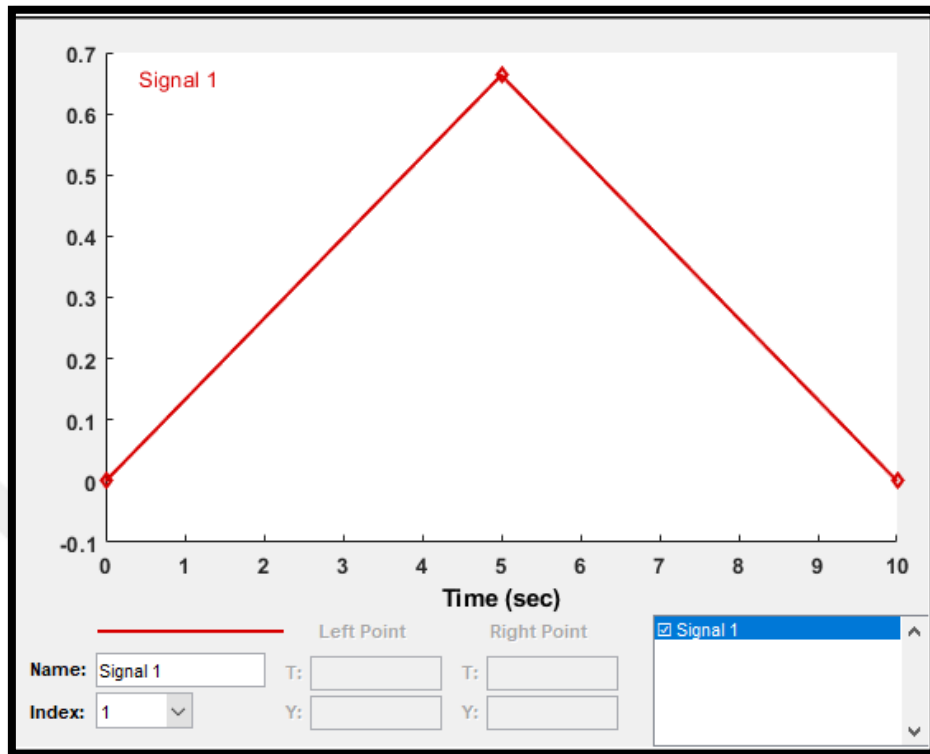
Figure 20 Lateral Move Velocity Profile (m/s)
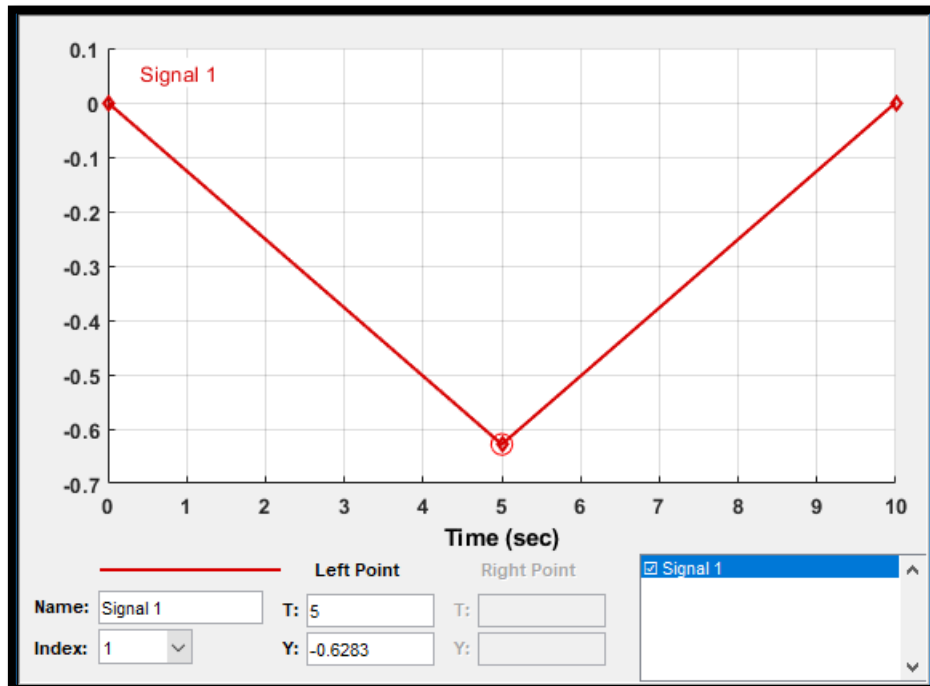
Figure 21 Angular Move Velocity Profile (rad/s)

According to these displacements and velocity requirements, the selection of electrical motors is given in the following section.

2.2 Motor Calculations

Rotational Movement Motor Calculations
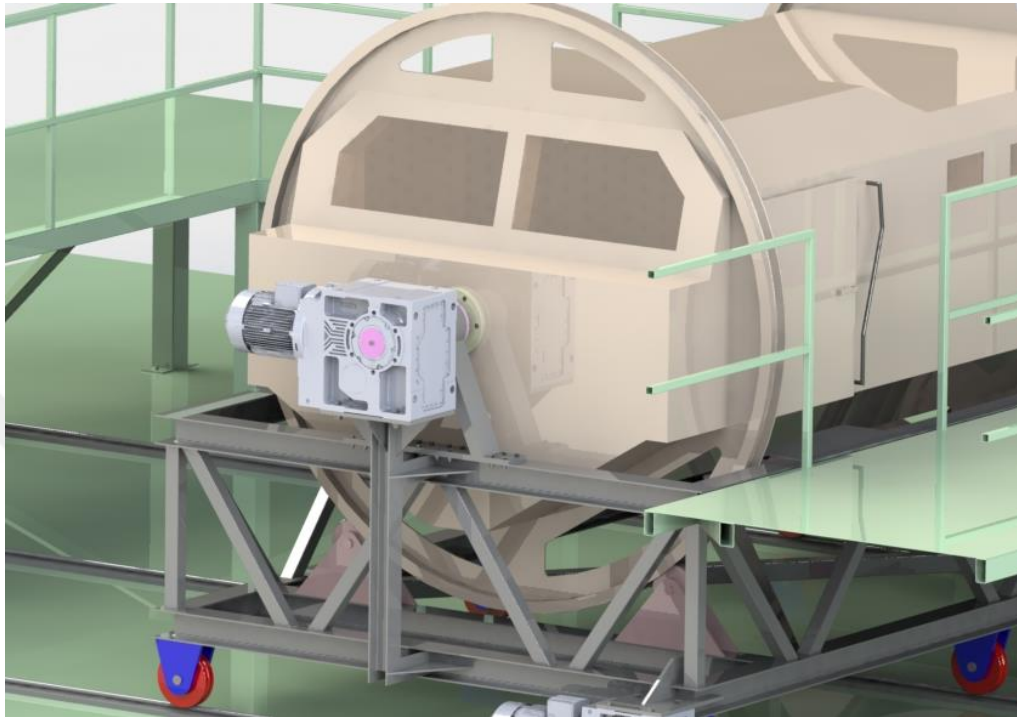
Figure 22 Rotation Motor's Placement

Maximum rotational movement speed is determined as 0.6283 rad/second, which equals 6 rpm based on the velocity profile given in Figure 21.

The rotational movement occurs against the moment created by the frictional forces and the center of gravity which is not on the axis of rotation. So the selected electrical motor must be able to handle the total moment that occurred because of these forces.

There are 4 wheels on the movable platform these contact with the rail surface of the simulator cabin. These contacts create friction, and this friction creates a rolling resistance. Consequently, the motor should overcome this resistance. The system is a combination of steel wheels on rails, so friction factor C_r is taken as 0.27 [32].

On the other hand, for the effect of the moment which is created by the center of gravity, there were 3 different conditions investigated while selecting the rotation motor because of the center of the mass changes with different sitting configurations. In the first case no load was applied, in the second case fully load was applied. In the third case, one side asymmetric load was applied.

So for these 3 different loading conditions, the following power calculations are performed:

$$P = M \times w / 0.975 \qquad (2.1)$$

P: Power (W)

w: Angular velocity (rpm)

$$M_T = M_f + M_L \qquad (2.2)$$

M_T: Total Torque (kgm)

M_f: Frictional Torque (kgm)

M_L : Load Torque (kgm)

$$M_f = m \times d_1 \times C_r \qquad (2.3)$$

$$M_L = m \times d_2 \qquad (2.4)$$

m: resultant mass of the simulator and load applied (kg)

d_1: distance between center of the mass of the simulator cabin and rotation axis (m)

C_r : steel wheels on rails rolling resistance factor

d_2: distance between center of the mass of the simulator cabin and support wheel (m)

<u>First Case: No External Load</u>

$d_1 = 3014mm/2 = 1.507\ m$

$d_2 = 10.41mm = 0.01041\ m$

$m = 3804.75\ kg$

From Equation 2.2;

$M_T = m \times d_1 \times C_r + m \times d_2$

$M_T = 3804.75\ kg \times (1.507\ m \times 0.27 + 0.01041m) \approx 1587.72\ kgm$

$V = 6\ rpm$

From Equation 3.1;

$P = 1587.72 \times 6 / 0.975$

$P \approx 9770.6\ W = 9.77\ KW$
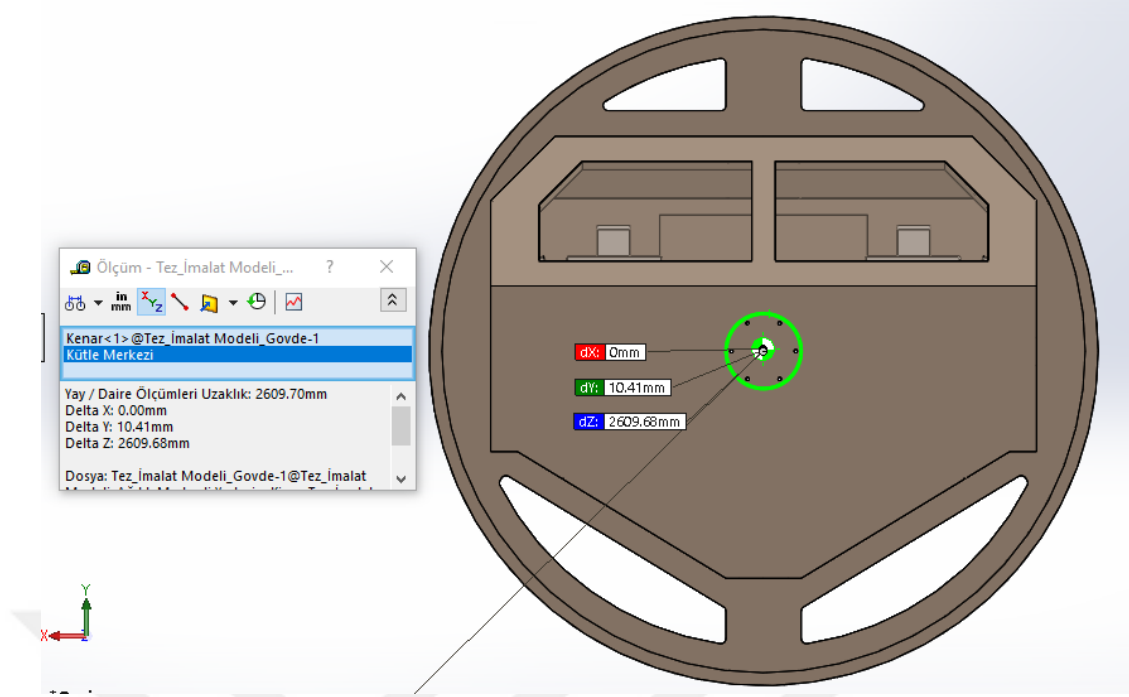
Figure 23 Mass Center for No External Load Case
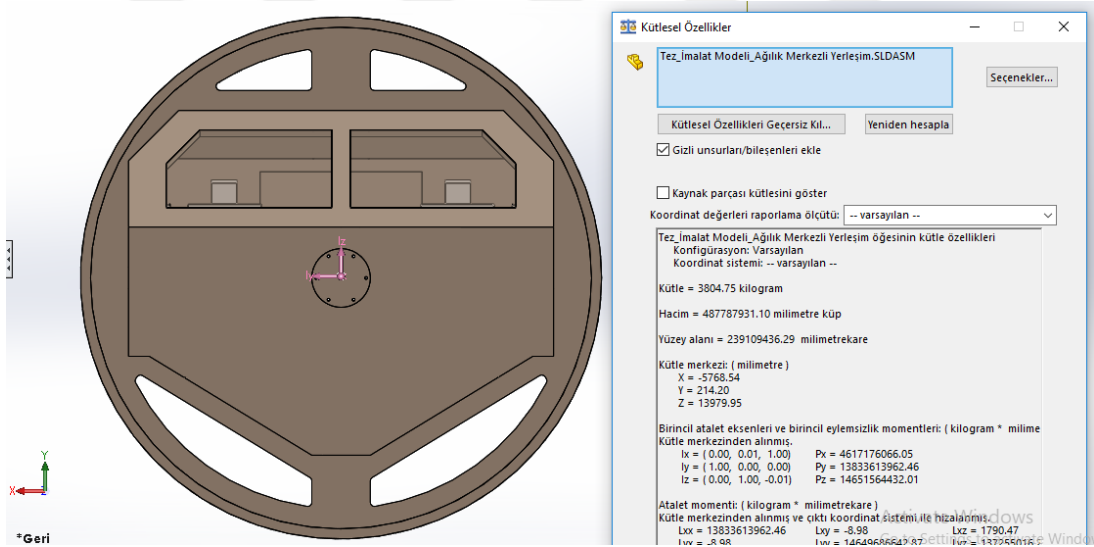
Figure 24 Mass Properties for No External Load Case

<u>Second Case: Full load</u>

Distance between center of the mass of the simulator cabin and rotation axis under full load condition is zero, so no external load moment occurs.

$d_1 = 3014mm/2 = 1.507\ m$

$d_2 = 0\ m$

21

m = 4719.04 kg

From Equation 2.2;

$M_T = m \; x \; d_1 \; x \; C_r + m \; x \; d_2$

M_T = 4719.04 kg x (1.507 m x 0.27 + 0 m) ≈ 1920.13 kgm

V = 6 rpm

From Equation 2.1;

P = 1920.13 x 3 / 0.975

P ≈ 118164W = 11.8 KW
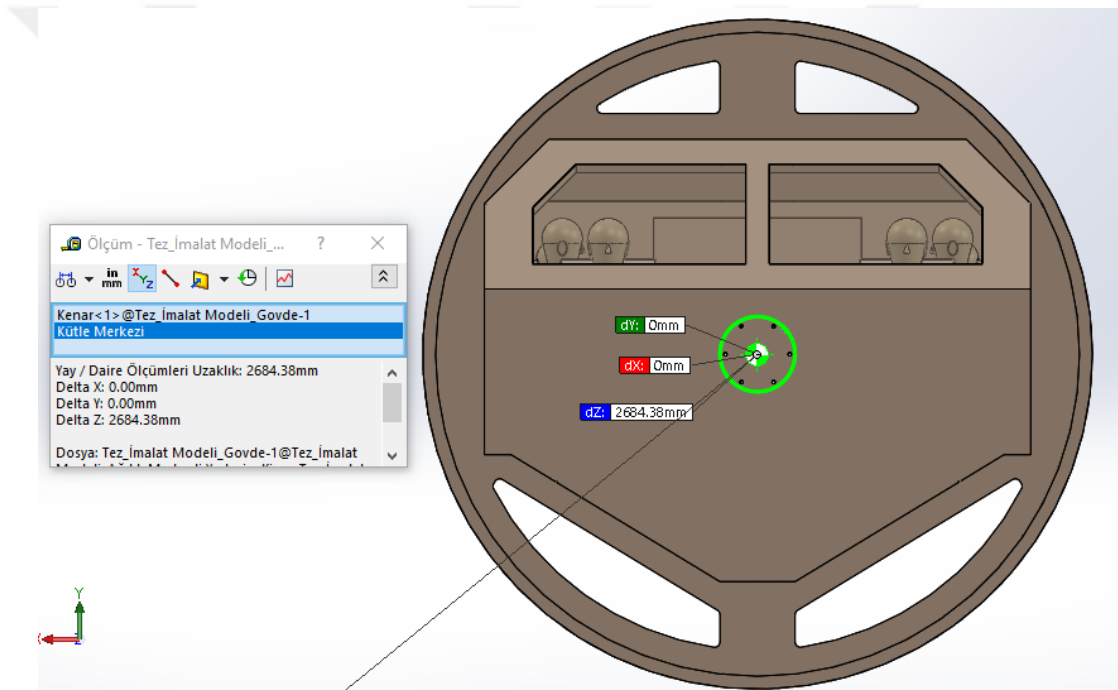
Figure 25 Mass Center for Full Load Case
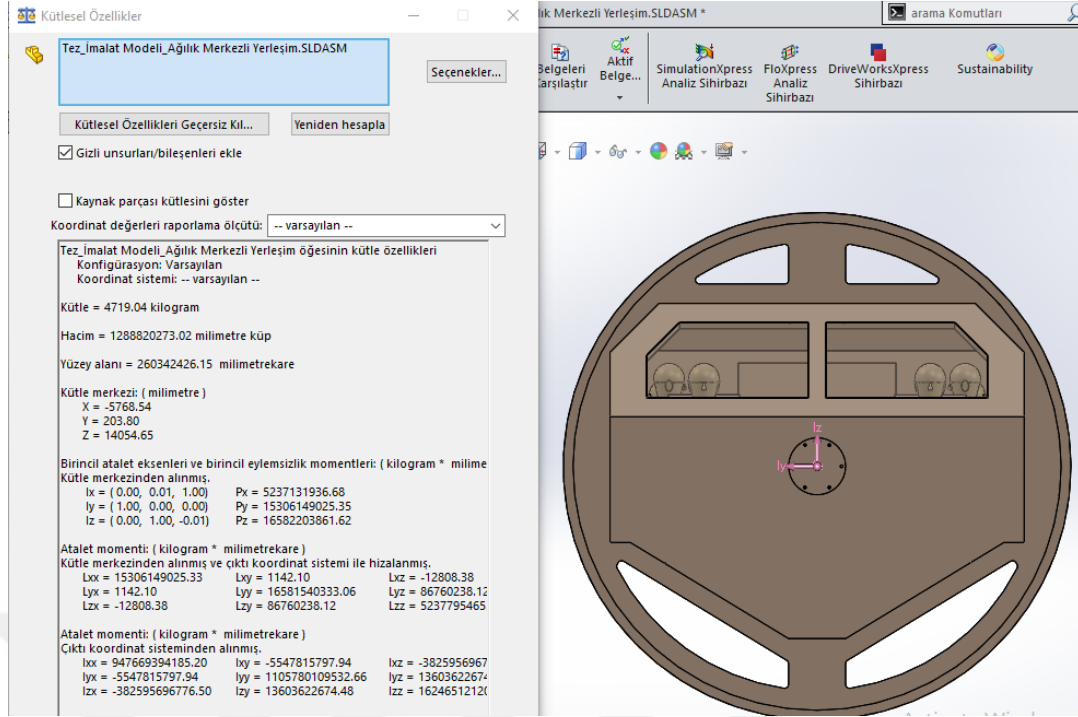
Figure 26 Mass Properties for Full Load Case

Third Case: Asymmetric Load

$d_1 = 3014mm/2 = 1.507\ m$

Distance between center of the mass of the simulator cabin and rotation axis under no-load condition is: $\sqrt{(79,34)^2 + (4,65)^2} = 79.48\ mm$

$d_2 = 79.48mm = 0.07948\ m$

$m = 4261.89\ kg$

From Equation 2.2;

$M_T = m\ x\ d_1\ x\ C_r + m\ x\ d_2$

$M_T = 4261.89\ kg\ x\ (1.507m\ x\ 0.27 + 0.07948m) \approx 2072.85\ kgm$

$V = 6\ rpm$

From Equation 2.1;

$P = 2072.85\ x\ 6\ /\ 0{,}975$

$P \approx 12756W = 12.8KW$

23
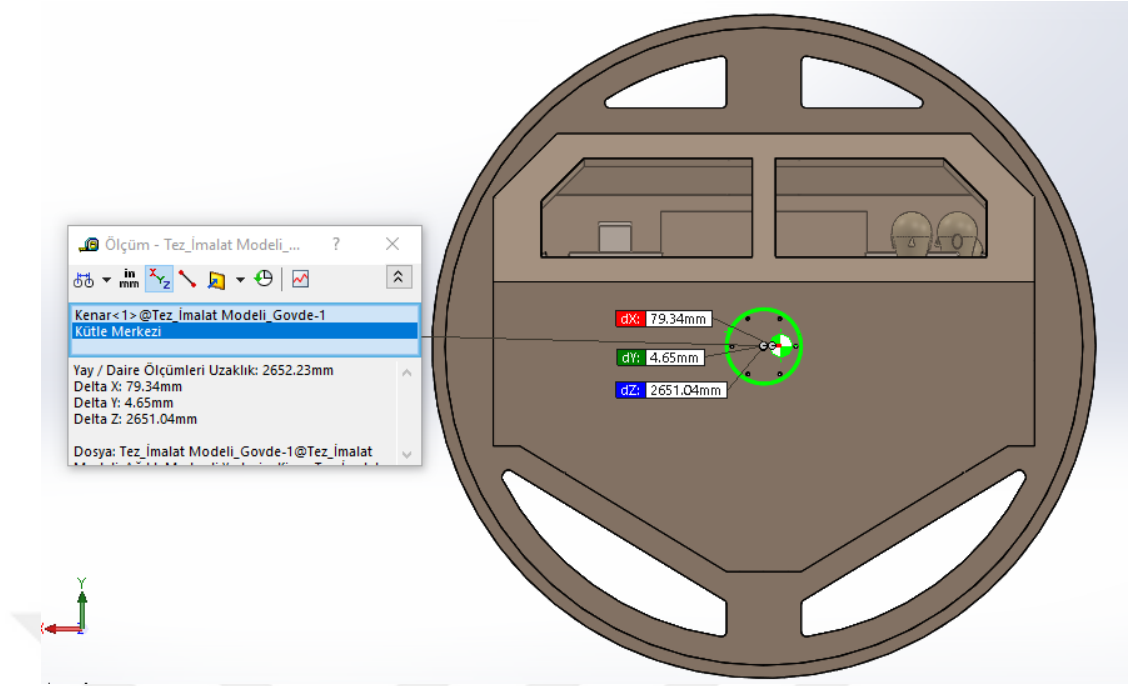
Figure 27 Mass Center for Asymmetric Load Case
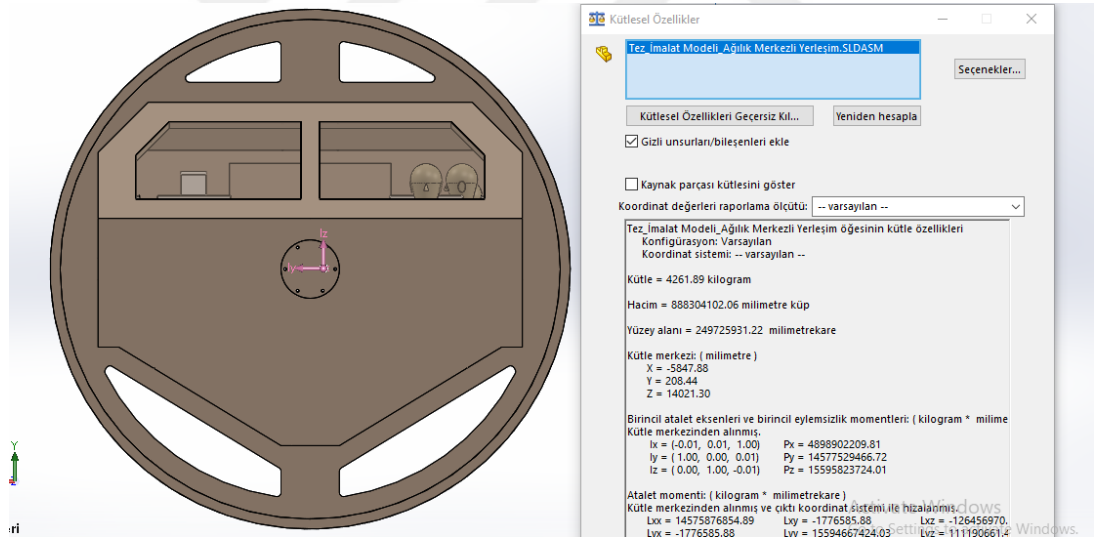
Figure 28 Mass Properties for Asymmetric Load Case

The maximum required power is determined at the third case with the asymmetric load which is 12.8 KW. So in this case the electrical motor should provide the following requirements:

Power: *12.8 KW*

Rotation speed: *6 rpm*

Torque: *20334.5 Nm*

> Lateral Movement Motor Calculations

The lateral movement of the simulator is provided by a pair of coupled, wheel and electric motor. The following calculations are applied to select the electrical motor.
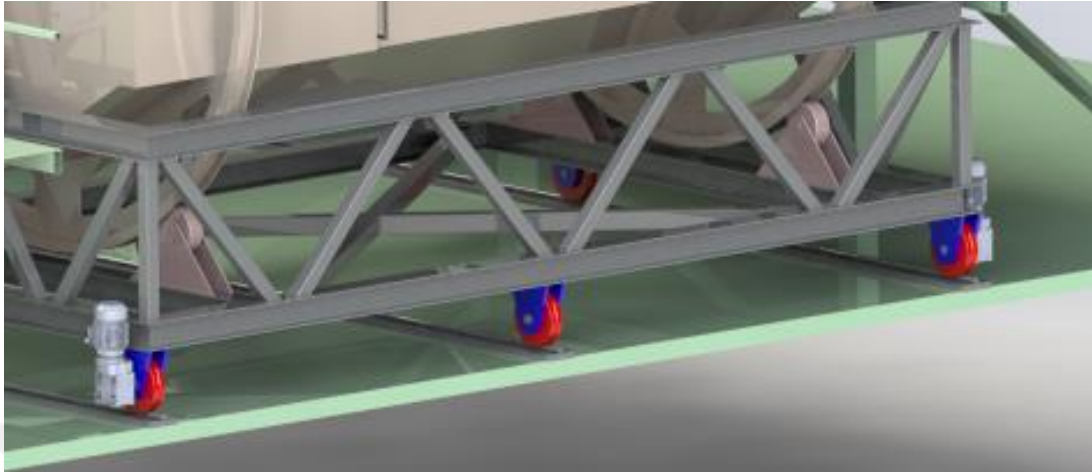
Figure 29 Lateral Movement Motor's Placement

Friction Force :

$$F_f = m \; x \; \mu \qquad (2.5)$$

m: the resultant mass of the simulator and load applied (kg)

$$m = m_{total\;personel} + m_{simulator\;cabin} + m_{movable\;platform} + m_{rotation\;motor} \qquad (2.6)$$

m = 76 kg x 12 + 3605 kg + 2296 kg + 725 kg = 7538 kg

There are 6 wheels that move on rails. These wheels create friction and this friction creates a rolling resistance. So the motor should overcome this resistance. The system occurs from steel wheels on rails, so friction factor C_r is taken as 0.27. [32].

$\mu =$ kinematic friction factor between steel and steel $= 0.27$

From Equation 2.5;

$F_f = 7538 \; kg \; x \; 0.27 \; \approx 2035.3 \; kg$

There are two motors coupled wheel use in the simulator so;

m = 2035.3 kg load

$$P = M \; x \; V / \; 0.975 \qquad (2.1)$$

$$w = v \; / \; 2\pi r \qquad (2.7)$$

$$w_{max} = v_{max} \; / \; 2\pi r \qquad (2.8)$$

w_{max}: Angular velocity (rpm)

v_{max}: Maximum lateral speed of the simulator = *0.663 meter/second*

r = radius of the wheel = *150 mm = 0.15 m so;*

From Equation 2.8;

$w_{max} = 0.663 \; (m/s) \; / \; 2 \; x \; 3.1514 \; x \; 0.15m \; = \; 0.7035 \; rps \approx 42 \; rpm$

$$M = m \; x \; d \qquad\qquad (2.4)$$

m: the resultant mass of the simulator and load applied (kg)

d: distance between center of wheel and the surface

From Equation 2.4;

M =2035.3 kg x 0.15 m = 305.3 kgm

V = 42 rpm

From Equation 2.1;

P = 305.3 x 42/ 0,975

P = 13151.4 W = 13.2 KW

So in this case each electrical motor should provide the following requirements:

Power: *6.6 KW*

Rotation speed: *42 rpm*

Torque: *1495.9 Nm*

CHAPTER 3

STATIC STRUCTURAL ANALYSIS

In this chapter, static structural analysis is performed to provide the strength of the material that is used in the simulator to make sure if it is capable to endure the external loads these are applied while the use of the simulator.

Simulator Cabin and Movable Platform which carry the simulator cabin are focused on statical analysis. The 3D design is performed on SolidWorks sketching program, and statical analysis is also performed by the static structural tool of the same program.

3.1 Simulator Cabin Analysis

3.1.1 Simulator Cabin Model

The simulator cabin is a resultant product of sheet metal plates that are bent and welded to each other. Four types of sheet metals are used which have the same material type with different thicknesses. The thickness values are given in Figures 13, 14, and 16. The steel type is St37-2, and its material properties are given in the following figure:

Figure 30 St-37 Type Steel Material Properties
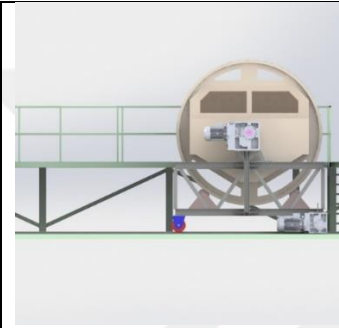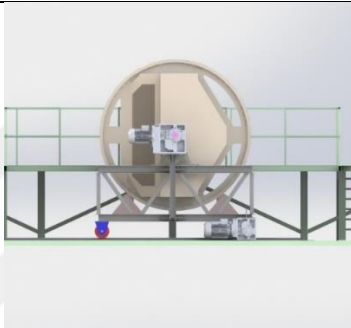
For the FEM solution method, the model is simplified by removing the doors because they do not carry any external load. For the representation of the doors, their

masses are applied to the model as external load. Details are given in the Loads Section.

3.1.2 Loads

The simulator cabin is the place where trainees sit and tie themselves. The design of the cabin is symmetrical from the half-section plane of the short side of the simulator so it has a symmetrical loading case but it also rotates so the loading case changes with time. An approximation is taken place for load cases. The static analyses repeated for three different positions of the simulator. These are;

Table 2 Simulator Cabin Static Analysis' Cases

| 0º Case | 90º Case | 180º Case |

One of the external loads that applied to the cabin is the mass of the chairs. On the other hand, the chairs that are located in the cabin are stock parts so it is not necessary to design and include for the simulator. Instead of this approach, the masses of the sittings are applied to certain places that they are located. So total external forces applied to the simulator model are:

$$M_{individual\ place} = (M_{trainee} + M_{sitting}) \tag{3.1}$$

$$M_{individual\ place} = (76\ kg + 22\ kg) = 98\ kg$$

$$M_{total} = (M_{trainee} + M_{sitting}) \times Number\ of\ the\ trainee \tag{3.2}$$

$$M_{total} = 98\ kg \times 12 = 1176\ kg$$

But only these masses do not represent enough load cases acting on the structure. According to the F.E.M 1.001 standard [33], a dynamic coefficient should be applied to the total load. The F.E.M 1.001 standard generally represents the hoist standards but in our case, there is no special standard for simulators so it is logical enough to use this standard in this study. According to standard, the dynamic coefficient must be no less

than 1.15 for the hoist system which withstands the load usually through a rope mechanism which is more unstable than the direct load applied simulator like in this study. So the dynamic load coefficient $C_{dynamic} = 1.15$.

$$L = M \times C_{dynamic} \tag{3.3}$$

$$L_{individual\ place} = M_{individual\ place} \times C_{dynamic} \tag{3.4}$$

$$L_{individual\ place} = (78\ kg + 19.5\ kg) \times 1.15 = 112.1\ kg \approx 1100\ N$$

$$L_{total} = M_{total} \times C_{dynamic} \times Number\ of\ Trainee \tag{3.5}$$

$$L_{total} = 112.1\ kg \times 12 = 1345.2\ kg \approx 13196.4\ N$$

So 1100 N external load added to 12 places as in the following figure.
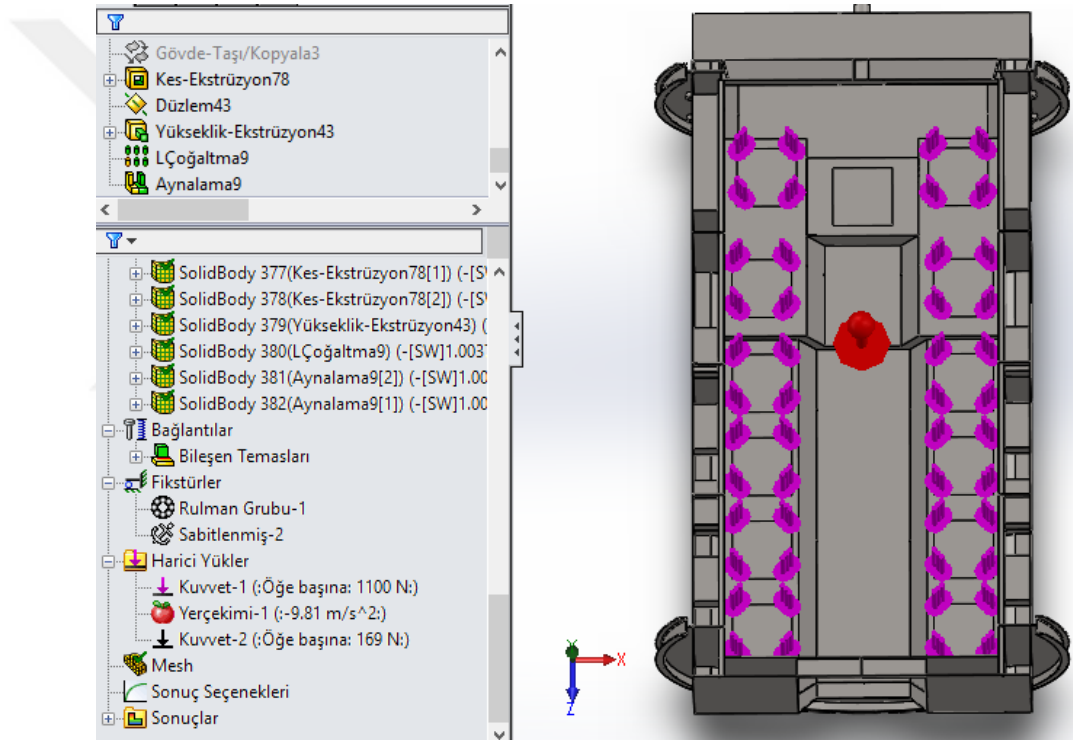
Figure 31 External Loads of Simulator Cabin - 1

To simplify the model, the doors of the simulator are excluded. Instead of the actual model, their masses are added as external loads. The mass of each door which is designed to be manufactured from sheet metal is approximately 30kg. They are integrated into the cabin with two hinges. So the external load is approximately for each hinge is 169 N with dynamic coefficient factor (as 1.15) and applied to the analysis as in the following figure. Also, the red arrow represents the gravitational force.
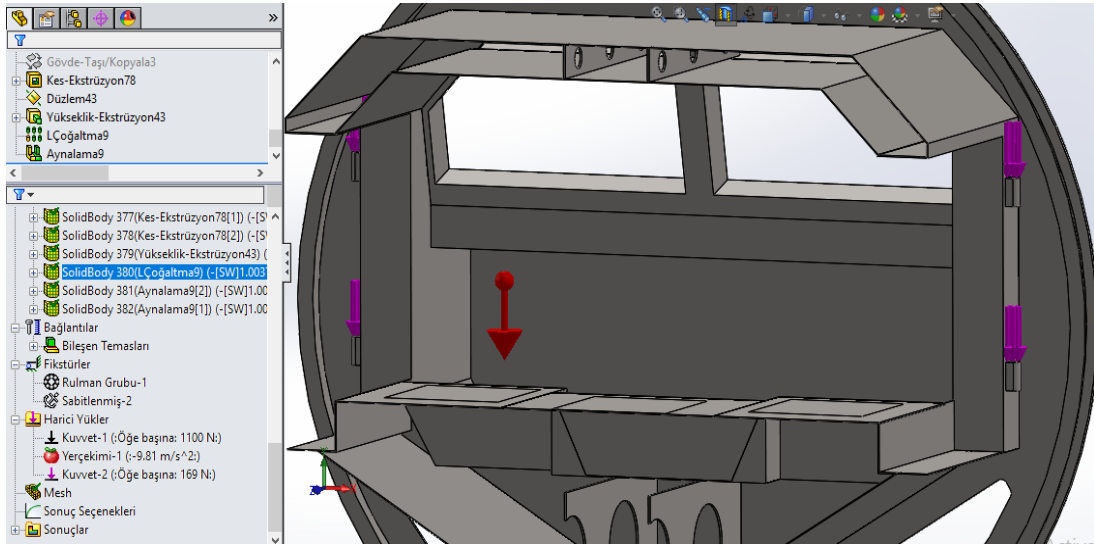
Figure 32 External Loads of Simulator Cabin - 2

3.1.3 Fixed Surfaces

The cabin is supported by four wheels and one bearing housing. For static analysis, they are represented as fixed points (green ones are the wheels, and the blue one is the bearing housing) as in the following figure.
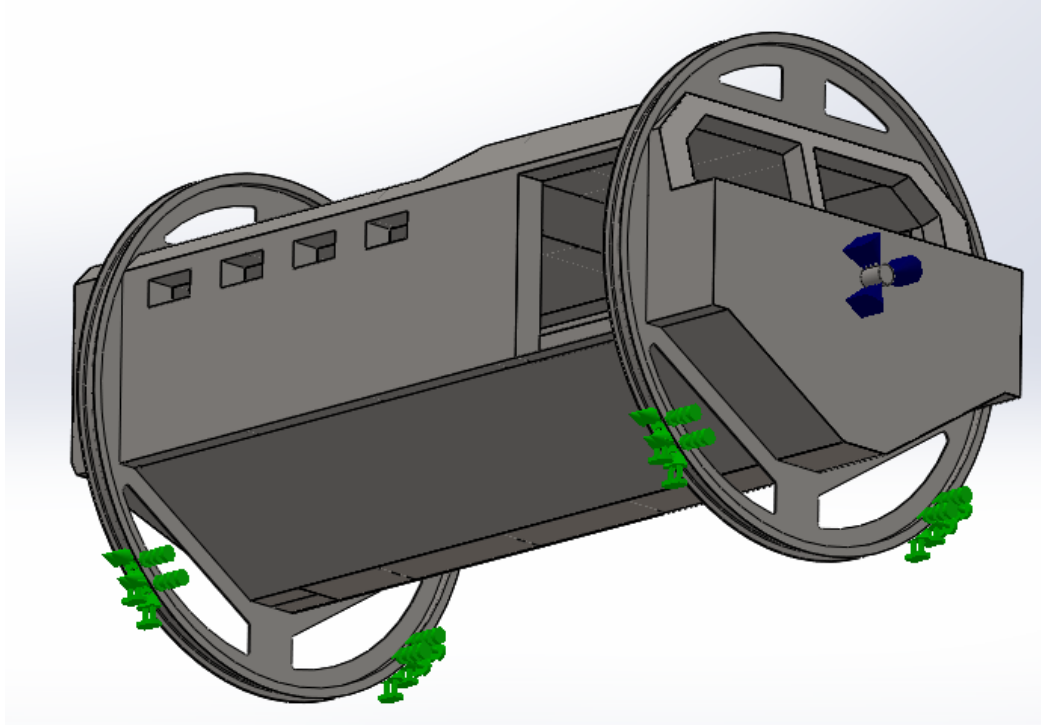
Figure 33 Fixed surfaces of Simulator Cabin

3.1.4 Results

The stress, displacement, and safety factor results are given under this section.

- 0$^\text{o}$ Case Results
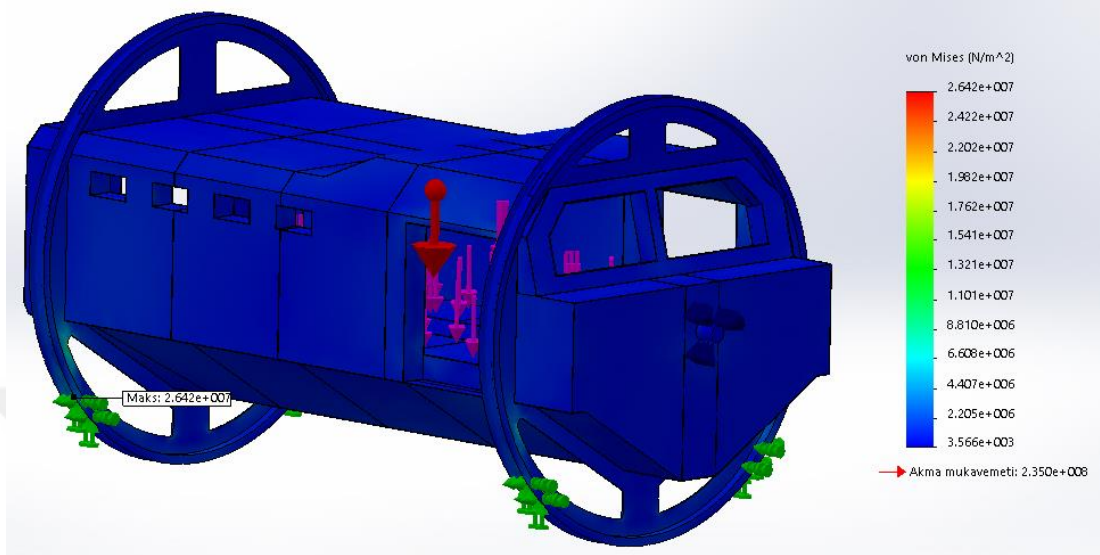
Figure 34 0$^\text{o}$ Case Stress Graph
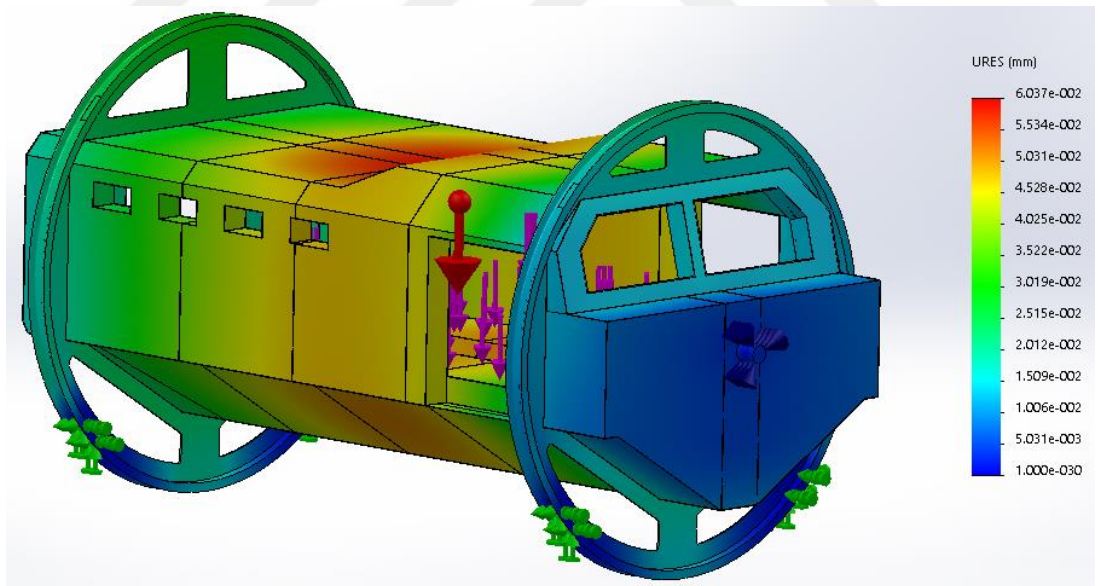
Figure 35 0$^\text{o}$ Case Displacement Graph
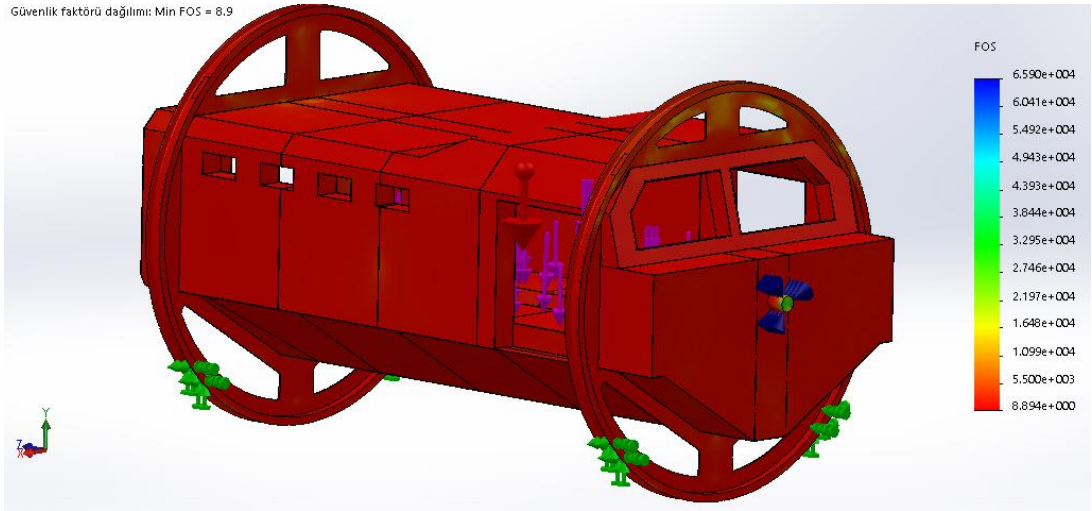
Figure 36 0° Case Safety Factor Graph

- 90° Case Results

Figure 37 90° Case Stress Graph

32
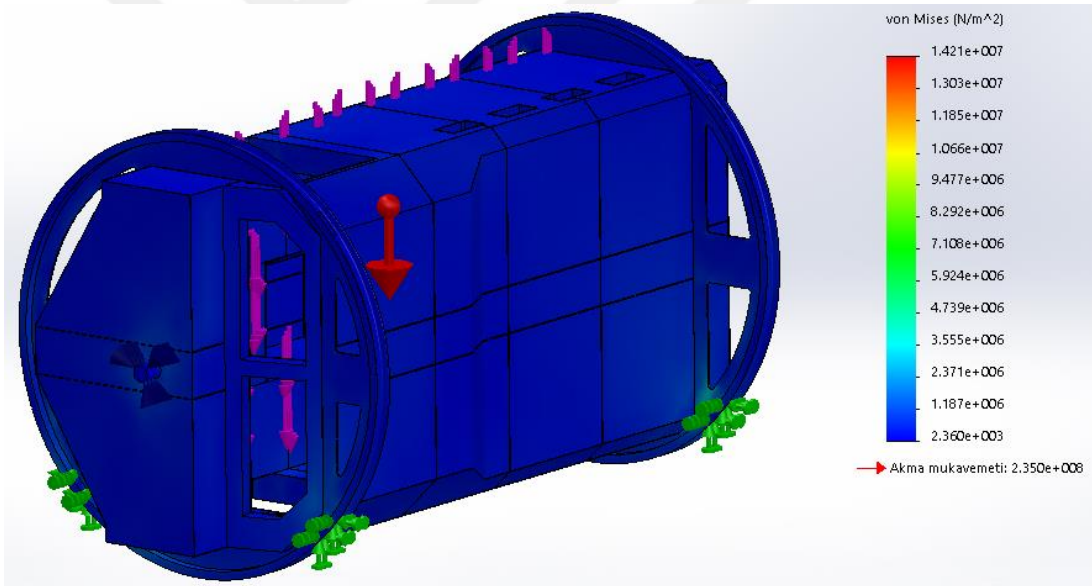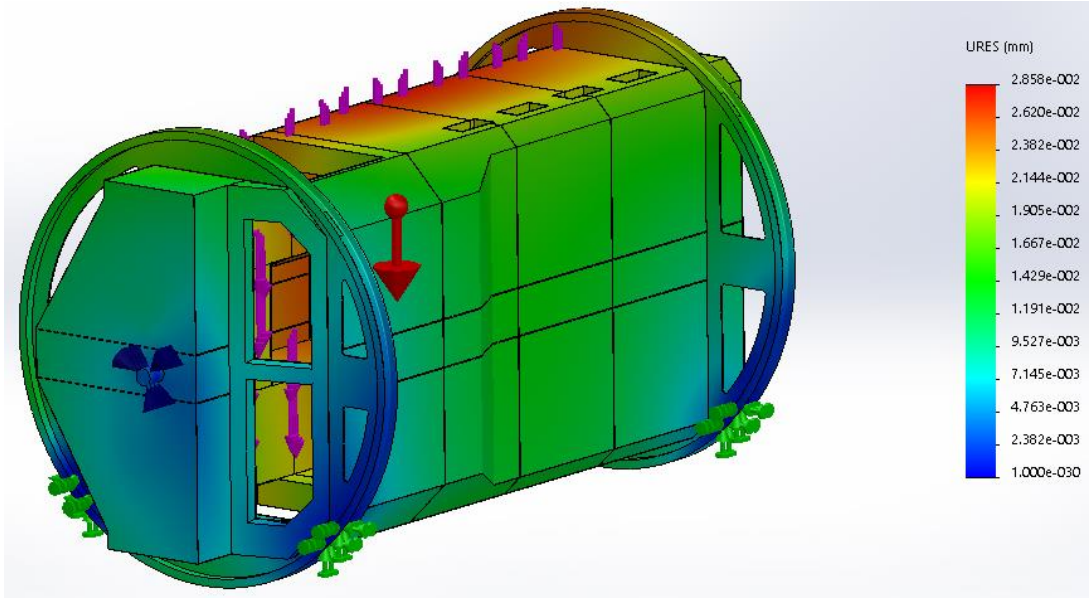
Figure 38 90° Case Displacement Graph
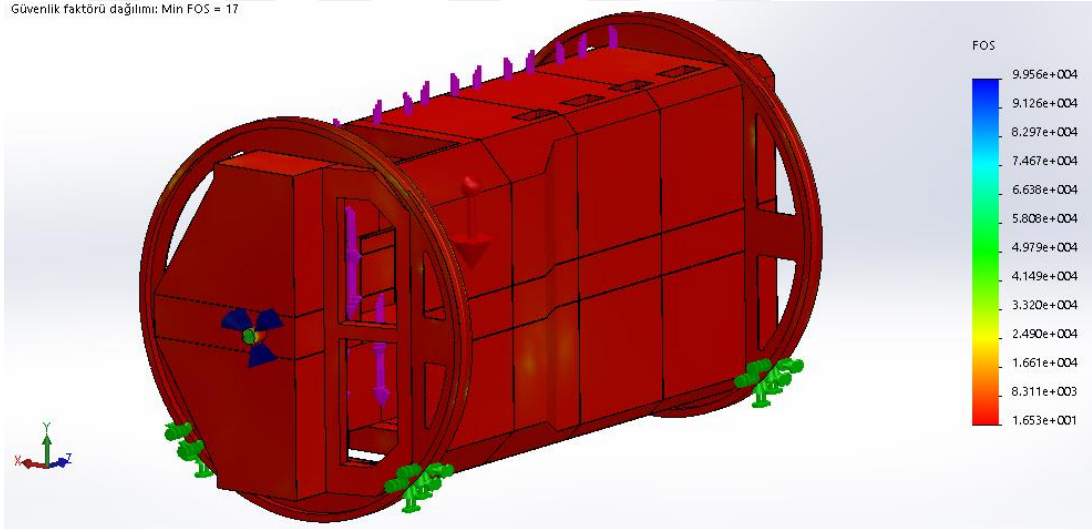
Figure 39 90° Case Safety Factor Graph

- 180° Case Results
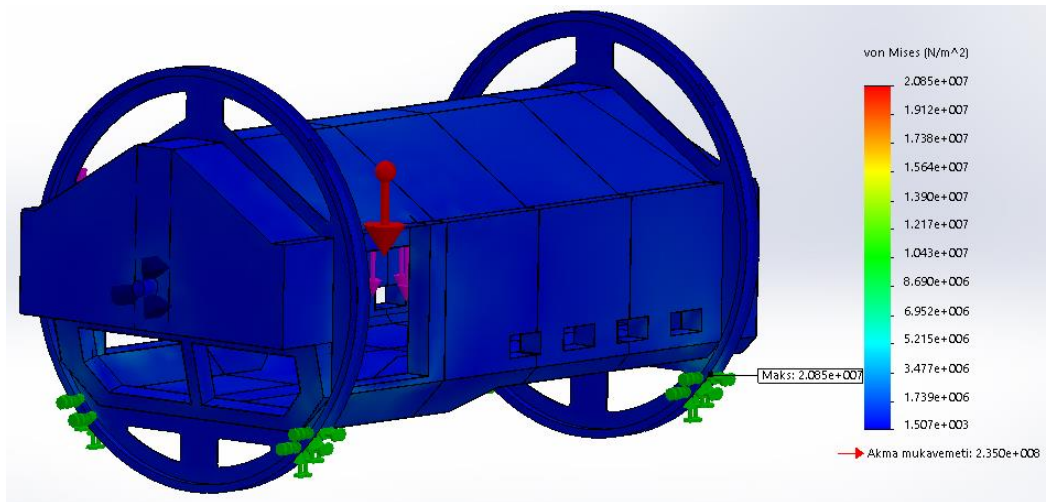
Figure 40 180° Case Stress Graph
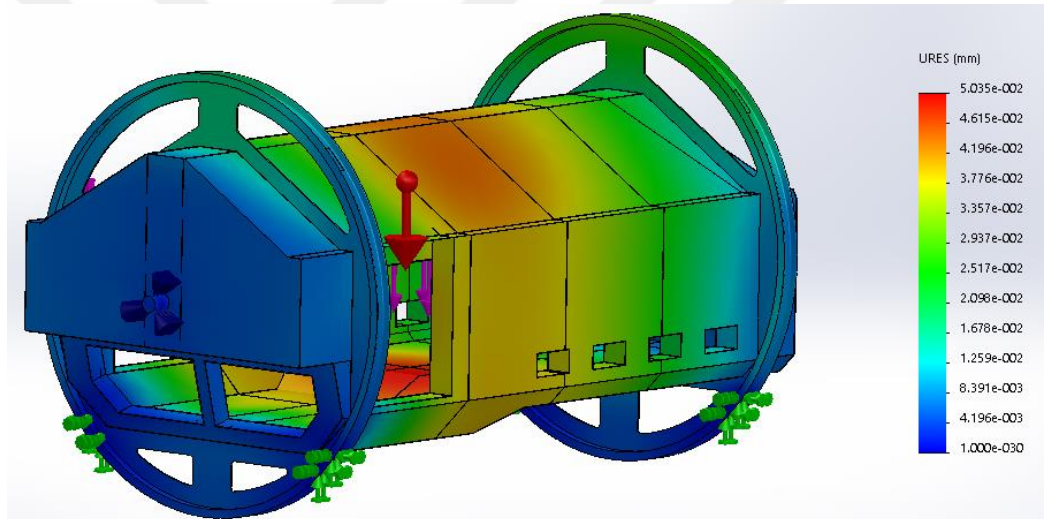
Figure 41 180° Case Displacement Graph
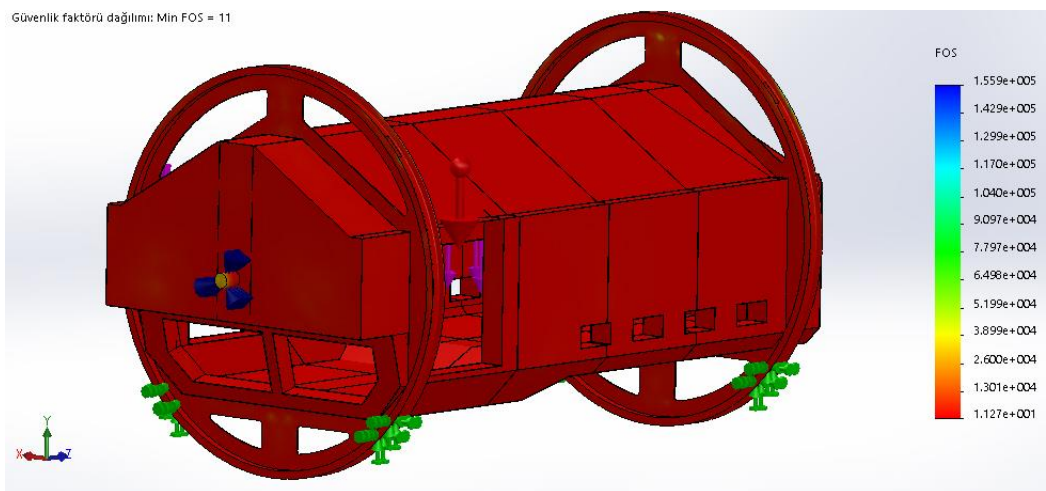
Figure 42 180° Case Safety Factor Graph

3.2 Movable Platform Analysis

3.2.1 Movable Platform Model

The movable platform is a resultant product of steel profiles that are welded and bold connected.

3.2.2 Loads

The movable platform carries the simulator cabin with full load condition and rotation motor. So one of the external load that applied as the mass of the cabin with trainees in it, and the other one applied as the mass of the motor. The mass of the cabin carried by 5 different regions is estimated as they carry the load equally. Four of them are the carrying wheels' construction, and the other one is the rotation motor's bearing housing. The mass of the simulator cabin under full load conditions is given in Figure 26 as 4719.04 kg.

$$L = M \text{ x } C_{dynamic} \qquad (3.3)$$

$$L_{Cabin} = M_{cabin} \text{ x } C_{dynamic} \qquad (3.3)$$

$L_{Cabin} = 4719.04 \, kg \, x \, 1.15 = 5426.9 \, kg \approx 53238 \, N$

For each region: $53238 \, N / 5 = 10648 \, N$
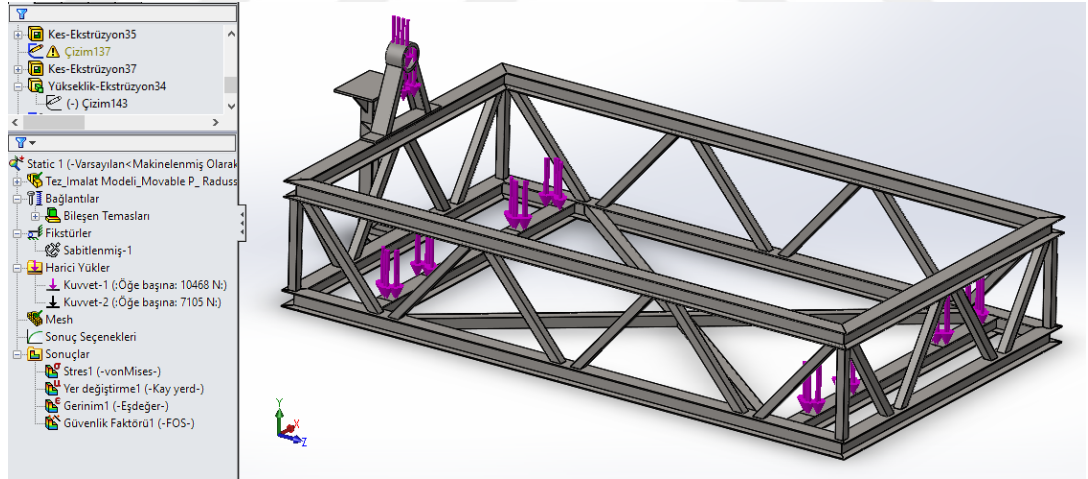
Figure 43 Simulator Cabin Load on Movable Platform

The mass of the motor is 725 kg which approximately equals 7105 N. The motor is stable and fixed so there is no dynamic factor applied on simulation.
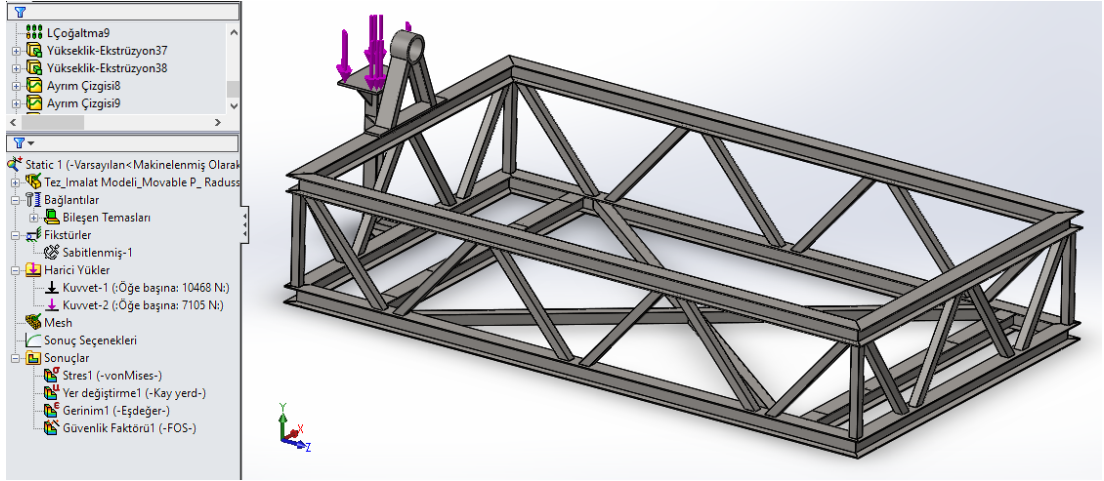
Figure 44 Simulator cabin load on the movable platform

3.2.3 Fixed Surfaces

The platform is supported by six wheels. For static analysis, they are represented as fixed points (green ones are the wheels) in the following figure.
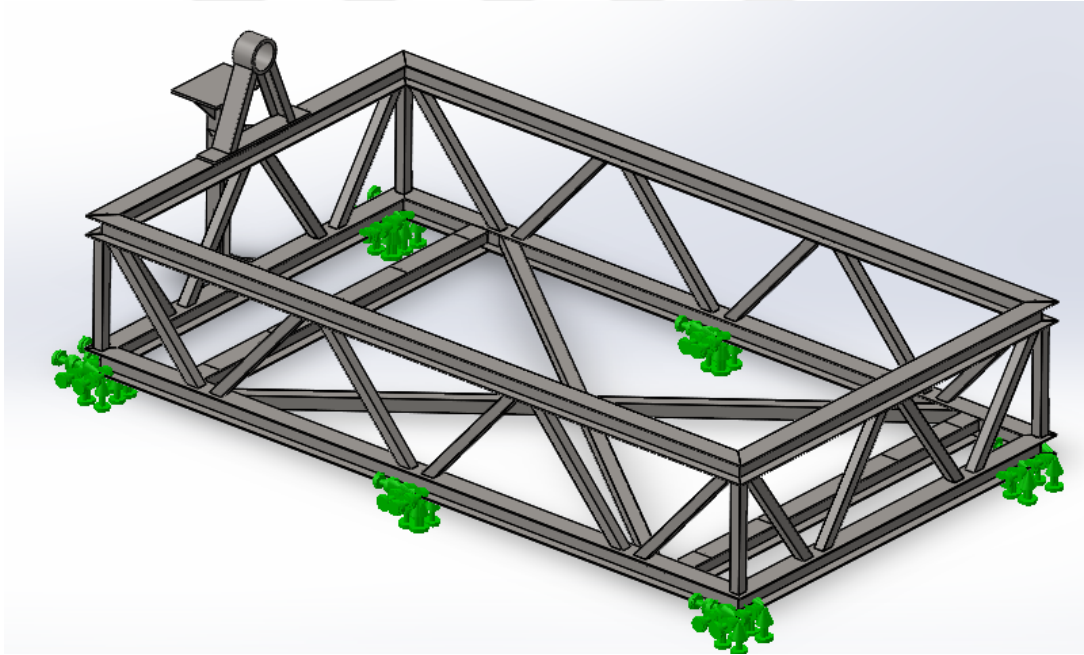
Figure 45 Fixed supports of movable platform

3.2.4 Results

The stress, displacement, and safety factor results are given under this section.
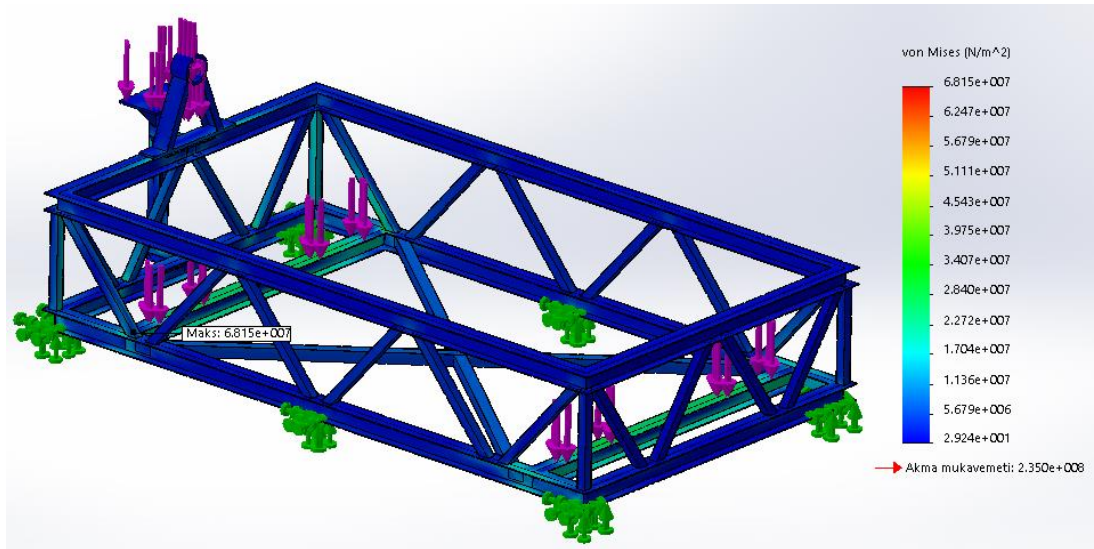
Figure 46 Movable Platform Stress Graph
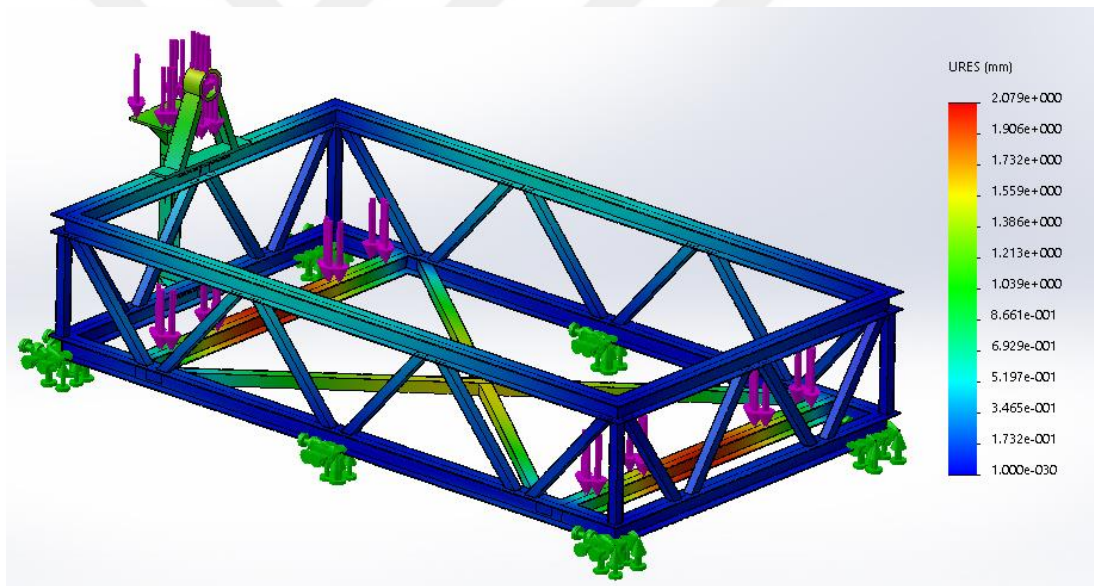
Figure 47 Movable Platform Displacement Graph
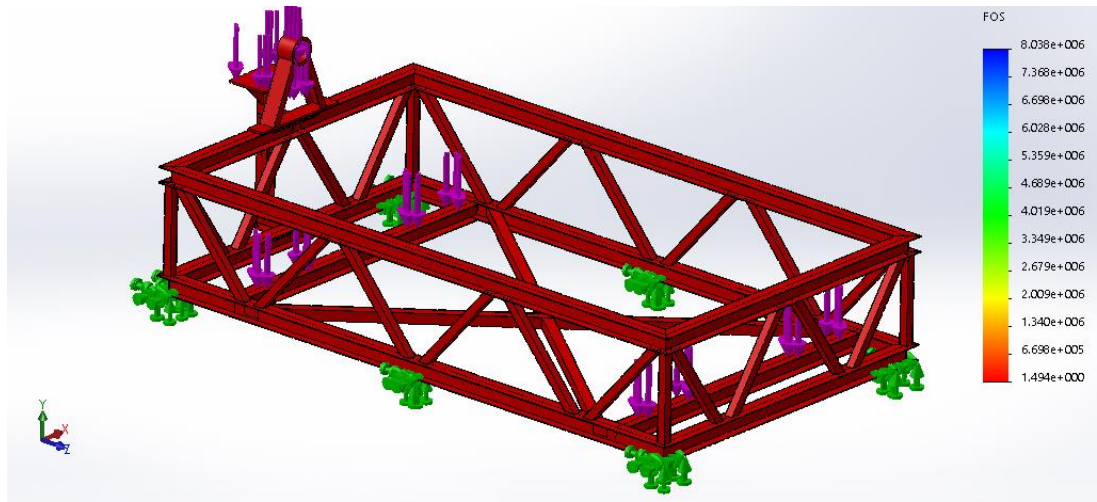
Figure 48 Movable Platform Safety Factor Graph

CHAPTER 4

DYNAMIC SIMULATION

4.1 Dynamic Simulation Methodology

The simulator system is modeled in SolidWorks 3D modeling program and converted into .xml format which is an acceptable format for the MATLAB Simulink environment. In that way, the model is transferred to MATLAB.

The purpose of simulating the system in MATLAB Simulink is to determine the limit velocity and acceleration values according to the human model inside the simulator. So the design of the dummy is an important issue.

4.1.1 Human Model

Using a dummy instead of an actual human is a common way for testing devices or certain activities, safely. These tests began before the computer-based simulation technologies and still continues. So since the beginning of this kind of tests, researchers have tried to replicate the most similar anthropomorphic test devices which drive human body behavior for actual tests. In the early years, the researcher mostly used devices that have non-active joints because they were using actual cadavers. But this was an inefficient and unsustainable way. So in recent years more efficient dummies with active joints developed. These types of joints include damping parameters which represent the anatomical proportions and muscular structure of the human body. Chhor, Yun Choi, Lee [34] showed the advantages of active joints over non-active joints in the case of a rollover situation. Similar types of joints are used for developing a biomedical model in the case of impact simulation by T. Silva and A.C. Ambrósio [35] In another study, Hyun et al. used active joints for designing human-friendly robots and tried to determine proper stiffness values in case of different sized collisions. So active joints that have internal stiffness and dumping force are also used in this study.

Active Joint resistance represents the muscles' behavior and prevents the unacceptable positions of the model. [36]. For this representation two physical internal resistance

models - a viscous torsional damper and a non-linear torsional spring- are applied to the joint. The representation of the torsional damper and torsional spring represented by the properties of stiffness coefficient and damping factor of the revolute joint in Simulink. These values and details of the Simulink model are given in Section 4.2.
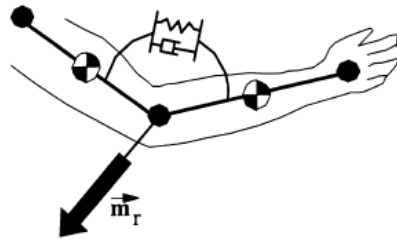
Figure 49 Representation of Active Joint [36]

In the case of rollover accidents, the most important injuries occur on the neck area - unless lack of head and vehicle roof contact- because it can cause permanent disability. According to [37] Funk, Cormier, and Manoogian's study focus on the comparison of risk factors for cervical spine, head, serious and fatal injury in rollover crashes. The most common injury type is fatal head injury, and the second one is the fatal cervical spine injury. Even though, we have to remember that the data used in their study, were obtained from the National Automotive Sampling System- Crashworthiness Data System (NASS-CDS), which contains a large population of police-reported crashes. So in an actual rollover accident, the integrity of the vehicle disappears, and the victims do not have any protective stuff, sometimes not even the seat belts. But in this study, a simulator that simulates the rollover accident is designed so the integrity of the simulator does not disappear, and the trainees always wear protective clothes and seat belts. Consequently, under these conditions, cervical spine injuries are the most possible and risky issue for our case, and the limiting joint is determined as the human neck joint.

In a real human neck, there are seven spine parts, but for this simulation model, it is simplified to one revolute joint with its own angular limits and resistance. On the other hand, the other joints of the rest of the body are considered as fixed joints because they do not affect neck injury, like Arienti and Cantoni [38] did in their publication called Lightweight Seat Design and Crash Simulations. In Yang Wang 's thesis [39] single joint representation is also used just like M. Simoneau et al.'s [40] study.

For the body mass properties of the human model, the study of Yoganandan et, al. [41] is used. This study is a compilation of some studies about the human body, and it gives some average values about the masses of the total body weight and a head weight of the human body. So based on these average values and the 3D human model, the total mass of the human model is considered 76 kg, and the head mass is considered as 4.5 kg.

According to the simulation that is going to run the velocity and acceleration values for the neck of the human model are going to be determined but they are meaningless without the answer to this question: May these values cause injury? To answer this question, researchers developed some equations called injury criteria corresponding to experimental results, especially, from the know-how gotten from car crash tests. In this study, two of them are used.

Neck Injury Criterion – 1 (NIC1):

Based on the National Highway Traffic Safety Administration's (NHTSA) regulations Ford Motor Company and General Motors designed some test setups which are usually performed on pigs, in the 1980s, and by these test results, a criterion is developed as follows: [42]

$$NIC1 = \frac{F_z}{F_{int}} + \frac{M_z}{M_{int}} \qquad (4.1)$$

F_z is the axial load and F_{int} is the critical intercept load on the neck. M_z is the bending moment, and M_{int} is the critical bending moment on the neck. The critical force and moment values are given in the following table which is taken from Kleinberg, Sun, and Eppinger's study [42]. These values are determined from the experimental results which are performed by Hybrid III type dummies.

Table 3 Experimental Force and Torque Results [42]

Dummy Type	Tension (N)	Compression (N)	Flexion (Nm)	Extension (Nm)
Crabi 12 month old	2200	2200	85	25
Hybrid III 3 year old	2500	2500	100	30
Hybrid III 6 year old	2900	2900	125	40
Hybrid III small female	3200	3200	210	60
Hybrid III mid-sized male	3600	3600	410	125

Neck Injury Criterion – 2 (NIC2):

The following criterion is developed according to experiments firstly performed on pigs before humans. [43]

$$NIC2 = a_{rel} \; x \; 0.2 + v_{rel}^2 \qquad (4.2)$$

where a_{rel} and v_{rel} are the horizontal velocity and acceleration difference between the T1 (bottom) and C1 (top) of the cervical spine. Constant multiplication number 0.2 represents the neck length of the pigs which also can represent the length of the human neck.

The result of NIC2 should be less than 15 m²/s². On the other hand, this criterion is a generalized equation, and its effects can be changed from person to person. For example, Herring and others performed [44] some crash tests on some volunteers, and one of them had minor injury and neck pain up to 10 days even the NIC was 11.8 m²/s².

4.2 Simulation Components and Inputs
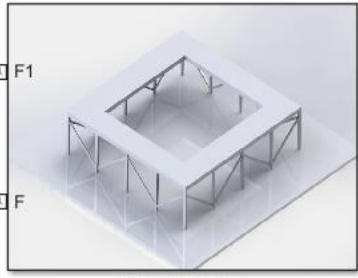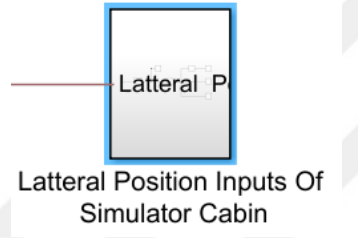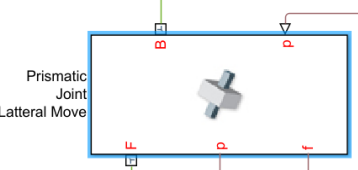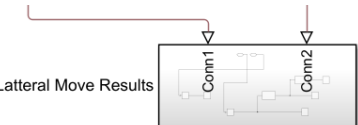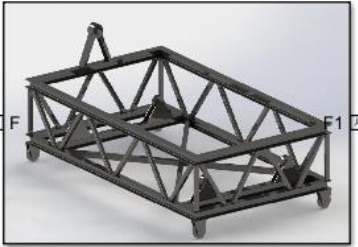
A Simulink diagram was created for simulation. It's a complicated model so given section by section in the following figures and tables.
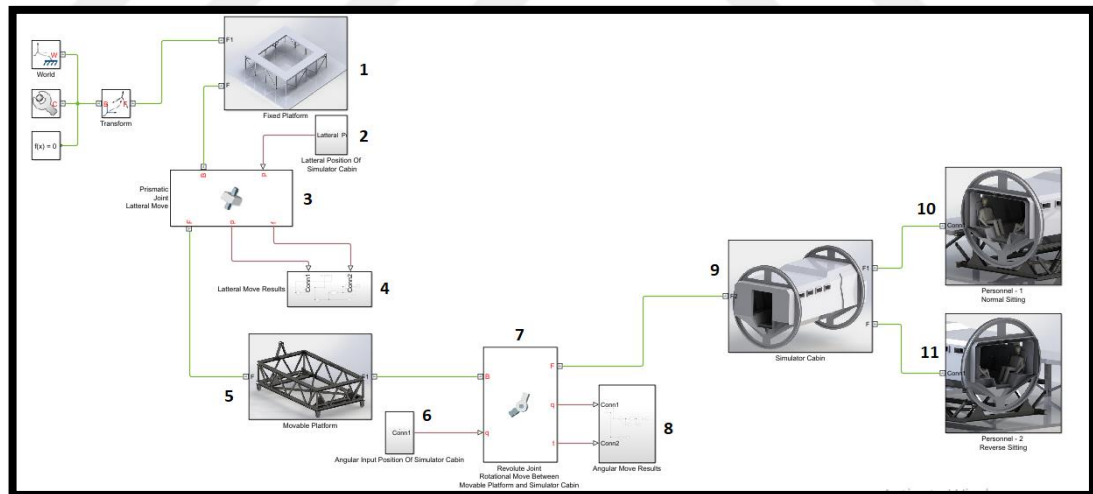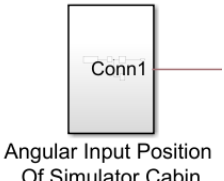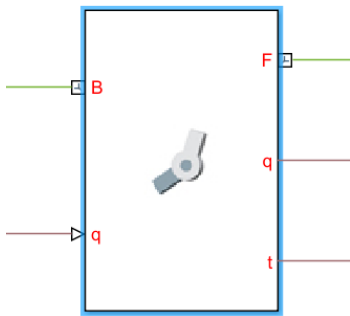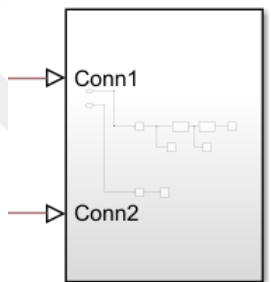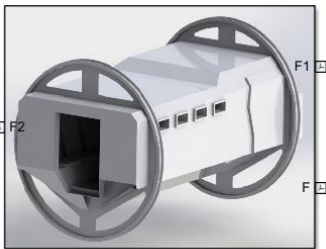
Figure 50 General Model of Simulink Model
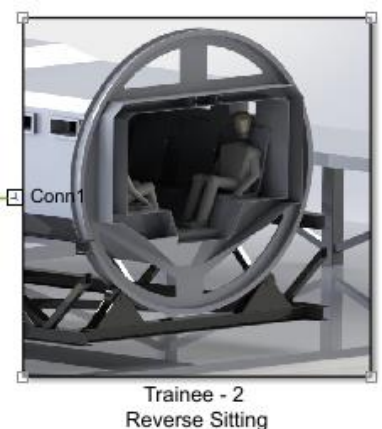
There are 11 subcomponents created for the model in the main section. Details are given in the following sections.

Table 4 MATLAB Simulink Components used in Simulation Diagram

#	Symbol	Component Name	Function
1	 Fixed Platform	Fixed Platform	Represents the fixed platform of the simulator. It is connected to world frame and prismatic joint between fixed platform and movable platform.
2	 Latteral Position Inputs Of Simulator Cabin	Lateral Position Inputs Of Simulator	Lateral position of simulator provided by the position input of the prismatic joint.
3	 Prismatic Joint Lateral Move	Prismatic Joint for Lateral Movement	Lateral position of simulator provided by the prismatic joint.
4	 Latteral Move Results	Lateral Position Results Of Simulator	Lateral position results of simulator given under this component. Details are given under results section.
5	 Movable Platform	Movable Platform	Represents the movable platform of the simulator. It is connected to fixed platform and revolute joint between movable platform and simulator cabin.

6	Conn1 Angular Input Position Of Simulator Cabin	Angular Position Inputs Of Simulator	Angular position of simulator provided by the position input of the revolute joint.
7	F B q q t Revolute Joint Rotational Move Between Movable Platform and Simulator Cabin	Revolute Joint for Rotational Movement	Angular position of simulator provided by the revolute joint.
8	Conn1 Conn2 Rotational Move Results	Angular Position Results Of Simulator	Angular position results of simulator given under this component. Details are given under results section.
9	F1 F2 F Simulator Cabin	Simulator Cabin	Represents the simulator cabin. It is connected to movable platform and Trainees in the simulator.
10	Conn1 Trainee - 1 Normal Sitting	Trainee-1 Normal Sitting	The trainee who sits in the simulator with sitting position through lateral movement. Sub components are given in following figures.

11	Trainee - 2 Reverse Sitting	Trainee-2 Reverse Sitting	The trainee who sits in the simulator with sitting position through reverse of lateral movement. Sub components are given in following figures.

The human model, its seat belt design, and Neck Injury criteria are given in the following diagram. The components of normal sitting and reverse sitting trainees are the same, so only the details of the normal sitting trainee are given in the following figures.
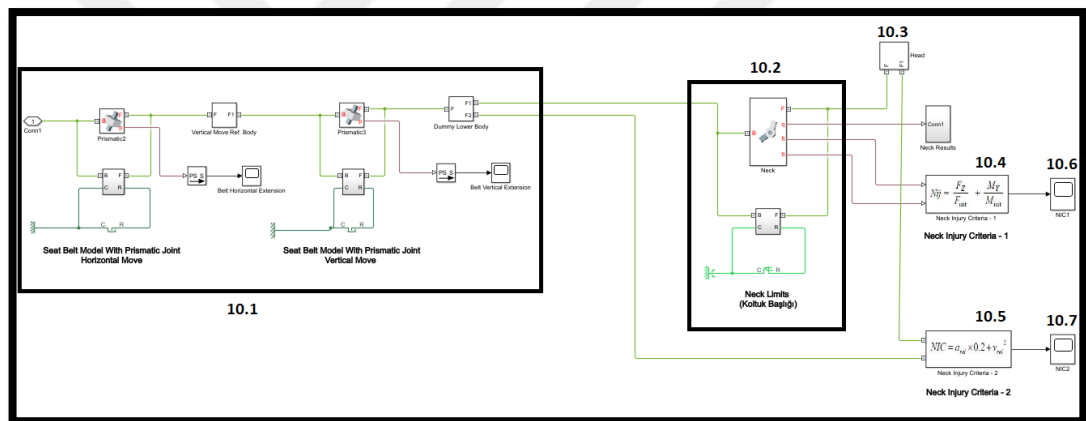
Figure 51 Human model with NIC
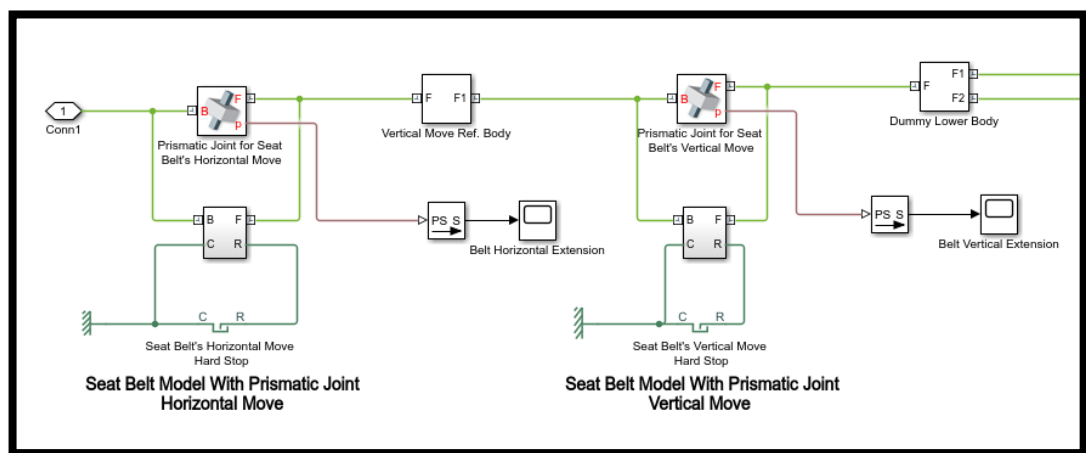
Figure 52 10.1 Seat Belt Model

The seat belt is modeled by two proportional prismatic joints between the dummy's lower body and the simulator's seat. One prismatic joint represents the horizontal movement, and the other one represents the vertical movement with 30mm ranges. At the 30mm limit, hard stops are added just like real seat belts which lock themselves in case of emergency. The representation of seat belt was similar in "Seat belt control: from modeling to experiment" book [45] which takes spring stiffness as 124 kN/m and damping coefficient as 100 N/m and the same values used both for prismatic joints and their hard stops, in this study.
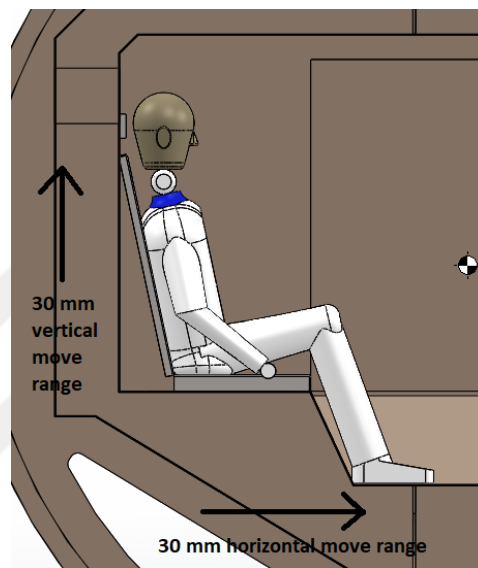
Figure 53 Seat Belt's Working Ranges

The body of the human is connected to the head by a revolute joint which is mentioned at the beginning of the chapter.
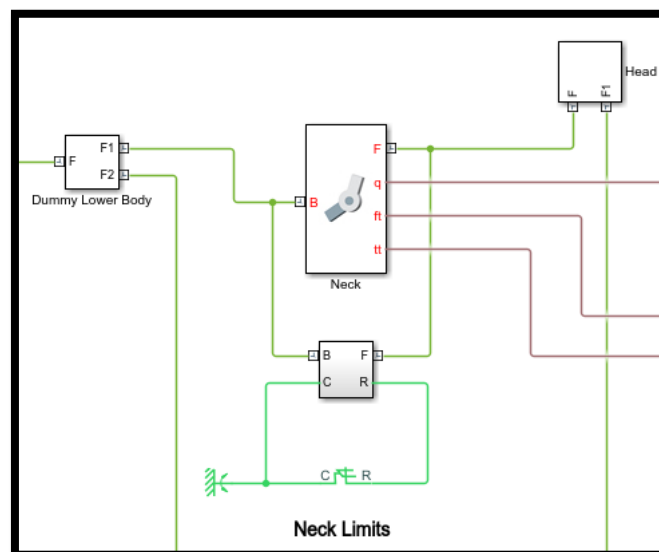
Figure 54 10.2 Neck Model

To represent the active joint, torsion spring's stiffness and torsional damping coefficients must be placed into the input variables of the revolute joint. The stiffness and damping values change person to person or relaxed and tensioned position of the neck. There are many different studies on these values. For example, in M. Simoneau et al.'s [40] study on neck stiffness and viscosity values, the neck stiffness values vary from 14 Nm/rad to 22 Nm/rad and the damping factor varies from 1.8 to 2.4 Nm-s/rad. In Yang Wang 's thesis [39] which is about the neck responses against whole-body vibration, the stiffness and damping coefficient values vary based on the number and type of joints which represent the neck. For example, a single degree of freedom passive joint's (non-muscle activated) stiffness is 9.14 Nm/rad and the damping factor is 0.36 Nm-s/rad. On the other hand, for two degrees of freedom muscle-based joints, stiffness values are k_1=65.81 Nm/rad and k_2=37.05 Nm/rad, and damping factors are c_1=2.30 Nm-s/rad and c_2=0.09 Nm-s/rad. Grewal, Paver, and Khatua's study [46] the neck stiffness and damping coefficient for a single DoF joint are determined as 234.9 Nm/rad and 10.88 Nm-s/rad. So the previous studies prove that there is a large range on this topic but when the literature checked more deeply a study was found which is named "An optimization approach for modeling the cervical spine as a single-joint system." [47]   For the selection of these values, knowledge of this paper is used. Portero et al get experimental results from their setup given in Figure 55 which is designed for determining the stiffness and damping coefficient values.
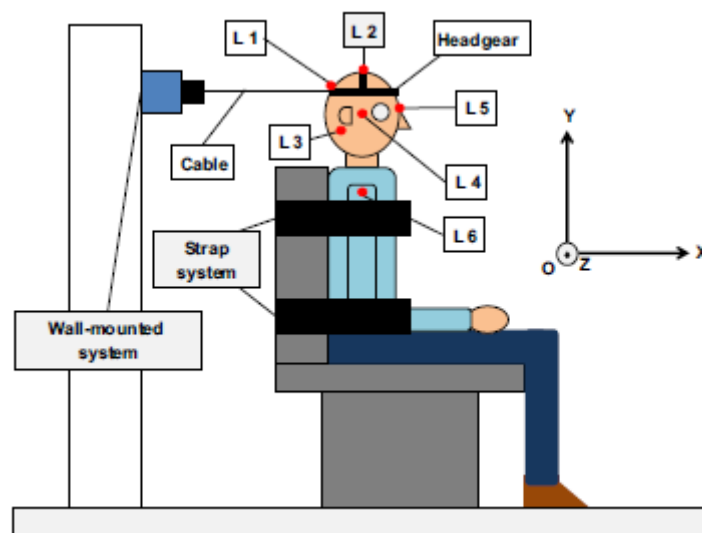
Figure 55 Portero et al's Experiment Setup [47]

The experimental results developed a relationship between torque applied on the neck

and musculotendinous stiffness which are given in the following figure.
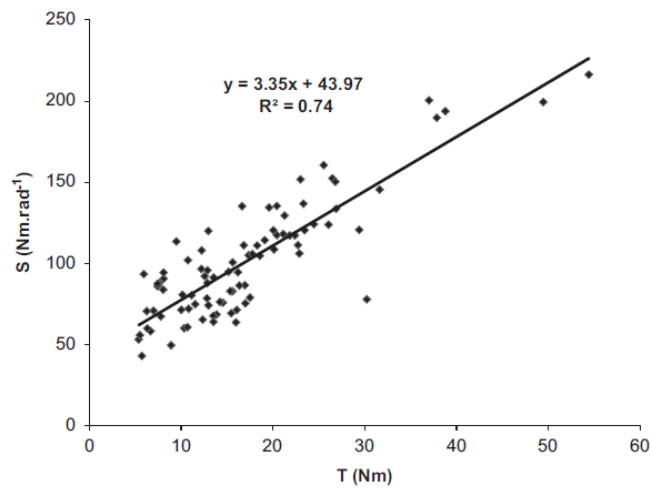
Figure 56 The relationship between Torque and Neck Stiffness [47]

To determine the torque on the neck, acceleration of the neck needs to be determined. The acceleration of the simulator cabin is known so the acceleration of the head can be determined by planar kinematic calculations.

4.2.1 Planar Kinematics

The traditional style rollover simulation systems perform only rotation movement training, but our improved one can perform lateral move additionally. Yet, the movement is two-dimensional in both systems. So, the kinematic movement with respect to the ground frame is planar for each trainee inside the vehicle. Block diagrams are given in the following figures.
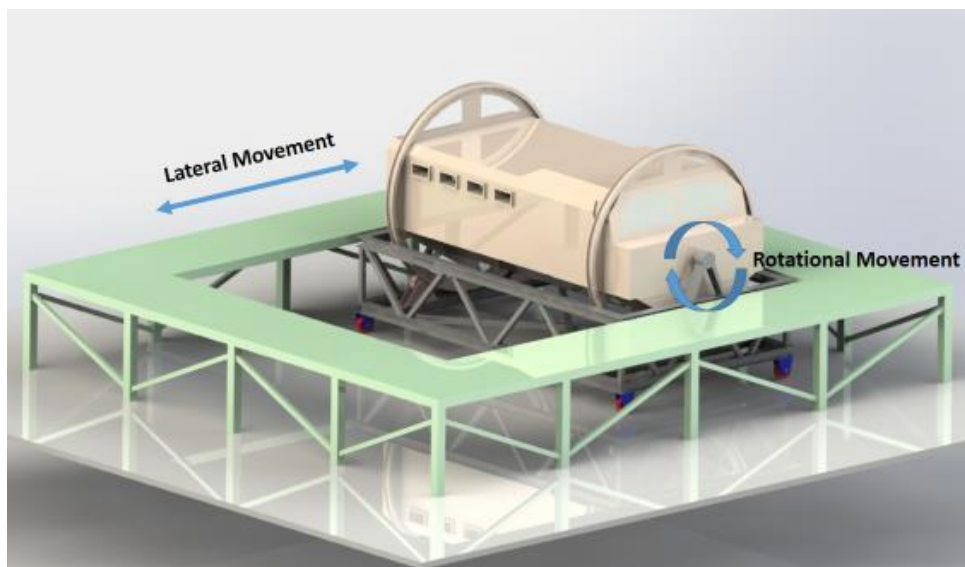
Figure 57 Move Abilities of Simulator

48

$\mathcal{F}_G$ = Ground frame

$\mathcal{F}_o$ = Platform Frame

$\mathcal{F}_S$ = Simulator Cabin - Moving (translating and rotating) frame

$\vec{u}_1^{(o)}$ and $\vec{u}_2^{(o)}$ = Unit vectors of $\mathcal{F}_o$

$\vec{u}_1^{(s)}$ and $\vec{u}_2^{(s)}$ = Unit vectors of $\mathcal{F}_s$

θ = The angle between $\vec{u}_1^{(o)}$ and $\vec{u}_1^{(a)}$

$\vec{r_s}$ = Position vector between O and S

$\vec{r}$ = Position vector between S and P

$\vec{r_p}$ = Position vector between P and G

$\vec{r_l}$ = Position vector between O and P

$\overrightarrow{s_{12}}$ = Distance between the ground frame and platform frame
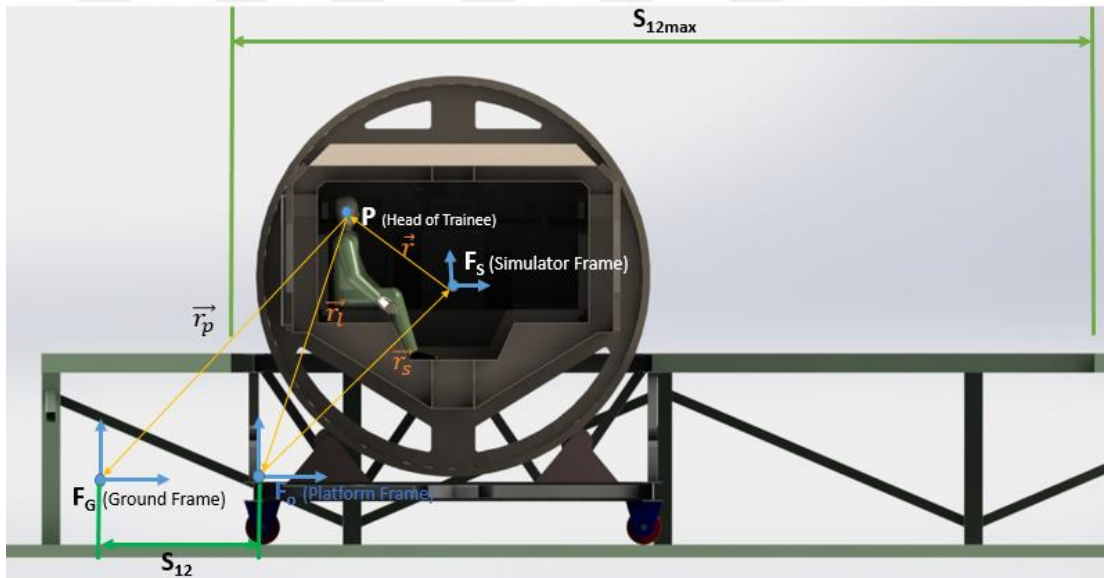
Figure 58 Frames of Simulator

P point represents the head of the personnel who gets the training. Personnel is fixed to the simulator cabin by a seat belt. In this step of the kinematic calculations, the motion of the P point has been neglected for this case but in the second step of the calculations, the motion and the angle difference are determined by the energy method.

$$\vec{r_l} = \vec{r_s} + \vec{r} \text{ according to } \mathcal{F}_o \text{ (Platform Frame)} \quad (4.3)$$

$$\vec{r_p} = \vec{r_s} + \vec{r} + \overrightarrow{s_{12}} \text{ according to } \mathcal{F}_G \text{ (Ground Frame)} \quad (4.4)$$

$$\vec{v_l} = D_o\vec{r_l} = D_o\vec{r_s} + D_o\vec{r}$$

$$\vec{v_l} = D_o\vec{r_l} = D_o\vec{r_s} + D_s\vec{r} + \vec{w} \times \vec{r}$$

$$\vec{v_l} = D_o\vec{r_s} + D_s\vec{r} + \vec{w} \times \vec{r}$$

$D_s\vec{r}$ is the derivative of $\vec{r_s}$ relative to $\mathcal{F}_o$ but in that case S point has no motion (r_s is constant) relative to the moving frame $\mathcal{F}_s$ so $D_o\vec{r_s} = 0$

$D_s\vec{r}$ is the derivative of $\vec{r}$ relative to $\mathcal{F}_s$ but in that case, P point has no motion (r is constant) relative to the moving frame $\mathcal{F}_s$ so $D_s\vec{r} = 0$

$$\vec{v_l} = \vec{w} \times \vec{r} \quad \text{according to } \mathcal{F}_o \text{ (Platform Frame)} \tag{4.5}$$

$$\vec{v_p} = \vec{w} \times \vec{r} + \vec{s_{12}} \quad \text{according to } \mathcal{F}_G \text{ (Ground Frame)} \tag{4.6}$$

$$D_o\vec{v_p} = D_o(\vec{w} \times \vec{r})$$

$$D_o(\vec{w} \times \vec{r}) = \vec{a} \times \vec{r} + \vec{w} \times D_o\vec{r}$$

$$D_o\vec{r} = D_s\vec{r} + \vec{w} \times \vec{r}$$

$$D_s\vec{r} = 0$$

$$D_o\vec{r} = \vec{w} \times \vec{r}$$

$$D_o(\vec{w} \times \vec{r}) = \vec{a} \times \vec{r} + \vec{w} \times (\vec{w} \times \vec{r})$$

$$D_o\vec{v_l} = \vec{a} \times \vec{r} + \vec{w} \times (\vec{w} \times \vec{r})$$

$$\vec{a_l} = \vec{a} \times \vec{r} + \vec{w} \times (\vec{w} \times \vec{r}) \quad \text{according to } \mathcal{F}o \text{ (Platform Frame)} \tag{4.7}$$

$$\vec{a_p} = \vec{a} \times \vec{r} + \vec{w} \times (\vec{w} \times \vec{r}) + \vec{s_{12}} \quad \text{according to } \mathcal{F}_G \text{ (Ground Frame)} \tag{4.8}$$

where, $\vec{\alpha}$ is the angular acceleration of the simulator cabin.

$$\vec{a_p} = \vec{\alpha} \times \vec{r} + \vec{w} \times (\vec{w} \times \vec{r}) + \vec{s_{12}}$$
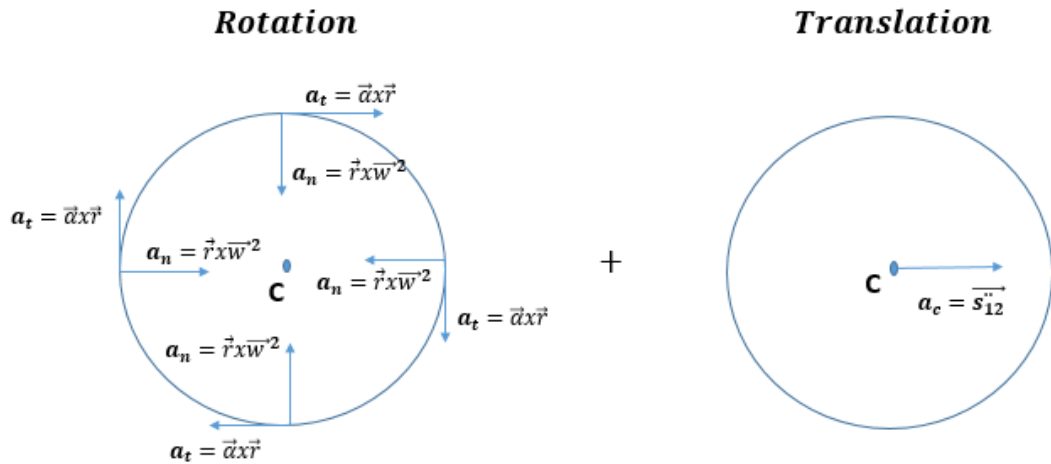
Figure 59 Components of Acceleration

The top position is used as a reference for determining the scalar acceleration value because it has the maximum velocity and acceleration values. It is used for the determination of neck stiffness values. So;
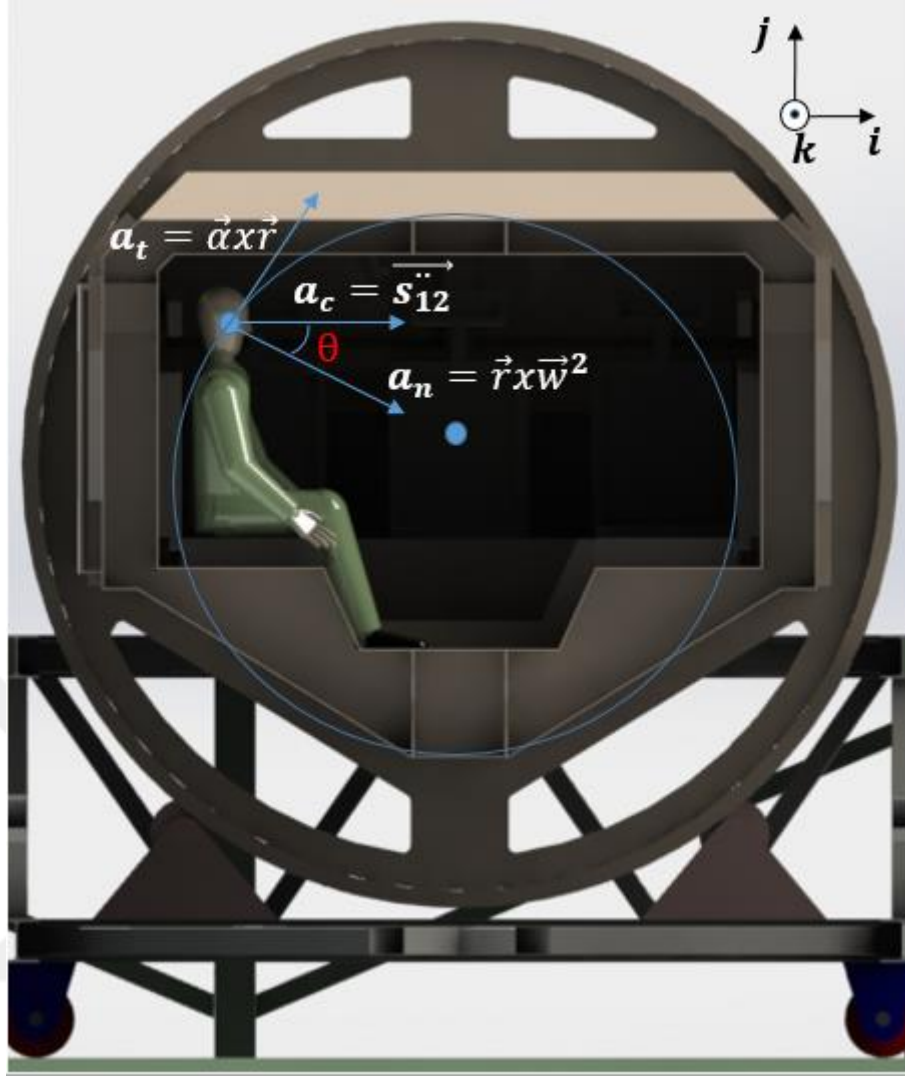
Figure 60 Vectorial Scheme of Acceleration

$$\overrightarrow{a_p} = \vec{\alpha}k \; x \; (\vec{r}sin\theta j + \vec{r}cos\theta i) \; + \vec{w}k \; x \; (\vec{w}k \; x \; (\vec{r}sin\theta j + \vec{r}cos\theta i)) + \overrightarrow{\ddot{s}_{12}}i \quad (4.9)$$

$$\overrightarrow{a_p} = (-\vec{\alpha} \; rsin\theta i + \vec{\alpha} \; \vec{r}cos\theta j) \; + (\vec{w}^2 \; rsin\theta j - \vec{w}^2\vec{r}cos\theta i) + \overrightarrow{\ddot{s}_{12}}i \quad (4.10)$$

$$\overrightarrow{a_p} = (\vec{r}cos\theta \; + \; \vec{w}^2 \; rsin\theta)j - (\vec{\alpha} \; rsin\theta + \vec{w}^2\vec{r}cos\theta - \overrightarrow{\ddot{s}_{12}})i \quad (4.11)$$

4.2.2 Simulation Inputs for Determining Maximum Values

The purpose of this chapter is to determine the limit values of the simulator according to NIC values. These simulations run many times with different velocity and acceleration values. Based on that trials the limiting values nearly reached around 1 second simulation time so the velocity values of 1 second simulation time used in the following calculations.

    a.   Constant Stiffness Case

According to the angular velocity versus time graph given in Figure 61 angular

acceleration of the simulator is;

$$a = 12{,}566 \ \text{rad}/s^2$$
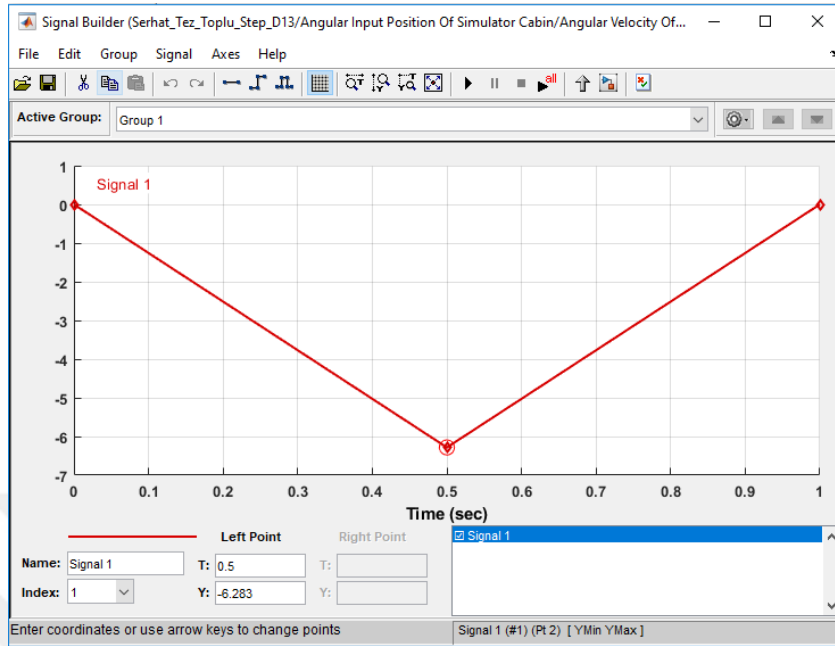
Figure 61 Angular velocity of the Simulator

According to the lateral velocity versus time graph given in Figure 62 linear acceleration of the simulator is;

$$\ddot{s}_{12} = 13{,}26 \ \text{m}/s^2$$
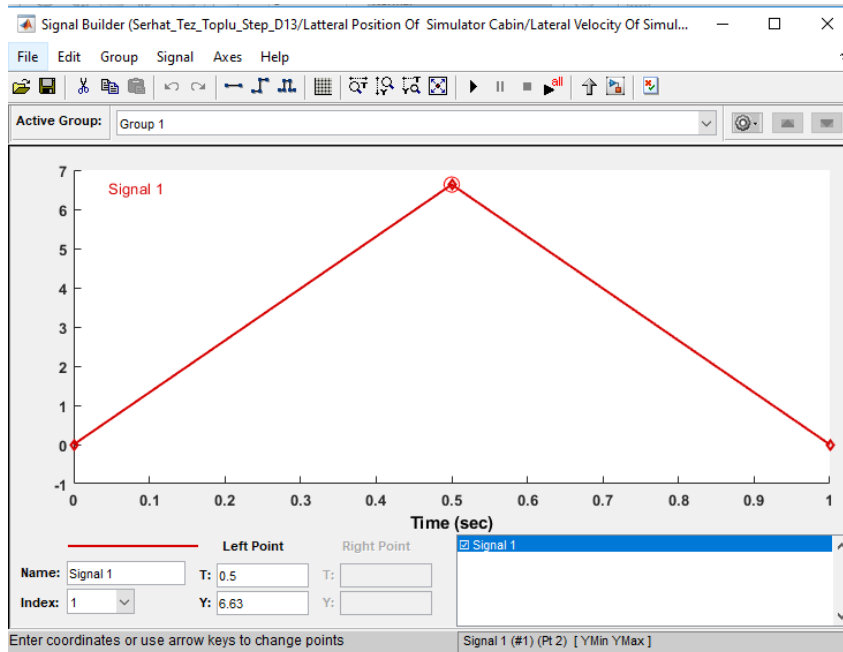
Figure 62 Linear velocity of the Simulator

$$\overrightarrow{a_p} = (\vec{\alpha}\, r cos\theta \ + \ \vec{w}^2\, r sin\theta)j - (\vec{\alpha}\, r sin\theta + \vec{w}^2 \vec{r} cos\theta - \overrightarrow{\ddot{s}_{12}})i \qquad (4.11)$$

52

$r = 1.02$ m (r is shown in Figure 58)

$\theta = 17.10^{\circ}$

$w = 6.283$ rad/s

$a = 12.566$ rad/s^2

$\ddot{s}_{12} = 13.26$ m/s^2

From Equation 4.11;

$$\vec{a_p} = [12{,}566 \text{ rad/s}^2 \ x\ 1.02\ m\ cos(17.10^{\circ})$$
$$+ (6.283 \text{ rad/s})^2\ 1.02\ m\ sin(17.10^{\circ})]\ j$$
$$- [12{,}566 \text{ rad/s}^2\ x\ 1.02\ m\ sin(17.10^{\circ})$$
$$+ (6.283 \text{ rad/s})^2\ 1.02\ m\ cos(17.10^{\circ}) - 13{,}26 \text{ m/s}^2]\ i$$

$$\vec{a_p} = (24.091)j + (28.994)\ i$$

$$\vec{a_p} = 37.7 \text{ m/s}^2$$

$$T = Fr \tag{4.12}$$

$$F = ma \tag{4.13}$$

$$F = 4.5kg\ x\ 37.7\text{m/s}^2 = 169{,}65\ N$$

$$T = Fr = 169{,}65\ N\ x\ 0.151\ m$$

$$T = 25.61\ Nm$$

Stiffness of Neck formulation according to Figure 56;

$$k = 3.35\ x\ T + 43.97$$

$$k = 129.78\ Nm/rad$$

The stiffness of the neck is determined, so the theoretical limiting angle can be calculated by the energy method.

Translation: The kinetic energy equation for a rigid body that has a mass m and translating its particles with the same velocity:

$$T = \frac{1}{2}mv^2 \tag{4.14}$$

Rotation about a fixed-axis: The kinetic energy equation for a rigid body that has a

mass m and rotating about a fixed-axis O:

For an arbitrary point called i:

$$T = \frac{1}{2}m_i v_i{}^2$$

$$v_i = w r_i \tag{4.15}$$

$$T = \frac{1}{2}m_i(wr_i)^2 \tag{4.16}$$

$$I_o = m_i r^2 \tag{4.17}$$

$$T = \frac{1}{2}I_o w^2 \tag{4.18}$$

So for the general plane motion of a rigid body:

$$T = \frac{1}{2}mv^2 + \frac{1}{2}I_o w^2 \tag{4.19}$$

Work done by all forces acting on a body can be expressed as the kinetic energy difference between its two positions which is called the Work energy equation:

$$T_2 = U_{1-2} + T_1 \tag{4.20}$$

For the simulator initial state $T_1 = 0$

The second stage is considered as the half time of the movement where the lateral and angular velocities are maximum.

$$T_2 = U_{1-2} + T_1$$

$$U_{1-2} = \frac{1}{2}mv^2 + \frac{1}{2}I_o w^2 \tag{4.21}$$

For the trainee in the simulator:

$m_{Head} = 4.5\ kg$

$v = 6.63\ m/s$

$w = 6.283\ rad/s$

$I_o = m_i r^2$ $where\ r = 0.151\ m$

$r\ is\ the\ distance\ between\ the\ rotation\ point\ and\ head's\ mass\ center$

$$\Delta E_{Kinetic} + \Delta E_{potatial} + \Delta E_{Elastic} = 0 \tag{4.22}$$

$$\Delta E_{Kinetic} = \frac{1}{2}mv^2 + \frac{1}{2}I_o w^2 \tag{4.23}$$

$$\Delta E_{potatial} = mg\Delta h \tag{4.24}$$

$$\Delta E_{Elastic} = \frac{1}{2}k\theta^2 \tag{4.25}$$

$$\frac{1}{2}k\theta^2 = \frac{1}{2}mv^2 + \frac{1}{2}I_o w^2 + mg\Delta h \qquad (4.26)$$

For maximum reached θ angle;

$$\frac{1}{2}k\theta^2 = \frac{1}{2}(4.5\ kg)(6.63\ m/s)^2 + \frac{1}{2}(0.101\ kgm^2)\left(6.283\frac{rad}{s}\right)^2$$

$$+ (4.5kg)(9.81\ m/s^2)(0 - 1.02m)$$

$$\frac{1}{2}k\theta^2 = 98.90 + 1.99 - 52.97$$

$$\frac{1}{2}k\theta^2 = 47.92$$

$$129.78\left(\frac{Nm}{rad}\right)\theta^2 = 95.84\ kg\ m^2\ rad/s^2$$

$$129.78\left(\frac{Nm}{rad}\right)\theta^2 = 95.84\ Nm\ rad$$

$$\theta = 0.859\ rad = 49.23\ deg$$

So, the theoretical maximum θ angle is 49.23°. Simulation results of the neck angle which are simulated without a headrest are also given in the results section.

According to the stiffness value which is calculated and read from Figure 56 entered as input variable into the neck block diagram. The damping coefficient is proportionally taken from Grawel, Pavel, and Khatua's study as 1.31 Nm/(rad/s). [46] But this is not enough because there is a headrest at the backside of the head so there is a limitation. To determine the limit of the revolute joint, firstly initial sitting position of the dummy was investigated. In Sławiński, Malesa, and Świerczewski's [48] study which focuses on external explosion effects on military vehicle personnel, they determined the proper sitting position of the dummy in an MRAP type vehicle. So their data and figures are used to determine the initial neck angle and the general body position which is given in Figure 63.

Figure 63 Sitting Position of Personnel in MRAP [48]

Secondly, the limiting angle of neck extension is determined as 18° according to the distance between the head and headrest. Thirdly, the limiting angle of the neck flexion was determined. The human neck's range of motion at flexion is approximately 80° to 90° according to the neck anatomy study of Swartz, Floyd, and Cendoma [49]. In this study 80° taken and 20° initial position is extracted, and finally, the flexion limit angle is determined as 60°.

According to $NIC1 = \frac{F_z}{F_{int}} + \frac{M_z}{M_{int}}$ formulation and Table-3 which gives us the force and torque values as $F_{int} = 3600N$ and $M_{int} = 125Nm$ the following Simulink diagram created which is given in Figure 64.
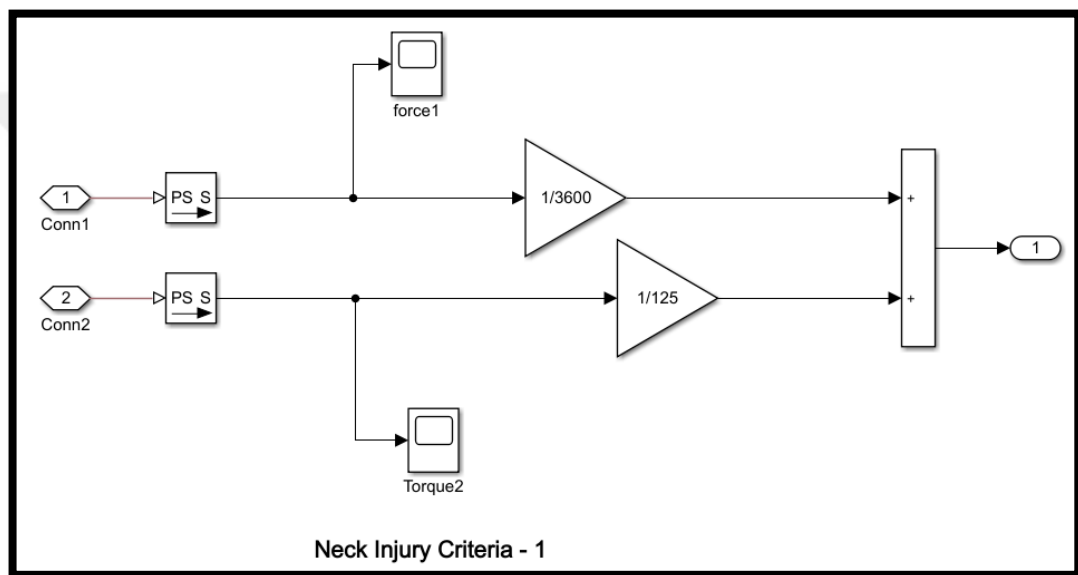

Figure 64 10.4 NIC-1

According to $NIC2 = a_{rel} \ x \ 0.2 + v_{rel}^2$ formulation of the following Simulink diagram created which is given in Figure 65.
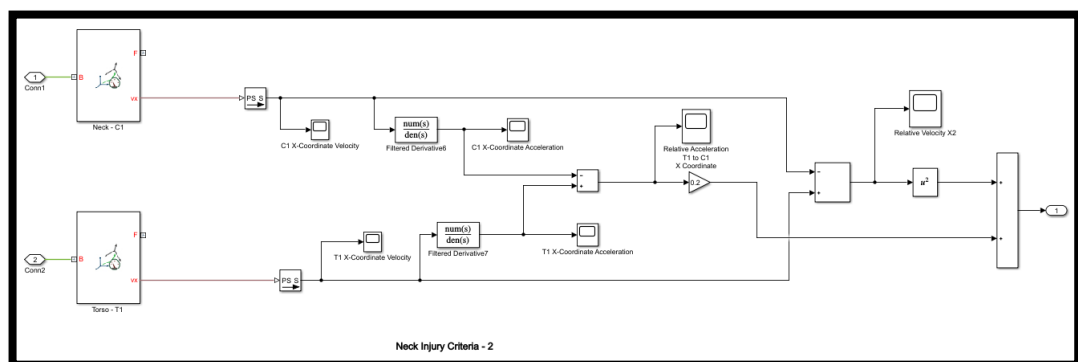
Figure 65 10.5 NIC-2

b. Variable Stiffness Case

Up to this point, the stiffness value of the revolute joint was determined by maximum limit inputs because only constant stiffness value can be inserted into the stock Simulink tool. On the other hand, a diagram specific to the variable stiffness case was created to examine the accuracy of the constant stiffness assumption and compare it with the results of the variable stiffness case. The variable stiffness situation diagram is created according to equations 4.11, 4.12, 4.13, and figure 56. The stiffness values obtained from this diagram, are embedded in another diagram prepared for the energy method according to equation 4.27, and neck angle results were obtained from it.
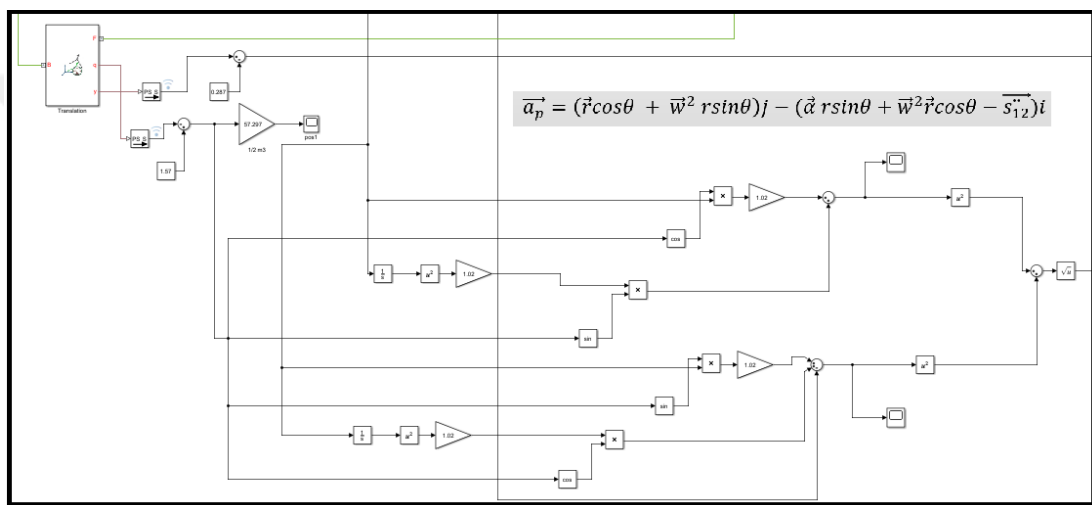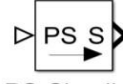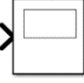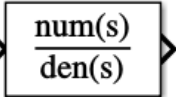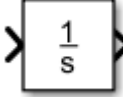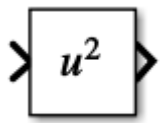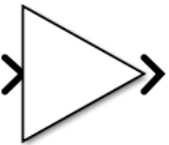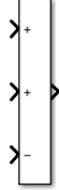
Figure 66 Variable Stiffness Case Diagram Part -1
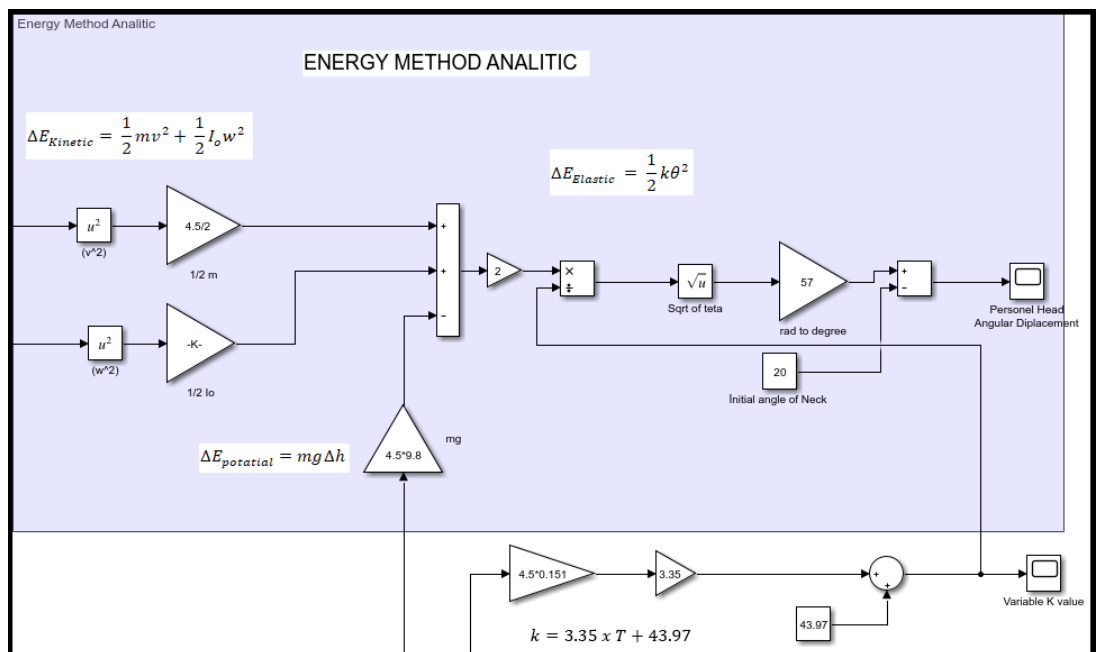
Figure 67 Variable Stiffness Case Diagram Part -2

Table 5 Other MATLAB Simulink Components used in Simulation Diagram

Symbol	Component name	Function
S PS Simulink-PS Converter	Simulink – PS Converter	This component converts Simulink signals to physical signals.
PS S PS-Simulink Converter	PS – Simulink Converter	This component converts physical signals to Simulink signals.
Scope	Scope	This component is for reviewing the data of physical signals which is run in simulation.
Group 1 Signal 1	Signal Builder	This component is used for inserting the input data of lateral and rotational movement of simulation.
$\dfrac{num(s)}{den(s)}$ Filtered Derivative	Filtered Derivative	This component is used for derivation. Usually used for position to velocity and acceleration converts. It's more accurate than the regular derivative block.
$\dfrac{1}{s}$	Integrator	This component is used for integration. Usually used for acceleration to position and velocity converts.

u^2	Square	This component is used for getting the square of desired data. It is usually used in diagrams of mathematical formulas.
$\sqrt{u}$	Square Root	This component is used for getting the root square of the desired data. It is usually used in diagrams of mathematical formulas.
	Gain	This component is used for getting the multiplication of desired data with a constant value. It is usually used in diagrams of mathematical formulas.
	Sum	This component is used for getting the addition or subtraction of desired data.

4.3 Results
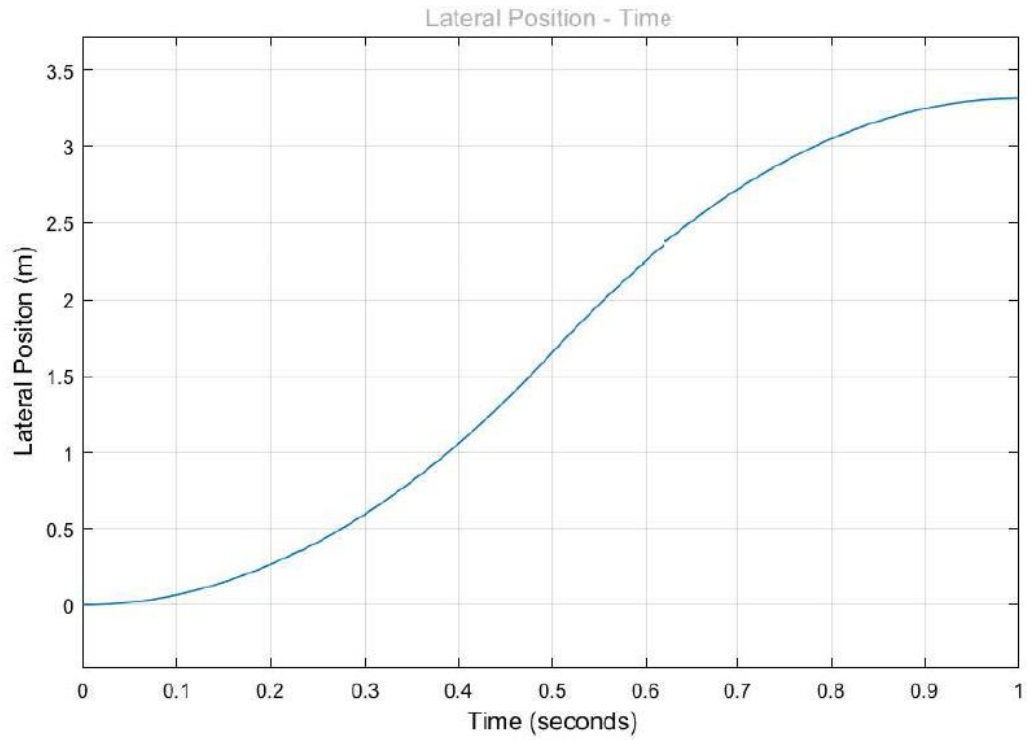
Figure 68 Lateral Position of Simulator Cabin
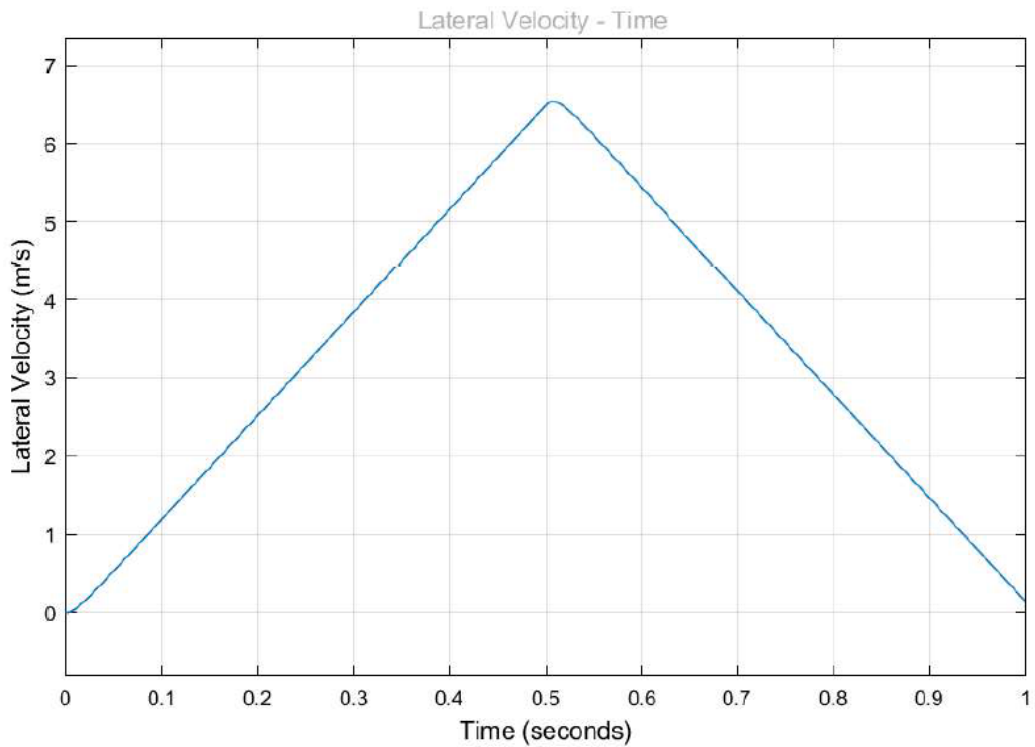
Figure 69 Lateral Velocity of Simulator Cabin
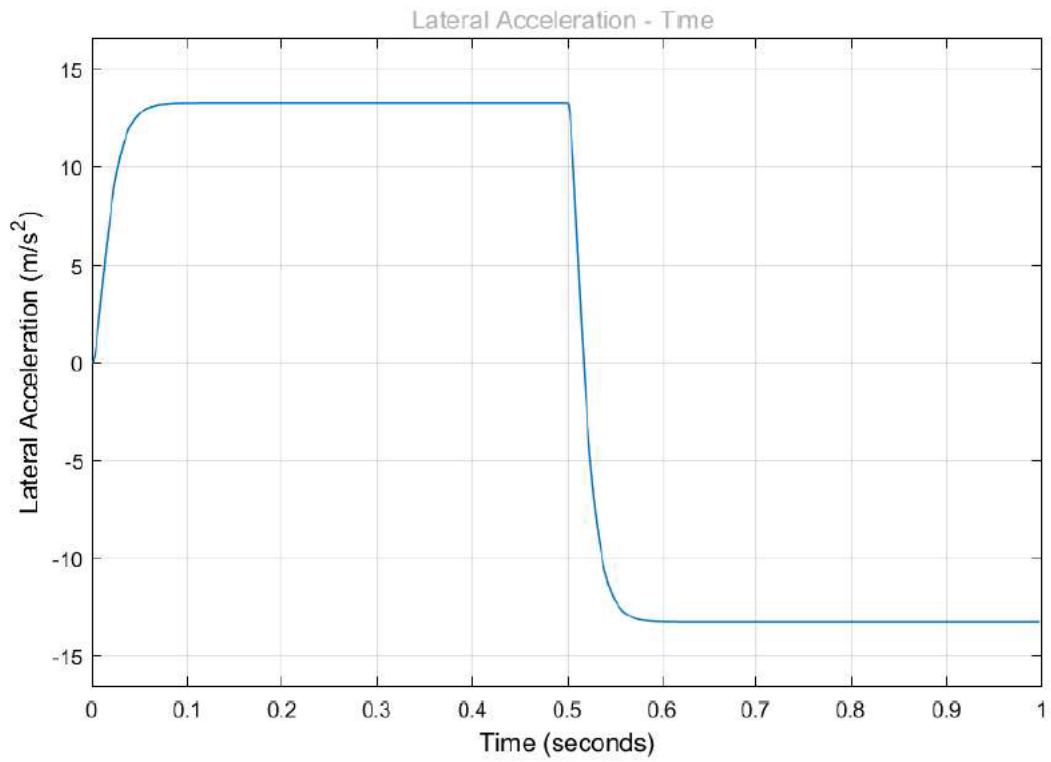
Figure 70 Lateral Acceleration of Simulator Cabin
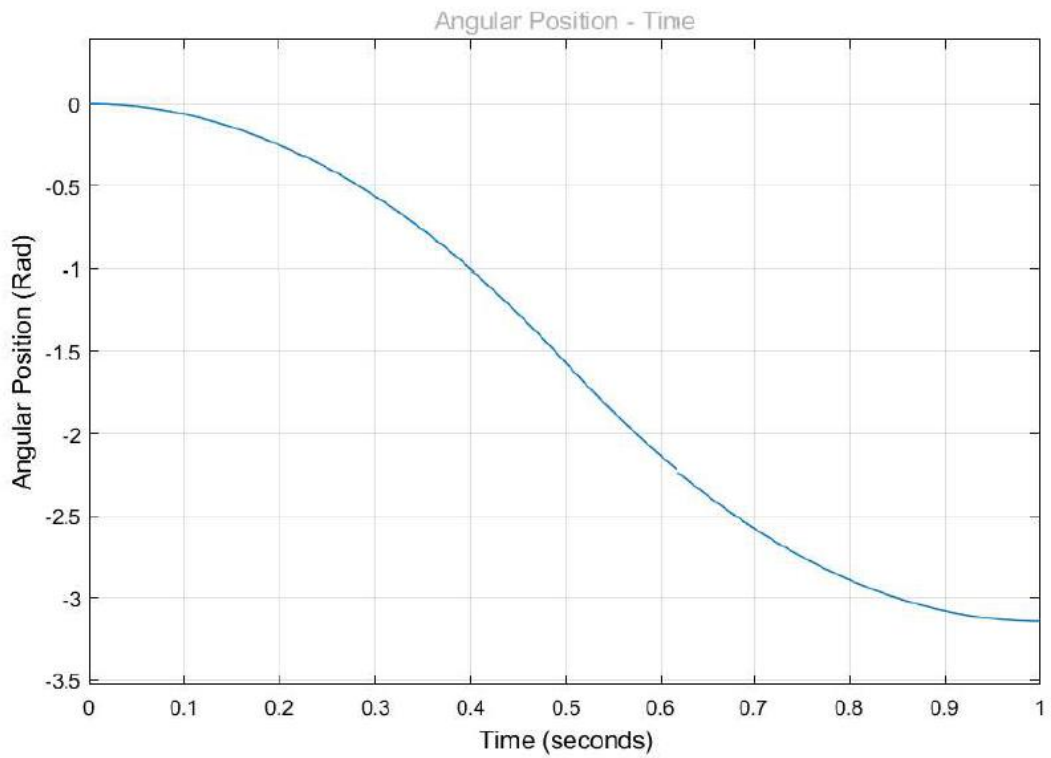
Figure 71 Angular Position of Simulator Cabin
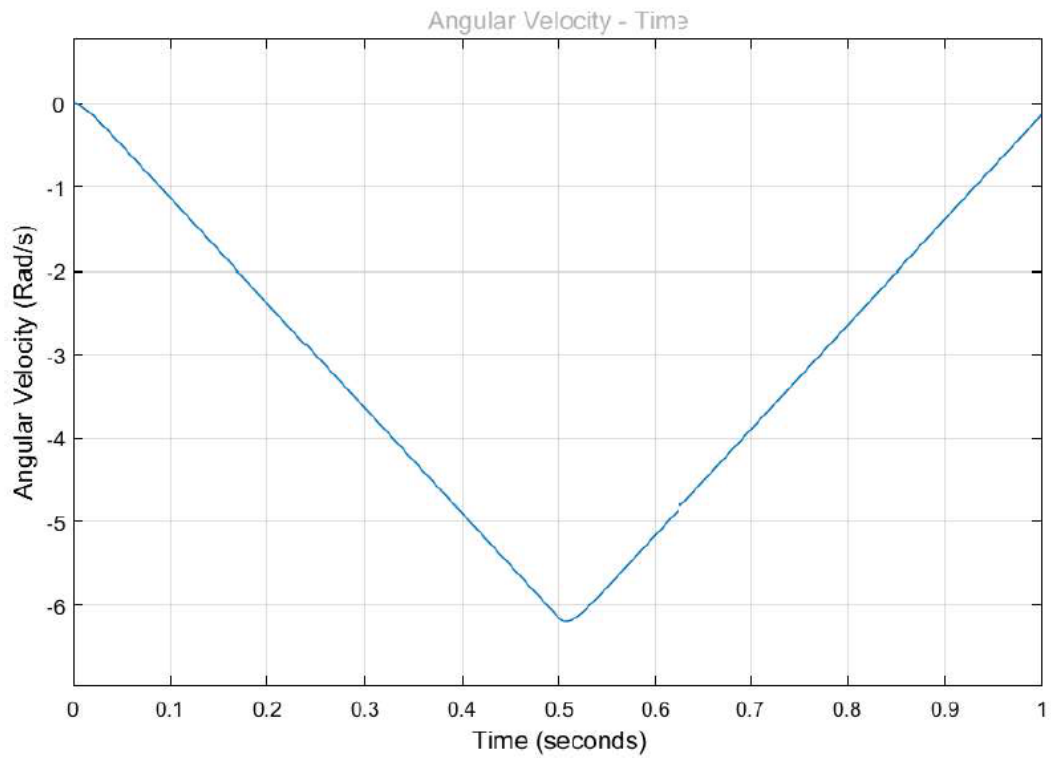
Figure 72 Angular Velocity of Simulator Cabin
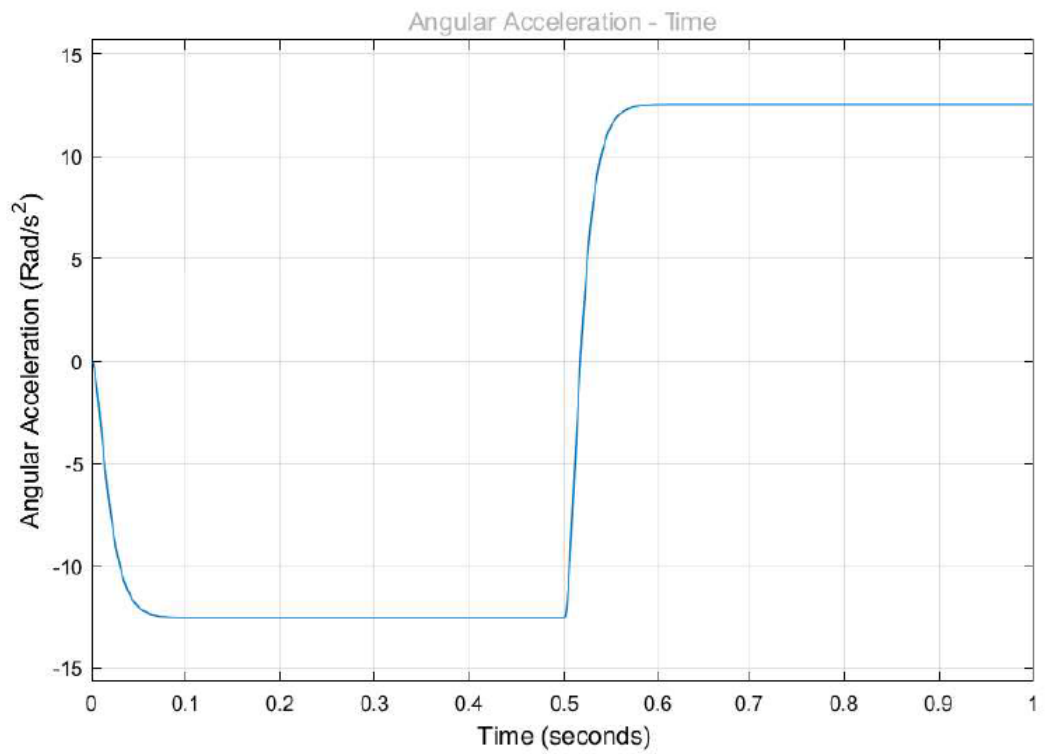
Figure 73 Angular Acceleration of Simulator Cabin
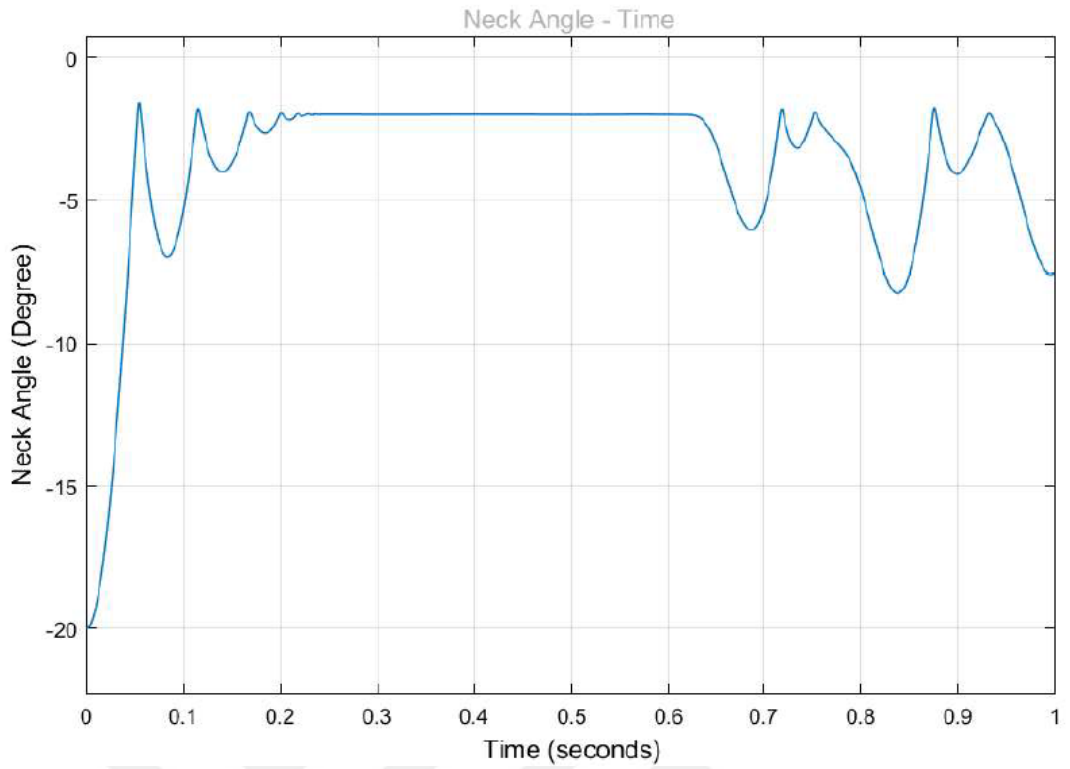
Figure 74 Neck Angle of Human Model with Constant Stiffness and with Headrest
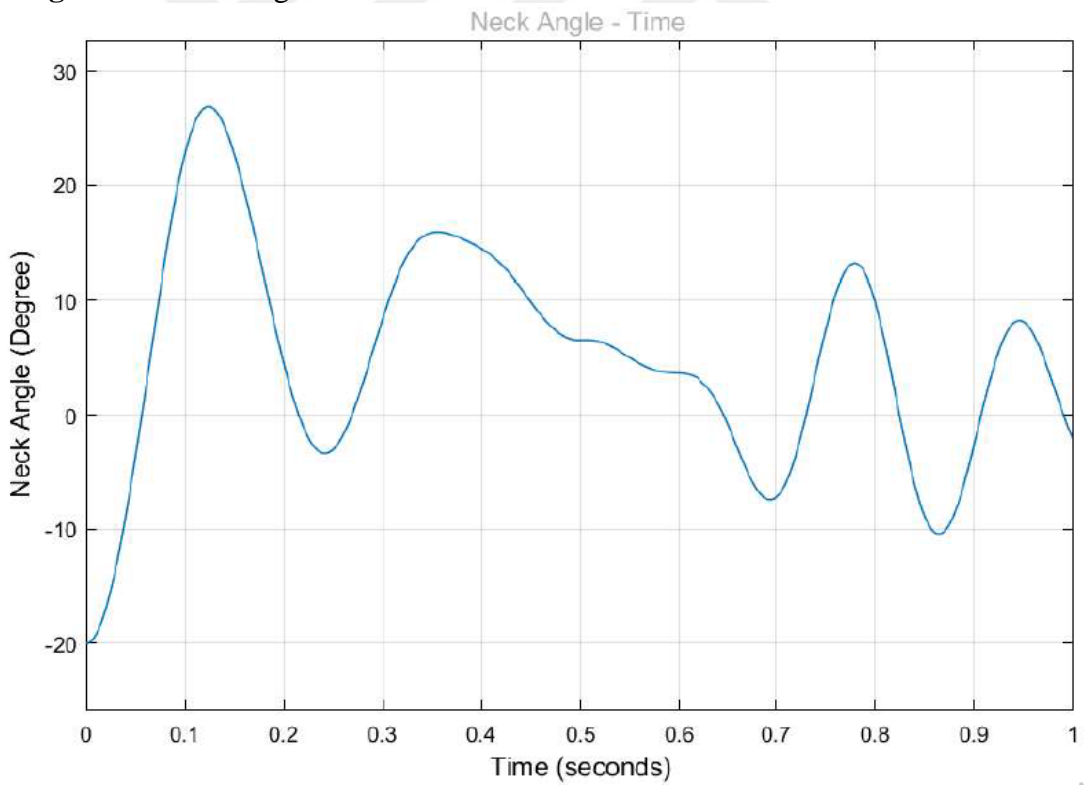
Figure 75 Neck Angle of Human Model with Constant Stiffness and without Headrest
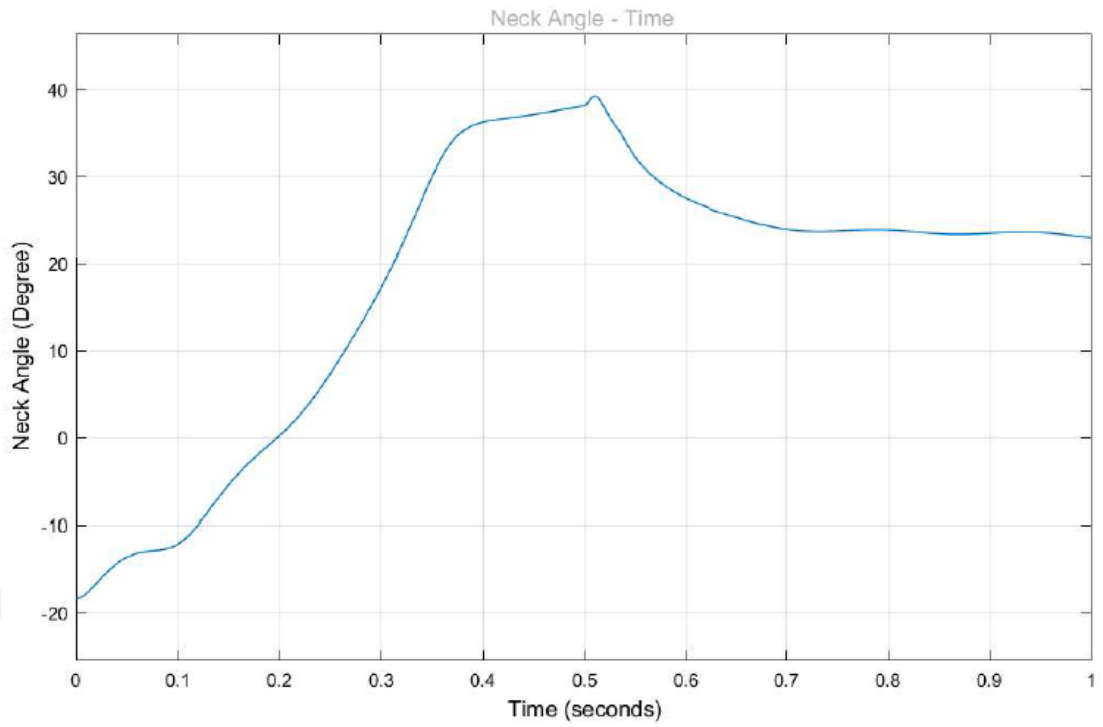
Figure 76 Neck Angle of Human Model with Variable Stiffness and without Headrest
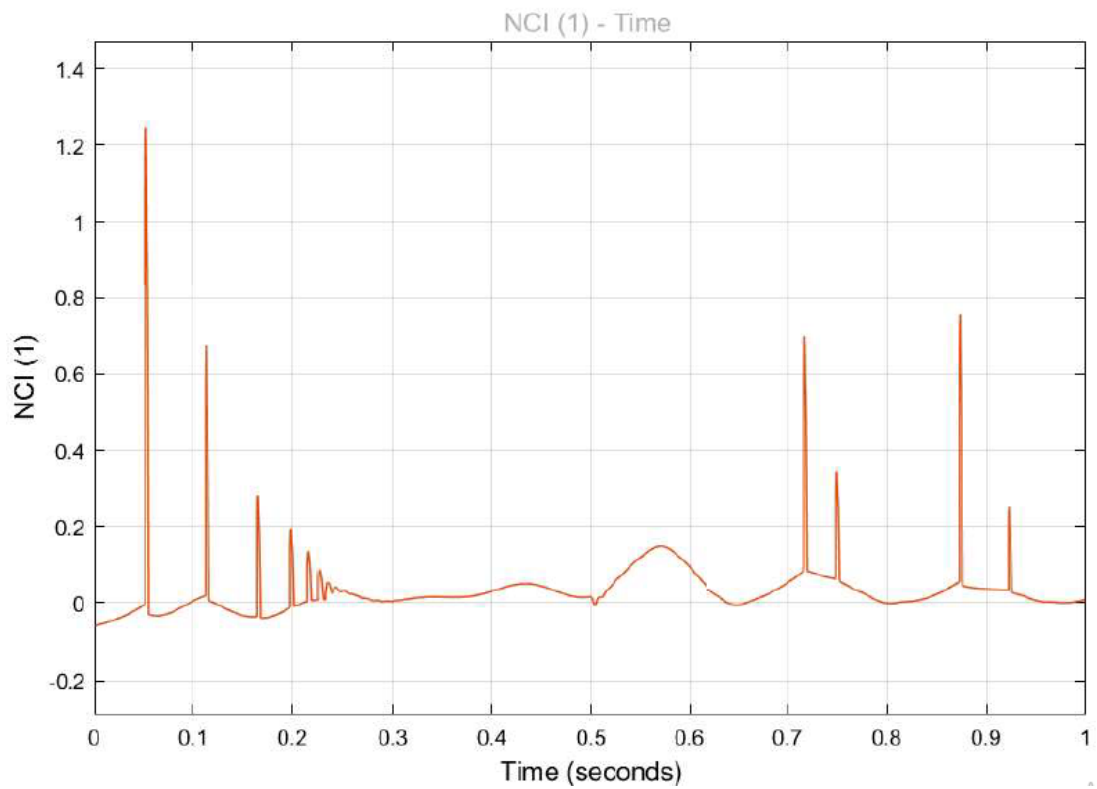
Figure 77 Neck Injury Criterion – 1 for Normal Sitting Trainee
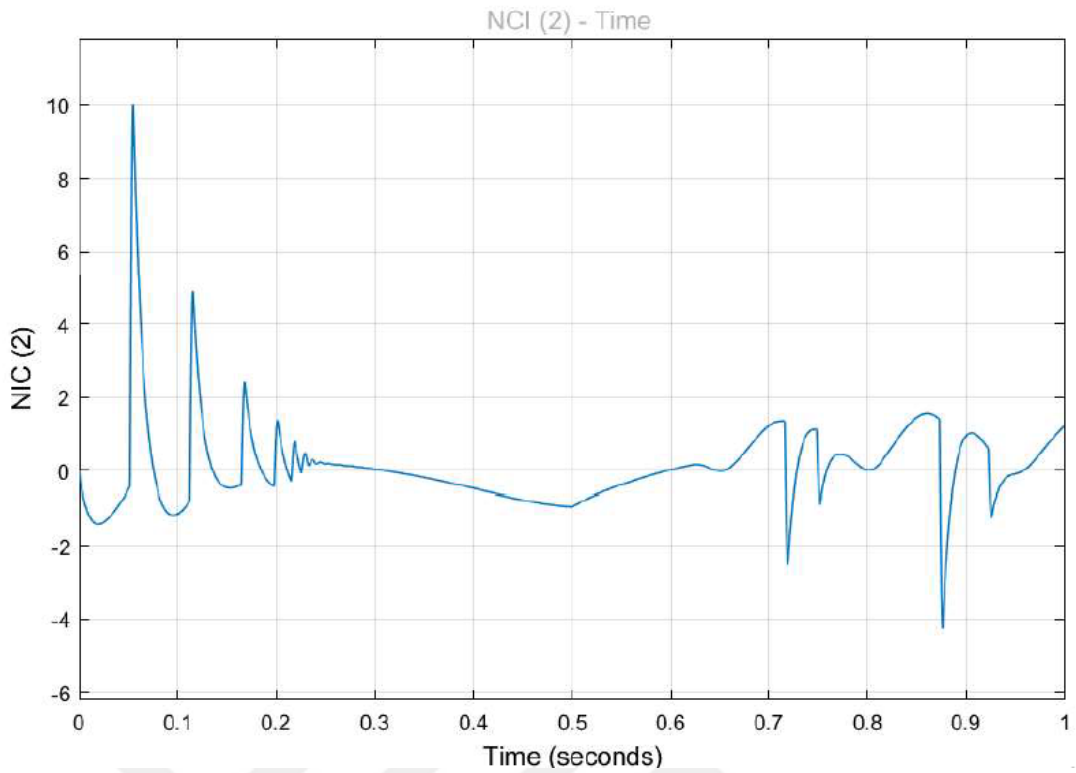
Figure 78 Neck Injury Criterion – 2 for Normal Sitting Trainee
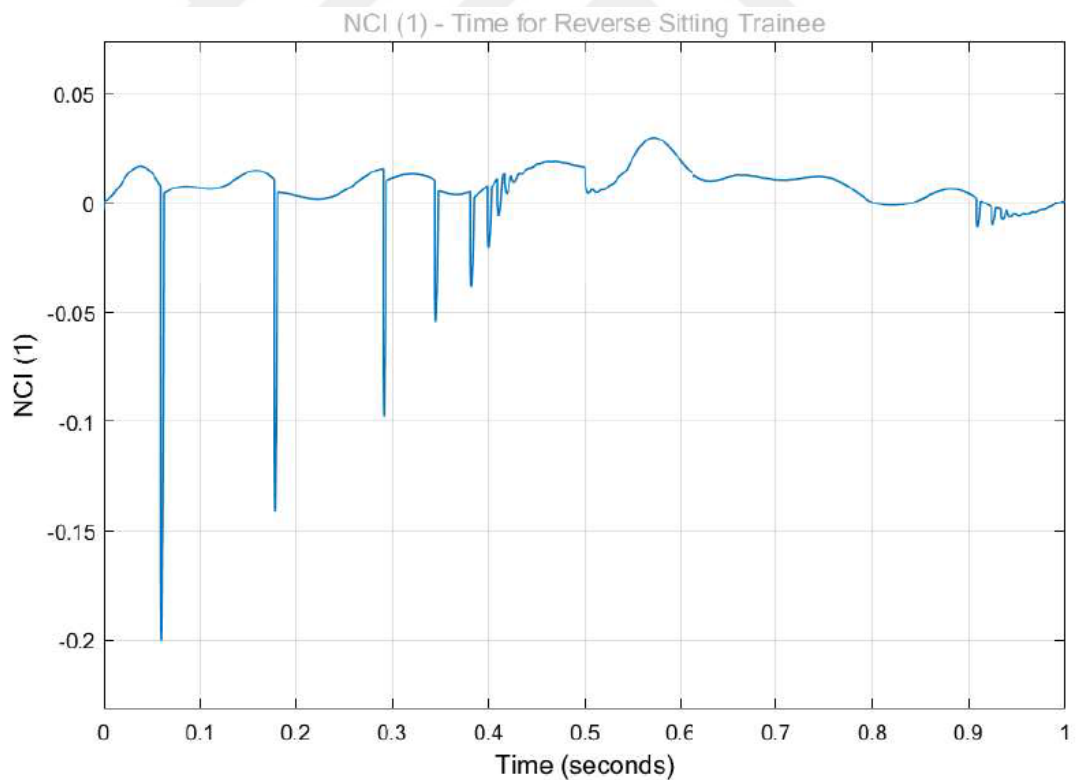
Figure 79 Neck Injury Criterion – 1 for Reverse Sitting Trainee

65
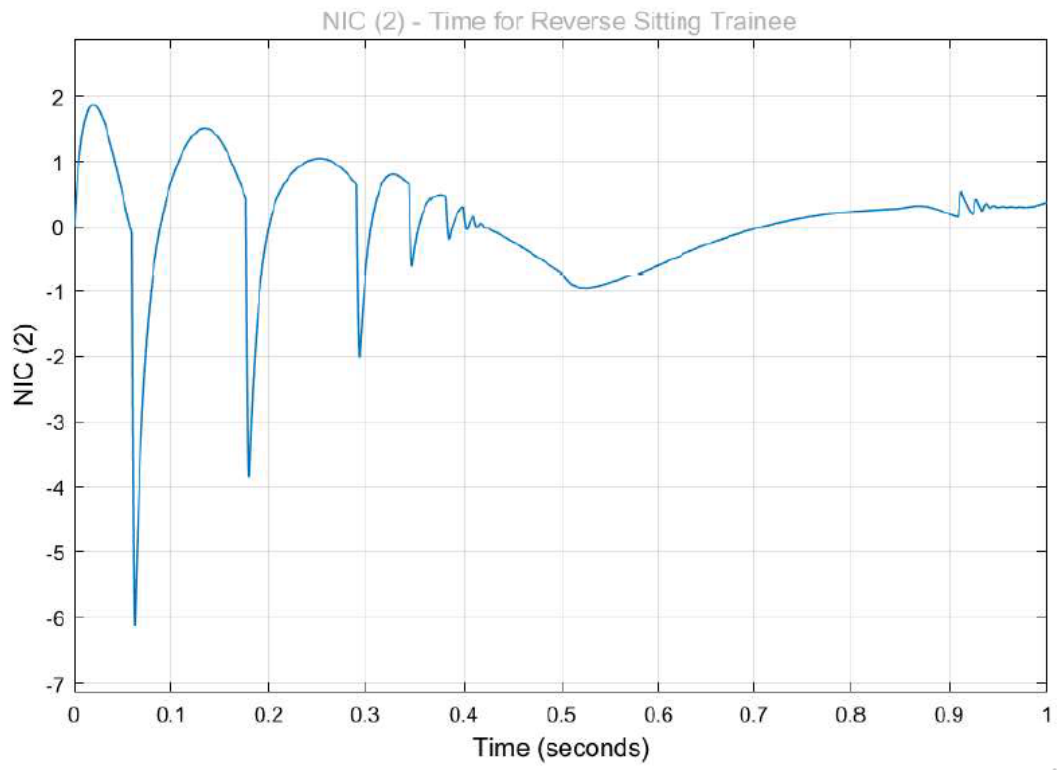
Figure 80 Neck Injury Criterion – 2 for Reverse Sitting Trainee

4.4 Discussion of Results

The position, velocity, and acceleration graphs for the lateral movement in figures 68-69 and 70 make sense because they have a harmony with the input velocity which is given in figure 62. The lateral position ends in the limits of the simulator area, moreover, velocity, and acceleration results are also consistent. The same things can be said for rotational movement too. The position, velocity, and acceleration graphs for the rotational movement in figures 71-72 and 73 also make sense because they have a harmony with the input angular velocity which is given in figure 61. The rotational movement position continues up to 180° rotation, moreover, velocity, and acceleration results are also consistent.

In figures 74-75 and 76, the neck angle results are given. In figure 74 and 75, the stiffness value of the revolute joint which represents the neck is constant. The neck angle results taken from the simulation with headrest is in figure 74 and without headrest is in figure 75. The obvious contacts of the head and the headrest is observed in figure 74. In figure 76, the stiffness value varies according to the torque value over the neck. Its maximum value is more than figure 75 because according to figure 56 the stiffness increases with time and torque so, in the beginning, the Musco-tensional reaction is less. Also, there is less fluctuation in figure 76 because it reacts more consistently to torque values so its resonance is less. In figure 75, the graph stabilizes itself about 0° because it is possible to add an equilibrium angle into the revolute joint as an input, in Simulink's stock tools. 0° is selected because at the end of the training, trainees' position is upside down and they will try to stabilize their neck around 0° by their will. But figure 76 comes from a Simulink diagram based on dynamical calculations so it is not stabilized around a selected equilibrium value, it is stabilized itself around 23° according to dynamical calculations.

But, this must be known, both figure 75 and figure 76 cases are theoretical because in the real-world the simulator has headrests. Both graphs reach to limit angle which represents the contact of head and headrest, approximately at the same time. And according to the following graphs of Neck Injury Criteria, the possible neck injuries occurs at that contact. So, for my study, using a constant stiffness value or a variable stiffness value does not really affect the neck injury criteria because both cases reach to first similar contact value at a similar time.

The results of neck injury criteria for the trainee who sits through lateral movement

are given in Figures 77 and 78. As mentioned previously, it can be observed that possible neck injuries occur at contact points of the head and headrest. For the first criteria in figure 77, the limit value is 1 (unitless) and it reaches the beginning of the simulation. For the second criterion in figure 78, the injury limit value is 15 m^2/s^2 but as mentioned previously, some people can have a neck injury and pain issues from 10 m^2/s^2. So when the sensitivity of the neck injury criteria is compared the first injury criterion is more sensitive than the second one.

Finally, the neck injury criteria results of the trainee who sits reverse through lateral movement are given in Figures 79 and 80. As seen in the figures, none of them reach their limit values. That means non-trainees has neck injury who sits at that side, but why? Because the trainees sit in the normal position, their neck is exposed to the extension. On the other hand, for the trainees who sit in the reverse position, their neck is exposed to flexion. The resistance capacity of neck flexion is higher than the neck extension as given in Table 3. This is why reverse sitting trainees do not have any injuries.

CHAPTER 5

CONCLUSION

In this study, the design and analysis of an MRAP-type military vehicle rollover simulator was applied. First of all, the structural design of the simulator cabin was created which was inspired by MRAP vehicles in use by the Turkish Army. Secondly, the movable platform which carries the simulator cabin, and the fixed platform which provides a height level for proper entrance and exit, was designed. All these designs are done by SolidWorks 3D program. After that, the movement trajectory of the simulator was determined. In this study, a modification was applied to standard type rollover simulators by adding a lateral movement to rotational movement. To provide this movement electrical motors were used whose selection calculations are given in the study. The simulator cabin and movable platform were statically examined by the SolidWorks Simulation tool, and their structural safety was proved. Finally, the simulator model was imported into MATLAB Simulink environment with two types of trainee models in it. One model represents the trainee who sits straight through the lateral movement, and the other one represents the trainee who sits reverse. The properties applied into the model and according to the velocity and acceleration values determined from simulation, Neck Injury Criteria are calculated. Based on the normal simulation time which was applied as 10s, there was no occurred injury. Following this, the theoretical maximum velocity and acceleration values were determined according to the neck injury criteria as angular velocity $w = 6.283$ rad/s, lateral velocity $v = 6.63\ m/s$, angular acceleration $a = 12{,}566$ rad/s^2, lateral acceleration $\ddot{s_{12}} = 13{,}26$ m/s^2.

REFERENCES

[1] A. Yılmaz, D. Yılmaz, A. M. Şenyiğit, B. K. Görür and V. İşler, "Genel Amaçlı Araştırma Simülatörü: Donanım ve Yazılım Altyapısının Tasarlanması ve Geliştirilmesi," *Savunma Bilimleri Dergisi,* pp. 147-161, May 2012.

[2] L. Stewart a, B. Durant, J. Wolfson, and G. Hegemier, "Experimentally generated high-g shock loads using Hydraulic," *International Journal of Impact Engineering,* vol. 69, pp. 86-94, 2014.

[3] U. B. Bayramoğlu, "Simulator Training and Practice for Reducing The Effect of Pilots in Aircraft Accidents," Master Thesis, Istanbul Technical University, 2019.

[4] M. Aebersold, "The History of Simulation and Its Impact on the Future," *AACN Advanced Critical Care,* vol. 27, no. 1, pp. 56-61, 2016.

[5] United States Government Accountability Office, "Army and Marine Corps Training: Better Performance and Cost Data Needed to More Fully Assess Simulation-Based Efforts," United States Government Accountability Office, 2013.

[6] M. . J. Taber and G. W. McGarr, "Confidence in future helicopter underwater egress performance: An examination of training standards," *Safety Science,* vol. 60, p. 169–175, 2013.

[7] M. J. Taber, "Simulation fidelity and contextual interference in helicopter underwater egress training: An analysis of training and retention of egress skills," *Safety Science,* vol. 62, p. 271–278, 2014.

[8] J. R. Hogue, F. . G. Anderson, C. . A. Pelz, R. W. Allen, S. Markham, and A. Harmsen, "Parachute Simulation Enhancements for Post-Ejection/Egress Training," in *36th Annual SAFE Symposium*, Phoenix, Arizona, 1998.

[9] J. Jennings, "Humvee Rollover Trainer: An Officer's Quest To Save Lives in Combat," *American Society of Safety Engineers,* vol. 55, no. 07, pp. 24 - 30, 2010.

[10] E. Baker, S. Budzik, and M. .. Reed, "Modeling Post-Accident Vehicle Egress," in *2nd International Digital Human Modeling Symposium*, 2013.

[11] J. . J. Glancy and S. . P. Desjardins, "A Survey of Naval Aircraft Crash Environments," Dynamic Science A Divisior of Marshall Industries, Phoenix,

Arizona, with Emphasis on Structural Response.

[12] C. J. Brooks, "The Human Factors of Surviving a Helicopter Ditching," North Atlantic Treaty Organization, Dartmouth, Nova Scotia, 2007.

[13] "scaffmag.com," 21 November 2013. [Online]. Available: https://scaffmag.com/2013/11/scaffolder-tells-story-survived-north-sea-helicopter-crash-killed-four/. [Accessed 17 November 2020].

[14] M. Taber and J. McCabe, "An examination of survival rates based on external flotation devices: A helicopter ditching review from 1971 to 2005.," in *SAFE Symposium*, Salt Lake City, Utah, 2005.

[15] [Online]. Available: https://www.dvidshub.net/image/1048085/marines-get-crash-course-helo-dunker-training. [Accessed 18 November 2020].

[16] [Online]. Available: https://everipedia.org/wiki/lang_en/OPITO. [Accessed 17 November 2020].

[17] "Huet Dunker," Seftec Group, [Online]. Available: https://www.seftec.ie/huet. [Accessed 17 November 2020].

[18] J. Croteau, J. Zolock, R. Larson, C. Bare, D. Peterson, and D. Parker, "Dynamic Response of Vehicle Roof Structure and ATD Neck Loading During Dolly Rollover Tests," *SAE Int. J. Passeng. Cars - Mech. Syst.,* vol. 3, no. 1, pp. 407-449, 2010.

[19] C. Chou, R. McCoy, and J. Le, "A literature review of rollover test methodologies," *Int. J. Vehicle Safety,* vol. 1, no. 1/2/3, pp. 200-237, 2005.

[20] J. R. Kerrigan, A. Jordan, D. Parent and et.al., "Design of a Dynamic Rollover Test System," *SAE Int. J. Passeng. Cars - Mech. Syst.,* vol. 4, no. 1, pp. 870-403, 2011.

[21] J. Hu, O. R. Nichole, R. Gruber and et.al, "Development of A New Dynamic Rollover Test Methodology for Heavy Vehicles," *SAE Technical Paper,* vol. 14, no. 57, pp. 1-7, 2017.

[22] A. Singh, D. A. Holtz, M. Megiveron and V. Paul, "Modeling Off-Road Rollover Using Terramechanics for Real-Time Driving Simulator," in *NDIA Ground Vehicle Systems Engineering and Technology Symposium*, Novi, Michigan, 2014.

[23] J. A. Tillapaugh, D. J. Murphy, H. J. Sommer III, and P. M. Garvey, "Operator Assessment of Tractor Roll Angle with and without a Tractor Stability Visual Feedback Device," *Journal of Agricultural Safety and Health,* vol. 16, no. 4, pp. 249-264, 2010.

[24] ITF, "Road Safety Annual Report," OECD Publishing, Paris, 2017.

[25] T. Rogoway, Acton Media Inc., 17 10 2017. [Online]. Available: https://www.thedrive.com/the-war-zone/15234/these-armored-vehicle-rollover-and-egress-simulators-ready-troops-for-a-bad-day. [Accessed 21 11 2020].

[26] M. C. Lo, R. P. Giffin, K. A. Pakulski, W. S. Davis, S. A. Bernstein, and D. V. Wise, "High-Mobility Multipurpose Wheeled Vehicle Rollover Accidents and Injuries to U.S. Army Soldiers by Reported Occupant Restraint Use, 1992–2013," *Military Medicine,* vol. 182, no. e1782, 2017.

[27] 01 July 2017. [Online]. Available: https://www.cumhuriyet.com.tr/amp/haber/kirpi-yine-takla-atti-88925. [Accessed 17 November 2020].

[28] J. T. Brooks, A. Ciavarelli, R. A. Grier, J. E. Morrison, C. G. Sanders, R. A. Wisher, and F. E. Hartman, "Analysis of System Training Impact for Major Defense Acquisition Programs (MDAPs): Training Systems Acquisition," Institute for Defense Analyses, Alexandria, VA, 2012.

[29] C. Hinneburg, 05 February 2016. [Online]. Available: https://americanmilitarynews.com/2016/02/incredible-pov-footage-from-inside-a-humvee-of-a-failed-roadside-bomb-attack/?utm_campaign=alt&utm_medium=facebook&utm_source=amn. [Accessed 18 November 2020].

[30] 01 September 2011. [Online]. Available: https://www.army.mil/article/64615/third_army_prepares_soldiers_for_dangers_of_a fghan_roads. [Accessed 18 November 2020].

[31] P. J. Sticha, M. J. Singer, H. R. Blacksten, J. E. Morrison and K. D. Cross, "Research and Methods for Simulation Design: State of the Art," U.S. Army Research Institute for the Behavioral and Social Sciences, Alexandria, VA, 1990.

[32] Y. Z. e. al, "Estimation of the friction coefficient between the wheel and rail surface using traction motor behavior," in *25th International Congress on Condition Monitoring and Diagnostic Engineering*, Huddersfield, United Kingdom, 2012.

[33] Federation of Europenne de la Manutention, "Booklet 2 - Classification and loading on structures and mechanisms," in *Rules for The Design of Hoisting Appliance*, 1998, pp. 23-84.

[34] A. Chhor, H. Y. Choi, M. Han, and I. Lee, "Rollover Simulation Using an Active Human Model," in *25th International Technical Conference on the Enhanced Safety of Vehicles (ESV)*, Detriot, Michigan, 2017.

[35] M. T. Silva, J. A. Ambrósio and M. PEREIRA, "Multibody System Dynamics,"

Biomechanical Model with Joint Resistance for Impact Simulation, vol. 1, p. 65–84, 1997.

[36] H. A. A. Hossein, A. SEDAGHAT, S. M. Mohsen and D. NADERI, "Determining and Optimization of Mass, Stiffness and Damping Coefficients of Tractor Seat by Quasi-Newton Method Using Coupled Human-Seat Model," *Journal of Agricultural Machinery Science,* vol. 4, no. 1, pp. 51 - 55, 2008.

[37] J. R. Funk, J. M. Cormier and S. J. Manoogian, "Comparison of risk factors for cervical spine, head, serious, and fatal injury in rollover crashes," *Accident Analysis and Prevention,* vol. 45, pp. 67-74, 2012.

[38] R. Arienti, C. Cantoni, M. Gobbi, and G. Mastinu, "Lightweight Seat Design and Crash Simulations," SAE Technical Paper 2015-01-1472, 2015.

[39] Y. Wang, "Passive and muscle-based predictive computer models of seated and supine humans in whole-body vibration," Ph.D. (Doctor of Philosophy) thesis, University of Iowa, 2012.

[40] M. Simoneau, M. Denninger and T. C. Hain, "Role of loading on head stability and effective neck stiffness and viscosity," *Journal of Biomechanics,* vol. 41, p. 2097–2103, 2008.

[41] N. Yoganandan, F. A. Pintar, I. Zhang, and J. L. Baisden, "Physical properties of the human head: Mass, the center of gravity and moment of inertia," *Journal of Biomechanics,* vol. 42, p. 1177–1192, 2009.

[42] M. Kleinberger, E. Sun and R. Eppinger, "Development of Improved Injury Criteria for the Assessment of Advanced Automotive Restraint Systems," National Transportation Biomechanics Research Center, 1998.

[43] O. Boström, M. Svensson and B. Aldman, "A new neck injury criterion candidate-based on injury findings in the cervical spinal ganglia after experimental neck extension trauma," in *International Ircobi Conference on The Biomechanics of Impact*, Dublin, Ireland, 1996.

[44] A. J. Croft, R. P. Herring, M. D. Freeman, and M. Haneline, "The neck injury criterion: Future considerations," *Accident Analysis & Prevention,* vol. 34, pp. 247-255, 2002.

[45] v. d. E. P. Laan, "Seat belt control : from modeling to experiment," Technische Universiteit Eindhoven, 2009.

[46] D. S. Grewal, J. G. Paver, and T. P. Khatua, "Simulation of BioSlD Head-Neck Motions," SAE Technical Paper Series, Detroit, Michigan, 1994.

[47] R. Portero, F. Quaine and V. Cahouet, "Musculo-tendinous stiffness of head–neck segment in the sagittal plane: An optimization approach for modeling the cervical spine as a single-joint system," *Journal of Biomechanics,* vol. 46, p. 925–930, 2013.

[48] G. Sławiński, M. Świerczewski, and P. Malesa, "Risk Assessment Regarding the Injuries of the Lower Limbs of the Driver of a Military Vehicle in the Case of an Explosion Under the Vehicle," *Biomechanics in Medicine and Biology,* pp. 179-193, 2019.

[49] E. E. Swartz, R. T. Floyd and M. Cendoma, "Cervical Spine Functional Anatomy and the Biomechanics of Injury Due to Compressive Loading," *Journal of Athletic Training,* vol. 40, no. 3, p. 155–161, 2005.